CARBON-CARBON BOND FORMATION METHODS FOR THE PREPARATION OF
SHAPE-PERSISTENT ARCHITECTURES

BY

AARON DEAN FINKE

DISSERTATION

Submitted in partial fulfillment of the requirements
for the degree of Doctor of Philosophy in Chemistry
in the Graduate College of the
University of Illinois at Urbana-Champaign, 2011

Urbana, Illinois

Doctoral Committee:

   Professor Jeffrey S. Moore, Chair
   Professor M. Christina White
   Professor Steven C. Zimmerman
   Professor Martin Gruebele

Abstract

Carbon-rich, conjugated organic scaffolding is a popular basis for functional materials, especially for electronic and photonic applications. However, synthetic methods for generating these types of materials lack diversity and, in many cases, efficiency; the insistence of investigators focusing on the properties of the end product, rather than the process in which it was created, has led to the current state of the relatively homogeneous synthetic chemistry of functional organic materials. Because of this, there is plenty of room for improvement at the most basic level. Problems endemic to the preparation of carbon-rich scaffolding can, in many cases, be solved with modern advances in synthetic methodology. We seek to apply this synthesis-focused paradigm to solve problems in the preparation of carbon-rich scaffolds. Herein, the development and utilization of three methodologies: iridium-catalyzed arene C-H borylation; zinc-mediated alkynylations; and Lewis acid promoted Mo nitride-alkyne metathesis, are presented as improvements for the preparation of carbon-rich architectures.

In addition, X-ray crystallographic analysis of two classes of compounds are presented. First, an analysis of carbazole-containing arylene ethynylene macrocycles showcases the significance of alkyl chain identity on solid-state morphology. Second, a class of rigid zwitterionic metal-organic compounds display an unusual propensity to crystallize in the absence of inversion symmetry. Hirshfeld surface analysis of these crystalline materials demonstrates that subtle intermolecular interactions are responsible for the overall packing motifs in this class of compounds.

For my friends and family

Acknowledgments

"You must try to generate happiness within yourself. If you aren't happy in one place, chances are you won't be happy anyplace." -- Ernie Banks

I figured Jeff would appreciate the Ernie Banks quote. Speaking of Jeff, I would first like to thank, and then apologize to, my advisor, Prof. Jeff Moore. Jeff has supported me, intellectually and financially, and my crackpot ideas since day one. By giving me the intellectual freedom and room to explore new ideas– things I neither deserved nor even knew I needed at first– he gave me the tools to succeed. Any success I had in grad school can be chalked up to the fact that he encouraged me to go along with my wild ideas, and never once discouraged me from letting my mind wander in new directions. For that I am infinitely grateful. At this time I would also like to apologize to my advisor, Prof. Jeff Moore, for the recurring "Flamin' Jeff" group meeting slide, my fake nanocar research proposal (or anything that had to do with nanocars/nanoputians in general), advocating to submit manuscripts in limerick form, voluminous emails about papers I just read, the Finke Marathon, the clown wig we made him wear for his birthday, and the Chicago Cubs.

You can't do science in a vacuum- not a sociological vacuum, anyway. Things would get rather stale. The support of many friends and colleagues were also paramount to my successes here. I would first like to thank the other members of my committee: Prof. Steve Zimmerman, Prof. Christina White and Prof. Martin Gruebele, for helpful discussions. The staff in the Organic Office: Stacy Olson, Susan Lighty, and Becky Duffield, were absolutely invaluable in making things run smoothly, and many thanks (and much Swiss chocolate!) are deserving. I'd also like to thank Jeff's secretary,

lab, which I more or less forbade him from using during my first year; more like his office, which was much safer. I'll always appreciate his puerile sense of humor (to augment my own) and knack for Simpsons quotes, our man-dates at Thara Thai, the epic bitch-sessions, David Caruso one-liners, not to mention him getting me hooked on "How I Met Your Mother." But most importantly, I am incredibly grateful for his support that got me through the most difficult semester of my life, when I oversaw a 600-student, 10-TA course. Without his experience and guidance, I wouldn't have gotten through that unscathed, and I don't think I ever got a chance to thank him for it. So… thanks, Phil. I mean it. Lastly but not leastly, I'd like to thank Josh Ritchey for being my main "actual" lab buddy, in that he was actually in the lab a lot. Josh was always great for tossing ideas around and for always challenging me to think about problems and ideas in different ways. I would also like to thank Dr. Dustin Gross and Dr. Zheng Xue for many helpful discussions and comments later on in my Ph.D career, and for feeding my "crystallography addiction." Thanks also go to the rest of the "RAL Crew:" Ron Smaldone, Erin Whitteck, Qilong Shen, Hideo Enozawa, Mitch Schultz, Jay Wackerly, James Herbison, Scott Sisco, and Nina Sekerak; and the "Beckman Crew:" Matty Kryger, Brian Steinberg, Hefei Dong, Aaron Esser-Kahn, Liz Glogowski, Susan Odom, Koushik Ghosh, Keith Porter, and Preston May, for their support.

At one point Jeff thought it wise to give me undergraduate minions, and he apparently does not regret this. I'd like to thank Mike Boyd, Joe Furgal, and especially Eric Elleby, for their hard work, despite their benevolent dictator's preference to, as Mike once put it, to "run a very tight ship." Eric was always there to put a smile on everyone's

face, usually with a bad joke, which never failed to put a grimace on mine. Despite this, Eric's limitless energy, enthusiasm, and friendliness was absolutely contagious, and he quickly became a fixture of the Moore Group. How he got paired up with the likes of me is anyone's guess. I wish them all the best in their future endeavors.

The support of my family and friends both at the U of I and outside were crucial to my stability. My friends at the U of I: Tim Flood, Mark Geiger, Greg Scott, Ian Dailey, Lindsay Sperling, Katie Brown, Kate Torrey, Adam Langenfeld, Emily Ayers-Johnson, I appreciate all the good times we had outside of lab. To my awesome co-blogger Jes Sherman: thanks a million for always being there for me. And to my family, thanks for supporting me 100% through this journey and the next. Lastly, I would like to thank Mark Ringenberg for his unconditional love and support through the last couple years of grad school. I couldn't have done it without you.

Table of Contents

Chapter 1

The Preparation of Carbon-Rich Scaffolding: An Overview[*]

"There's plenty of room at the bottom."

– Richard E. Feynman

1.1   Overview & Motivations

Carbon-rich, conjugated organic scaffolding is a popular basis for functional materials, especially for electronic and photonic applications. However, synthetic methods for generating these types of materials lack diversity and, in many cases, efficiency; the insistence of investigators focusing on the properties of the end product, rather than the process in which it was created, has led to the current state of the relatively homogeneous approaches to the preparation of functional organic materials. Because of this, there is plenty of room for improvement at the synthetic level. Problems endemic to the preparation of carbon-rich scaffolding can, in many cases, be solved with modern advances in synthetic methodology. This research takes this synthesis-focused paradigm to solve problems in the preparation of carbon-rich scaffolds. Herein, the development of three methodologies have been successfully applied to tackle basic problems: iridium-catalyzed arene C-H borylation for the preparation of dendritic polyphenylenes (Chapter 2); Pd-catalyzed alkynylations of aryl bromides promoted by zinc halides for rapid coupling without homodimerization (Chapter 3); and nitride-alkyne

---

[*]Portions of this chapter have been published: Finke, A. D.; Moore, J. S. Alkyne Metathesis Polymerization (ADIMET) and Macrocyclization (ADIMAC). In *Synthesis of Polymers*; Schlüter, A. D., Hawker, C. J., Sakamoto, S., eds. In press.

metathesis promoted by strongly Lewis acidic boranes for the rapid formation of metathesis-active molybdenum alkylidynes from readily-available precursors (Chapter 4).

In this chapter, the preparation of discrete (as opposed to polymeric) carbon-rich architectures will be discussed. A shape-persistent, "carbon-rich" architecture is one where the scaffold backbone is comprised solely of carbon-carbon bonds between either sp^2- or sp^3-hybridized carbons. Such discrete architectures can be divided into three main scaffolds: linear (oligomeric),[1,2] branched (dendritic),[3] and cyclic (macrocyclic).[4]

1.2   Kinetic Approaches to Carbon-Rich Scaffolds

Kinetic approaches to carbon-rich scaffolds, in which the shape-persistent backbone is generated by an irreversible C–C bond-forming step, dominate the landscape. This is mainly due to the fact that thermodynamic driving forces for the formation of architectures of discrete monomer length are not present for all but cyclic architectures. Modern preparation of carbon-rich architectures is dominated by transition metal-mediated cross-coupling reactions with Pd, Ni, and/or Cu catalysts. These reactions have provided convenient access to carbon-rich architectures of incredible diversity. Architectures that contain sp^2-sp^2 carbon linkages fall roughly into three categories: aryl-aryl, aryl-vinyl, and vinyl-vinyl linkages. General methodologies for bond formation for aryl and vinyl-containing scaffolds are different.

1.2.1   Architectures with C_{sp2}-C_{sp2} Vinyl Linkages

Aryl-aryl and aryl-vinyl scaffolds are more common than vinyl-vinyl scaffolds, due mainly to the relative instability of oligoenes. Despite this, oligoenes are a well-studied class of molecules and are readily found in nature. The large third-order nonlinear optical susceptibility of the natural product β-carotene led to studies of derivatives to optimize their nonlinear optical susceptibility.[5] Preparation of oligoenes typically follow two synthetic routes: Wittig-type olefination and Pd-cross coupling. Wittig olefination is a classic means by which many oligoenes are prepared; this is facilitated by the fact that many oligoene-dialdehyde natural product precursors are commercially available. Functionalization of the naturally-occuring **1** with donor and acceptor bearing phosphonium ylides is facile, and elongation by desymmetrization and Wittig olefination allows for the preparation of higher oligoenes with high *trans*-selectivity (Scheme 1.1).[6-9] Müllen[10] reported the formation of discrete oligoenes by Pd-catalyzed Stille olefination (Scheme 1.2).[11] Vinyl iodide **2** was prepared by hydroalumination of *tert*-butyl acetylene with DIBAL, followed by substitution with iodine. Optimal conditions for the preparation of tetraene **3** under Stille olefination required "ligandless" Pd catalysts, as the use of Pd(PPh$_3$)$_4$ gave no product after a week's time.

Olefin metathesis has also been used to make oligoenes, but discrete architectures utilizing this method have only recently been reported. A novel method for the formation of oligoenes was reported by Schrock in which strained cyclobutene **4** underwent ring-opening metathesis with a tungsten catalyst (Scheme 1.3).[12] Removal of the tungsten *via* Wittig-type replacement of the alkylidene with aldehyde and

subsequent heating and elimination of benzene led to a mixture of polyenes up to the 17-mer that were separated and analyzed by HPLC. Around the same time, Grubbs *et al.* reported the ring-opening metathesis polymerization of substituted cyclooctatetraenes with the same catalyst to form poly(acetylene)s.[13] An iterative method utilizing both Witting olefination and olefin metathesis for the formation of heterotelechelic oligo(phenylene vinylene)s was recently reported by Meyer (Scheme 1.4).[14] This clever approach exploited the difference in metathesis reactivity of styrenes lacking *ortho* functionalities (Type I olefins) and those bearing *ortho* functionalities (Type II olefins). Under metathesis conditions, Type I olefins metathesize with Type I and Type II olefins; Type II olefins, by contrast, do not react with other Type II olefins. The homologation strategy utilized a masked Type I olefin monomer **5** which was elucidated *via* Wittig olefination. Cross-metathesis of **5** with a Type II olefin led to the exclusive formation of a homologated Type I olefin terminus in good yield. Cross-metathesis with a Type II monomer **6** followed by Wittig olefination gave an oligomer with a Type II olefin terminus, completing the iterative cycle. The stilbene olefins generated in the process are inert to cross-metathesis (Type IV).

Dendritic scaffolds are limited to arylene-vinylene linkages. Two distinct methods stand out. Meier *et al.* reported a semi-convergent method that relied solely on Horner-Wadsworth-Emmons olefinations as the key coupling step.[15] Pillow *et al.* reported a more general, convergent strategy (Scheme 1.5), in which Pd-catalyzed Heck couplings were the key transformation.[16] In this case, the styrene focal point was masked with an olefin and elucidated by Wittig olefination. Subsequent Heck coupling with 3,5-

dibromobenzaldehyde gave the next generation dendron. Polymerization of the styrene competed with cross-coupling at high temperatures; the addition of the radical inhibitor 2,6-di-*tert*-butylcresol was necessary to inhibit polymerization.

1.2.2 Architectures with C_{sp2}-C_{sp2} Aryl-Aryl Carbon Linkages

Polyphenylene architectures, which consist solely of biaryl linkages, have only been extensively studied in the past 30 years due to the difficulty of generating polyphenylene scaffolds *without* cross-coupling. Early reports of oligomeric polyphenylene preparations contrast with modern methods.[17,18] An archetypal iterative method for oligophenylene construction *via* cross-coupling methods was reported by Schlüter, who utilized an aryltrimethylsilane as a mask for iodine functionalities and an aryl bromide mask for boronic acids, which cross-couple under Suzuki-Miyaura cross-coupling conditions (Scheme 1.6).[19] The lithiation of aryl bromides under strongly basic conditions is required and limits the utility of this otherwise satisfactory method.

Recently, "controlled" iterative cross-coupling strategies have overcome many of the limitations of previous iterative strategies for the preparation of oligophenylene scaffolds.[20] A strategy utilizing a "masked" boronic acid was developed independently by Burke[21] and Suginome.[22] Their approach utilizes an inexpensive and easily-generated functionality that is easily converted to a boronic acid under conditions orthogonal to Suzuki-Miyaura cross-coupling conditions (Scheme 1.7). Burke's boronic acid mask, *N*-methyliminodiacetic acid (MIDA), is rapidly hydrolyzed to the boronic acid upon treatment with aqueous base; anhydrous Suzuki cross-coupling conditions are

thus required to preserve the masked functionality. Suginome's mask is the 1,8-diaminonaphtalene (DAN) group, which is removed by aqueous acid. The latter has been utilized recently for the preparation of polyphenylene dendrons.[23] Hiyama has also reported the use of a protecting group for silanes active in cross-coupling.[24]

The preparation of cyclic oligo(phenylene)s remains a challenge. The first report of a cyclic polyphenylene, cyclohexa-*m*-phenylene, was reported by Staab in 1967.[25] Cu-promoted condensation of the bis-Grignard salt of 3,3'-dibromobiphenyl gave cyclohexa-*m*-phenylene in 11% isolated yield; as the length of the dibromide-terminated *m*-phenylene oligomer increased, so did the yield. This approach remained, with few exceptions,[26,27] the state of the art for polyphenylene macrocycle formation until the mid-1990's. This synthetic scheme was utilized by Cram for the preparation of shape-persistent cation-binding motifs.[28-31] Again, it was Schlüter who applied Suzuki-Miyaura cross-couplings to the formation of polyphenylene macrocycles, wherein the condensation of 2-3 monomeric units under Suzuki conditions gave large polyphenylene macrocycles in fair to good yields.[32,33] More recently, an impressive six-fold macrocyclization under Suzuki conditions was reported by Swager (Scheme 1.8).[34] Monomers **7** and **8** were condensed under Suzuki conditions to generate cyclohexa-*m*-phenylene **9** in 13% yield. The yield was extremely sensitive to the reaction conditions employed; slow addition and high dilution were found to be detrimental to the yield of **9**, indicating a potential templating effect. Other recent strategies, including electrochemical cyclization of Lipshutz cuprates[35] and Ni-catalyzed homocoupling,[36] have also proven useful for the formation of polyphenylene macrocycles. Recently, the

preparation of *p*-phenylene macrocycles has been achieved either using a rigid cyclohexane-based precursor to a *p*-phenylene moiety,[37,38] or reductive elimination from a platinum-hinged macrocyclic precursor.[39]

The pioneering work of Miller and Neenan in the early 1990's demonstrated the promises and limitations of the cross-coupling method for the preparation of polyphenylene dendrimers.[40,41] They found that Suzuki couplings were most efficient at generating 1,3,5-polyphenylene linkages. Their principal synthetic strategy relied on the elaboration of a "masked" boronic acid moiety at the focal point- in this case, a trimethylsilyl group which was converted to a boronic acid by BBr_3 followed by hydrolysis (Scheme 1.9). However, the third-generation masked focal point was unreactive to BBr_3, and a pseudo-divergent growth method was utilized for the preparation of higher generation building blocks. Since then, preparation of 1,3,5-polyphenylene dendrimers has followed a similar protocol, but other methods of boronic acid unmasking have been utilized, but nonetheless there appears to be a size limitation, as dendrimers larger than the third-generation have not been prepared. [23,42,43]

Müllen et al. has been able to overcome this apparent limitation by foregoing the 1,3,5-polyphenylene scaffold entirely.[44] The Diels-Alder reaction between tetraphenylcyclopentadienone and diphenylacetylene at high temperature generates, after cheletropic elimination of CO, hexaphenylbenzene in excellent yield.[45-47] Müllen utilized this reaction as the core strategy for the preparation of extremely large polyphenylene dendrimers (Scheme 1.10). [44,48-50] Key to this divergent strategy is exploiting the unreactivity of silylalkynes to Diels-Alder cycloaddition; triisopropylsilyl

(TIPS)-protected arylalkynes do not undergo the Diels-Alder cycloaddition reaction with tetraphenylcyclopentadienone. Thus, a TIPS-alkyne-substituted tetraphenylcyclopentadienone monomer **10** was prepared and reacted with a core polyalkyne. Removal of the TIPS group and subsequent reaction with the monomer gave the next generation in excellent yield. These dendrimers have been utilized in several materials applications and their electronic properties have been extensively studied.[51-55]. This method has been utilized in both convergent[56] and divergent[56] dendrimer growth.

1.2.3 Architectures With C_{sp}-C_{sp2} Linkages

The reactivity of terminal alkynes with metals has a rich chemistry that has been greatly exploited in the preparation of phenylene-ethynylene and vinylene-ethynylene scaffolds. The Sonogashira coupling has been utilized extensively for the preparation of phenylene-ethynylene architectures, including dendrimers (*vide supra*), polymers,[57] oligomers,[1] and macrocycles.[4,58] Our group has utilized Pd-catalyzed Sonogashira reactions to generate phenylene-ethynylene dendrimers of large size.[58-64] The success of this method is based on the facile formation and elaboration of "masked" aryl halides[65] and terminal alkynes (Scheme 1.11).

Our group has developed solid-phase preparative methods for phenylene-ethynylene heterosequence oligomers, enabling rapid preparation with minimal purification.[66] A key step in this method is the coupling of a grafted aryl bromide with a free alkyne. The use of Cu(I) inevitably leads to homocoupling of the alkyne, decreasing

yield. However, the use of superstoichiometric ZnBr$_2$ in conjunction with an active Pd catalyst enables rapid cross-coupling with no homocoupled byproduct.

1.3   Alkyne Metathesis: Dynamic Approaches to Carbon-Rich Scaffolds

Given the extraordinary achievements of olefin metathesis and its applicability across the entire spectrum of organic and polymer chemistry, it is both surprising and not that its cousin, alkyne metathesis, has only seen considerable synthetic utility in recent years. The driving force for the explosive popularity of olefin metathesis in polymer chemistry arguably rests on two foundations: 1) highly active, well-defined catalysts stable under ambient conditions; and 2) the living nature of metathesis-based polymerizations of strained cyclic olefins (ring-opening metathesis polymerization or ROMP). Alkyne metathesis does not share these primordial qualities. Nevertheless, the challenges facing alkyne metathesis as a general synthetic methodology belie its extraordinary potential, enabling transformations and reactivity that are simply not possible by other methods. In particular, the dynamic covalent nature of alkyne metathesis gives it a rare distinction in organic synthesis: the ability to directly generate carbon-carbon bonds under *thermodynamic control*.

The generally-accepted mechanism of alkyne metathesis, first proposed by Katz[67] and later verified experimentally by Schrock,[68] is shown in Scheme 1.12. Metathesis proceeds through a metallacyclobutadiene intermediate generated *via* a formal [2+2] cycloaddition. In general, dialkylalkynes react faster than alkylarylalkynes, which react faster than diarylalkynes.[69] Thus, for productive cross-metathesis of alkyl-

arylalkynes to occur, removal of the dialkylalkyne is crucial; otherwise, non-productive cross-metathesis of the dialkylalkyne will dominate the reactivity, "pseudopoisoning" the catalyst. Another undesired side reaction, addition polymerization of small alkynes such as 2-butyne, also competes with alkyne metathesis.[68,70] Metathesis of terminal alkynes also remains an unsolved problem as undesired alkyne polymerization predominates reactivity,[71] though there are a few reports of terminal alkyne metathesis of aliphatic alkynes.[72,73]

Olefin metathesis-mediated polymerizations generally fall into two categories: ring-opening metathesis polymerization (ROMP) and acyclic diene metathesis polymerization (ADMET). By contrast, there are few examples of ring-opening alkyne metathesis polymerization, due to both the difficulty of generating strained, cyclic alkynes and their relative instability.[74-76] In 1997, Weiss, Müllen and Bunz coined the term "acyclic diyne metathesis polymerization" (ADIMET),[77] shown in Scheme 1.13. This method was used to generate poly(phenylene ethynylene)s (PPEs) from bis(propynyl)benzene precursors, through the active removal of the dialkyne cross-metathesis byproduct. In addition to ADIMET, the shape-persistence of arylalkynes have brought forth a unique mode of reactivity for alkyne metathesis: *equilibrium*-driven cyclooligomerization of dialkyne monomers, which we term "acyclic diyne metathesis macrocyclization" (ADIMAC). This chapter is intended to be a brief overview of ADIMET and ADIMAC; for more detailed discussions on alkyne metathesis, several comprehensive reviews on these subjects have been published.[57,78-80]

1.3.1 Catalyst Development

Much like olefin metathesis, modern catalyst design for alkyne metathesis has typically focused on the efficacy of catalysts to promote reactions of small molecules.[79,81] Ring-closing metathesis of long, flexible alkyl chains dominates the methodological goal for chemists currently engaged in alkyne metathesis catalyst design. The number of catalysts that have shown efficacy in *polymerizations* is relatively small. Nonetheless, this short list boasts a diverse array of activity, functional group tolerance, and availability. Table 1.1 summarizes the catalysts which have demonstrated activity in alkyne metathesis polymerization. Well-defined alkyne metathesis catalyst precursors have been limited to high oxidation-state tungsten or molybdenum alkylidynes, though a silica-supported, well-defined rhenium alkylidyne was demonstrated to be alkyne metathesis-active.[82]

The Schrock tungsten alkylidyne $(Me_3CO)_3W\equiv CCMe_3$[69] is highly active in alkyne metathesis reactions, and to date is the only *well-defined* alkyne metathesis catalyst that is commercially available. $(Me_3CO)_3W\equiv CCMe_3$ is prepared from WCl_4 in three steps. Tungsten-based catalysts were the first to be utilized in ADIMET, however, its use in this realm has been supplanted by the more functional group-tolerant Mo catalysts. The high sensitivity of tungsten-based catalysts to ambient conditions and many common functional groups, particularly in comparison to the more general Mo catalysts, have diminished their usefulness in ADIMET. Despite this, the commercial availability and the relative ease of preparation of metathesis-active tungsten precatalysts, especially compared to their well-defined Mo counterparts, still makes

tungsten-based alkyne metathesis an attractive method. Several recently-reported tungsten alkylidynes with high metathesis activity show promise but their activity and scope in ADIMET have yet to be determined.[83-85]

The *in-situ* formation of alkyne metathesis catalysts from cheap, commercially available $Mo(CO)_6$ and 4-chlorophenol as developed by Mortreux[86-89] and Mori[90] is arguably the most popular method for the formation of linear polymers by alkyne metathesis polymerization. In general, the well-defined W and Mo alkylidyne catalysts display higher activity under milder conditions compared to the catalysts generated *in-situ* from $Mo(CO)_6$, but at the price of high sensitivity to ambient air and moisture. That air- and moisture-tolerant catalysts *do* exist, despite the fact that their active species is not currently known, marks an obvious target for future research and exploration.

The Mo(VI) precatalyst $EtC\equiv Mo[N(Ar)(CMe_3)]_3$[91] in conjunction with a phenol cocatalyst (typically 4-nitrophenol) to generate *in-situ* the active catalyst $EtC\equiv Mo(OAr)_3$, is a highly active and functional group-tolerant catalyst capable of metathesis activity near room temperature. We have reported an efficient method for generating $EtC\equiv Mo[N(Ar)(CMe_3)]_3$,[70,92,93] *via* a reductive-recycle strategy from Cummins' $Mo[N(Ar)(CMe_3)]_3$.[94] However, the nature of $Mo[N(Ar)(CMe_3)]_3$ as a potent activator of dinitrogen[95,96] requires that handling and use of this complex and its precursors be performed under an inert atmosphere of argon. Simpler handling and execution of related catalysts has been achieved through the use of grafting well-defined Mo precatalysts onto silica, lowering metal leaching while still enabling high activity.[97-99]

1.3.2 Poly(*p*-phenylene ethynylene)s *via* ADIMET

Poly(*p*-phenylene ethynylene)s (PPEs),[57,100,101] dehydrogenated analogues of the poly(*p*-phenylene vinylene)s, display desirable optoelectronic properties that have found extensive use as emissive materials.[102,103] PPE preparation is dominated by the Sonogashira Pd/Cu-catalyzed cross-coupling of aryl halides and terminal alkynes.[104] However, polymerizations under these conditions rarely achieve high molecular weight, and defects such as diyne formation and alkyne crosslinking in the polymer backbone are endemic.[57,105,106] Alkyne metathesis was envisioned as a complementary method to PPE synthesis, with much success.

A direct comparison between catalyst systems utilized in ADIMET can be found in Table 1.2, with the preparation of poly(2,6-dihexylphenylene ethynylene) **11** via ADIMET of 2,6-dihexyl-1,4-bis(1-propynyl)benzene, as a typical example. Weiss et al. were the first to report the formation of PPEs using ADIMET, using the Schrock alkylidyne catalyst $(Me_3CO)_3W{\equiv}CCMe_3$.[77] PPE **11** was generated in high yield after several days at 90 °C under vacuum-driven conditions. High degrees of polymerization (P_n) and polydispersities consistent with step-growth polymerization were attained. Later, Bunz reported the preparation of **11** using the Mortreux $Mo(CO)_6$ / phenol (4-chlorophenol or *p*-trifluorocresol) catalyst system after stirring at 120-150 °C overnight with a stream of nitrogen to remove 2-butyne.[107,108] Polymers of very high molecular weight and high PDI were attained, and a dependence on the molecular weight and PDI as a function of temperature was observed. The high polydispersity was explained to be a result of differing reactivity of the terminating alkyne upon oligomerization, and the

solubility of **11** at such high molecular weights appeared to be a limiting factor. We reported the synthesis of **11** with the EtC≡Mo[N(Ar)(CMe$_3$)]$_3$ / 4-nitrophenol catalyst system.[109] The use of the highly active catalyst enabled polymerizations close to room temperature, resulting in polymers of high molecular weight and normal PDI. Notably, in all of the above examples, *no defect structures of any kind* were observed. This is in contrast to Pd-catalyzed polymerizations which typically contain diyne defects and cross-linked structures.

Tungsten-based catalysts were the first to be utilized in ADIMET, but their use has been superseded by Mo catalysts. Schrock was the first to report alkyne metathesis polymerization of both cyclic (cyclooctyne) and linear alkynes (2,10-dodecadiyne) with W$_2$(OCMe$_3$)$_6$ and (Me$_3$CO)$_3$W≡CEt, respectively (Scheme 1.14).[75] Later, Bazan described the ring-opening polymerization of tetrasilacycloocta-3,7-diynes with (OCCF$_3$Me$_2$)$_3$W≡CCMe$_3$; notably, low polydispersities were achieved.[76] In 1997, Müllen, Weiss, and Bunz reported the first preparation of PPEs *via* ADIMET with (Me$_3$CO)$_3$W≡CCMe$_3$ (*vide infra*).

Of the catalyst systems in Table 1, the Mo(CO)$_6$ / 4-chlorophenol system has been most widely utilized for the preparation of linear PPEs, most notably by Bunz.[80] This "shake and bake" method boasts inexpensive starting materials, high ambient stability, and the use of undried, un-degassed solvents, making it an attractive polymerization catalyst system. Especially noteworthy is that these conditions do not require rigorously air- and moisture-free conditions for high conversion, in contrast to the much more sensitive Schrock catalysts. Heteroatoms also tend to be better tolerated

with this system than with the Schrock catalyst system, provided they are not *proximal* to the reactive alkyne.

The Mortreux catalyst system has shown extraordinary versatility in PPE synthesis, as can be seen in Scheme 1.15. PPEs generated by ADIMET of 1,4-dipropynylbenzenes with the $Mo(CO)_6$ / 4-chlorophenol system are characterized by polymers of very high molecular weight. The upper limit that is achievable appears to be dependent only on the solubility the side chain renders. $P_n > 100$ have been demonstrated, particularly with simple hydrocarbon monomers. This is in contrast to PPEs generated by palladium catalysis, whose P_n rarely exceed 100 unless electron-accepting groups are attached to the polymer main chain.[57] Optimization of polymerization conditions of 2,5-didodecyl-1,4-dipropynylbenzene **12d** by Bunz showed that the use of a carbonyl-free Mo precursor, $MoO_2(acac)_2$, in conjunction with Et_3Al and 2-fluorophenol, was most ADIMET-active, giving PPEs with $P_n > 100$ in a few hours at 105 °C.[110] The activity of the catalyst system was also found to be dependent on the *volatility* of the precursor; $Mo(CO)_6$ is sufficiently volatile at the high temperatures required for ADIMET that some loss of the precatalyst occurs. Reaction temperatures above 150 °C result in defects in the polymer backbone.[108]

Aside from simple PPEs, the Mortreux system has also been utilized for the formation of novel acetylene-containing polymers such as the poly(fluorenyleneethynylene) **13**.[111] Alternating PPE-stilbene polymers **14** are readily generated due to the tolerance of olefins.[112] Organometallic moieties such as Cp(CO)Co(cyclobutadienyl) have also been successfully incorporated into the PPE

backbone to generate unconjugated organometallic polymer **15**.[113,114] Dialkoxy-PPEs **16** can be prepared with a modified catalyst system, where 4-chlorophenol is replaced with 2-fluorophenol[115] or *via* pre-activation of the $Mo(CO)_6$ with 4-chlorophenol and 3-hexyne.[116] The preparation of novel PPE-containing copolymers is also possible with the Mortreux system (Scheme 1.16). ADIMET copolymerization of the naphthalene-containing monomer **17** and **12d** gave copolymer **19** in high yield with P_n roughly dependent on the ratio of **17** to **12d**. [117,118] Incorporation of the highly sterically-hindered 3,7-di-*tert*-butylnaphthyl group gave blue light-emitting polymers with high solid-state photoluminescent quantum yields. In another example, Bunz reported copolymers **20** containing the 3,6-diethynylcarbazole moiety **19**.[119] Polymers containing **19** showed emission quenching upon addition of acid and a high degree of fluorescence solvatochromism, with a significant blue shift upon addition of MeOH to a $CHCl_3$ solution of the polymer.

Despite the versatility of the Mortreux catalyst system, the high temperatures and long reaction times required for ADIMET are non-ideal. To date, ADIMET at low temperature still requires well-defined precatalysts. Although $(Me_3CO)_3W{\equiv}CCMe_3$ is metathesis-active at room temperature, its low functional group compatibility limits its scope. For example, metathesis of 2-thienylalkynes, precursors to poly(thienyleneethynylene)s (PTEs), presents a particular challenge, as neither tungsten-based catalysts nor the Mortreux catalyst system is capable of successfully metathesizing these substrates.[80] In contrast, the precatalyst $EtC{\equiv}Mo[N(Ar)(CMe_3)]_3$

with 4-nitrophenol is capable of polymerizing the thienyl monomer **21** at 30 °C under vacuum to give PTEs in good yield with $P_n > 100$ (Scheme 1.17).[109]

1.3.3 ADIMAC- Acyclic Diyne Metathesis Macrocyclization

Oligomeric arylene ethynylene scaffolds possess their own unique properties that distinguish themselves from their polymeric counterparts. In particular, arylene ethynylene macrocycles (AEMs) are of great interest due to their shape-persistent geometry and extended pi-systems, which offers unique solid-state properties that have been exploited in explosives detection devices.[120] Preparation of AEMs under kinetically-driven conditions are laborious, low-yielding, or both; stepwise addition of monomer units followed by a final macrocyclization step under pseudo-high-dilution conditions is typical, and more convergent approaches have only recently been reported. In the past few years, macrocyclization *via* dynamic covalent chemistry,[121] wherein the critical covalent bond-forming steps are under thermodynamic control, has proven itself to be a highly efficient means for the preparation of shape-persistent macrocycles.[4] While most dynamic covalent mechanisms involve bond-forming reactions of heteroatoms, only a handful are capable of the dynamic covalent formation of carbon-carbon bonds. Alkyne metathesis is among these few.

As noted by Schrock, the reactivity of diarylalkynes under metathesis conditions is markedly lower than that of monoarylalkynes or aliphatic alkynes.[69] While this has not hindered the preparation of linear PPEs from monoarylalkynes, exploiting the equilibrium nature of alkyne metathesis with diarylalkynes requires either forcing

conditions or highly active catalysts. The catalyst technology to establish equilibration between diarylalkynes under alkyne metathesis conditions is now readily available, and with correct monomer design, cyclooligomerization *via* alkyne metathesis can be a highly efficient process. This process may be termed ADIMAC, or Acyclic DIyne metathesis MACrocyclization, to distinguish it from ADIMET, whose target is *linear* polymers, and where reversible C≡C bond formation between diarylalkynes is counterproductive to the usual goal of high molecular weights and narrow molecular weight distribution.

In ADIMAC, active removal of undesired byproducts is necessary for productive bond-forming reactions to predominate, and the ease of removal of these byproducts is dependent on the scale of the reaction. The removal of volatile dialkylalkyne cross-metathesis products such as 2-butyne is facile on small scales (e.g. milligrams), either by passing a stream of inert gas over the reaction medium or performing the reaction under vacuum. However, large-scale (e.g. grams) preparation of AEMs via ADIMAC is inefficient under conditions that generate volatile byproducts. There are two reasons for this. First, removal of the 2-butyne (or 3-hexyne) byproduct is inefficient on larger scales, and pseudopoisoning cross-metathesis of dialkylalkynes predominates. Secondly, if 2-butyne is the leaving group, the catalyst can polymerize 2-butyne irreversibly at high concentrations; 3-hexyne is polymerized more slowly but is less volatile.

To overcome these limitations, we sought a different alkyne sidechain to exploit *solubility-driven* equilibrium. The 4-(4'-benzoylbiphenyl)yl group, upon alkyne cross-

18

metathesis, homodimerizes to form a diarylalkyne that is highly insoluble in chlorinated solvents, the preferred medium for ADIMAC.[122-124] In contrast, monomers and oligomers containing this group are soluble and enable the reaction to proceed, although solubility does vary from one monomer to another. This strategy can generate macrocycles on *gram scales* in high yield due to the immediate precipitation of the byproduct from the reaction mixture, allowing productive bond formation to occur. However, milligram-scale macrocyclizations tend to be more facile with the vacuum-driven method than the precipitation-driven method.

The preparation of [6]cycle **24** is illustrative of the necessity for dynamic covalent bond formation in the ADIMAC process (Scheme 1.18). First reported by Staab in 1974, Stephens-Castro coupling of **22a** generated **24a** in 4.6% isolated yield.[25] Nearly 30 years later, Bunz reported the preparation of **24b** from **23b** in 6% yield with the Mortreux catalyst system, clearly demonstrating the potential of alkyne metathesis for the preparation of macrocycles.[125] However, isolation of the desired [6]cycle from linear polymers was reported to be rather tedious. In 2004, we reported the preparation of **24b** from **23b** in 61% yield with $EtC{\equiv}Mo[N(Ar)(CMe_3)]_3$ / 4-nitrophenol in 1,2,4-trichlorobenzene at 1 mm Hg.[122]

Naturally, the question arises: what accounts for the dramatic difference in yields between these processes? Macrocyclization under *kinetic* control, as shown by the Staab example, is clearly not a favorable situation, as evidenced by the low yield of **24a**. In contrast, we have demonstrated that when alkyne metathesis macrocyclization is under *thermodynamic* control, [n]cycles are the lowest-energy product.[126] ADIMAC of

monomer **25a** under the conditions shown in Scheme 1.19 generate as the major

product [6]cycle **26** and [5]cycle **27** as a minor product. GPC analysis confirmed that

oligomeric products (both linear and cyclic) initially formed in the reaction are consumed

over time, and the [5-6]cycles are the major product upon completion. More

dramatically, when polymer **25b** was subjected to the same conditions, the major

products were smaller oligomers with **26** as the major product. An equilibrium *between*

macrocycles of different connectivity was also established when a 2:1 ratio of [3]cycle

28 and [6]cycle **29** subjected to ADIMAC conditions generated the mixed rhomboid

[4]cycle **30** as detected by FD-MS (Scheme 1.20).[123]

The favorable formation of [6]cycles from **25a** makes sense; the 120° angle

between reactive alkyne units suggests a hexagonal shape would generate a

macrocycle with the lowest angle strain. Theoretical calculations demonstrate that

[6]cycle formation from **25a** is favored enthalpically over smaller macrocycles due

largely to angle strain.[126] By contrast, larger macrocycles such as the [7-8]cycles are

disfavored entropically. Discrimination between the [5]cycle and [6]cycle under ADIMAC

conditions requires low temperatures, as the entropic factor becomes more pronounced

at higher temperatures; indeed, the product ratio [6]cycle:[5]cycle decreases from 6.5:1

at 30 °C to 2.9:1 at 95 °C, but returns to 6:1 upon cooling to 30 °C.[126]

Establishment of ADIMAC as a dynamic process leads to a rather simple but

nonetheless stunning conclusion: dynamic macrocycle formation is *intuitive* (Scheme

1.21). Simply calculating the bond angle between the reactive alkynes in a shape-

persistent dialkyne monomer can be an accurate predictor for the major product. As

shown above, the *m*-dialkynylbenzene monomer, with a 120° angle between reactive moieties, leads to predominantly [6]cycle formation, with the [5]cycle (containing an expected 108° angle for a regular pentagon) as the minor product. Likewise, *o*-dialkyne monomers with reactive alkynes 60° apart leads to a triangular [3]cycle as the major product, and *p*-dialkyne monomers with 180° spacing lead to linear polymers, as seen in ADIMET.

This predictability is not limited to benzene monomers. The 3,6-dialkynylcarbazole **19**, which has a roughly 90° angle between alkynes, leads to the square [4]cycle as the major product; and gram-scale preparation under precipitation-driven conditions gives the [4]cycle in excellent yield.[124] The use of well-defined catalysts is required, as use of the Mortreux system gives linear polymers with only trace amounts of [4]cycle.[119] These macrocycles have found considerable utility in nanofibril-based explosives detection devices.[120,127,128120,127,128120,127,128120,127,128]

ADIMAC has been utilized in the formation of many other kinds of novel macrocyclic scaffolds. Vollhardt reported the preparation of *o*-phenylene ethynylene macrocycles **31** with the Schrock catalyst $(Me_3CO)_3W\equiv CCMe_3$ in moderate yield (Scheme 1.22).[129] Notable was the unreactivity of monomers containing substituents *ortho* to the alkynes. The Mortreux catalyst system was utilized in the preparation of macrocycles from monomer **32** containing a disiloxane hinge, seen in Scheme 1.23. A mixture of macrocycles **33** and **34** were isolated in moderate yield.[130] A particularly impressive example of the utilization of ADIMAC for the preparation of large, extended

π-systems (Scheme 1.24) was shown by Haley, based on an *o*-phenylene ethynylene backbone to generate bicyclic (**35**) and tricyclic (**36**) scaffolds in excellent yield.[131]

1.4   Conclusions

Despite the fact that the potential for alkyne metathesis has clearly been demonstrated in the past ten years, alkyne metathesis has not yet replaced Pd catalysis for the preparation of linear oligomers and dendrimers. The generation of high-symmetry arylene ethynylene macrocycles has no serious competition to alkyne metathesis in terms of simplicity and efficiency. To overcome current limitations in alkyne metathesis methodology, further development of new catalyst systems which are highly active and more easily handled will further enable the utility and facility of this remarkable transformation.

1.5 Figures and Schemes
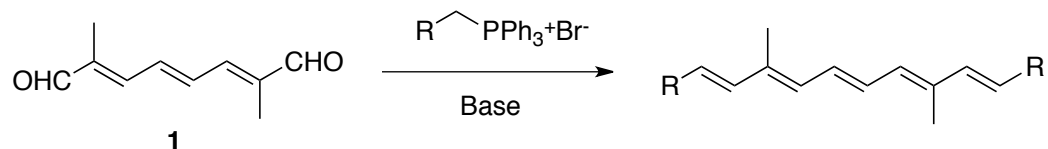
Scheme 1.1. General schematic of Witting-type olefination to form oligoenes.
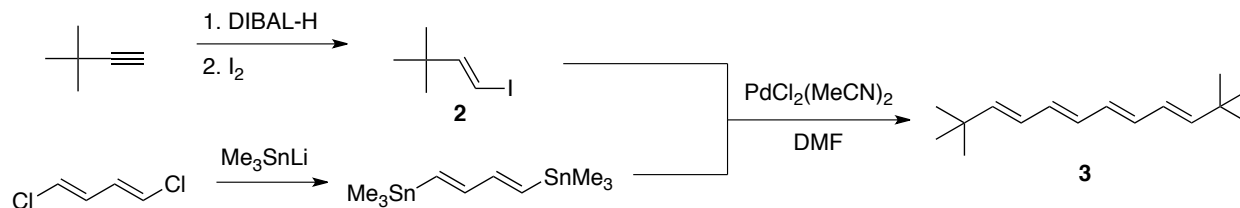
Scheme 1.2. Formation of oligoenes by Stille olefination.
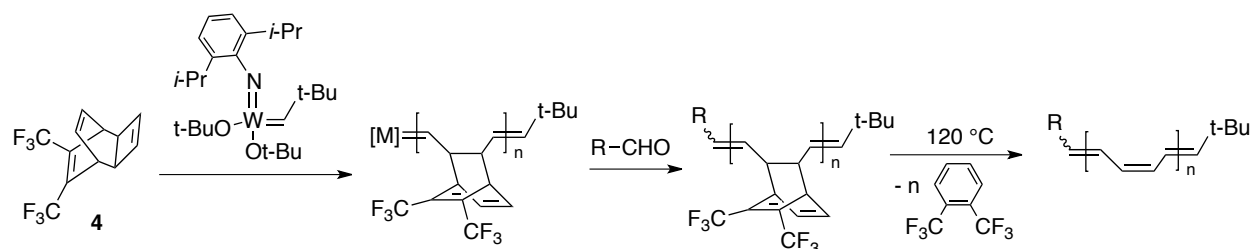
Scheme 1.3. Formation of oligoenes by ring-opening metathesis.
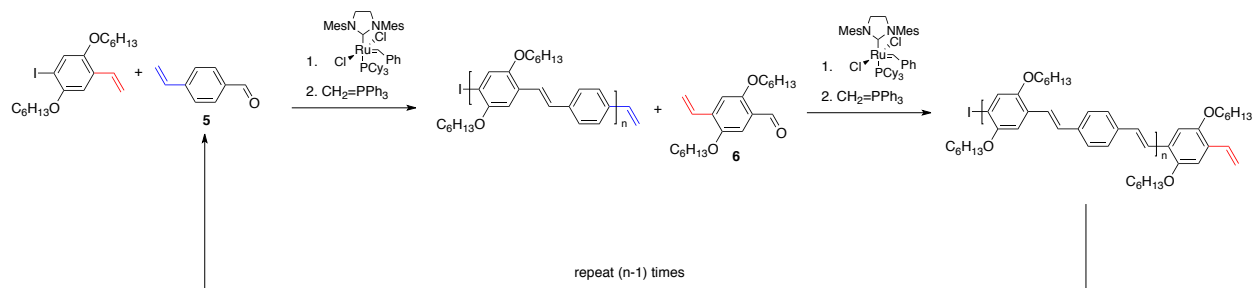
Scheme 1.4. Heterotelechelic oligo(phenylene vinylene)s by iterative cross-metathesis/olefination. Type I olefins in blue, Type II olefins in red.
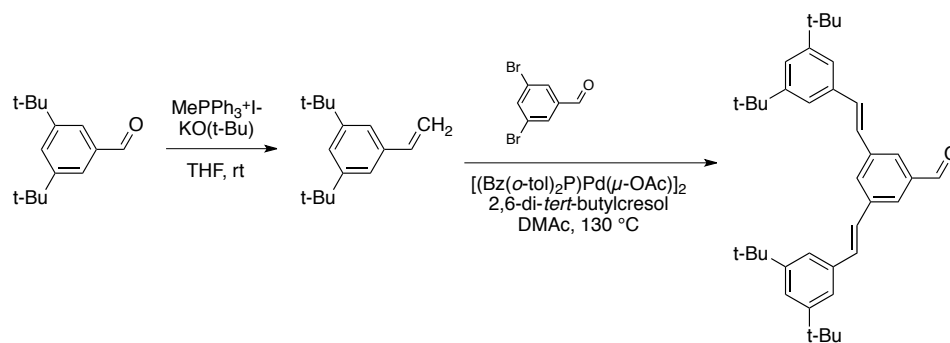
Scheme 1.5. Stilbene dendrons by iterative Wittig-Heck olefination.
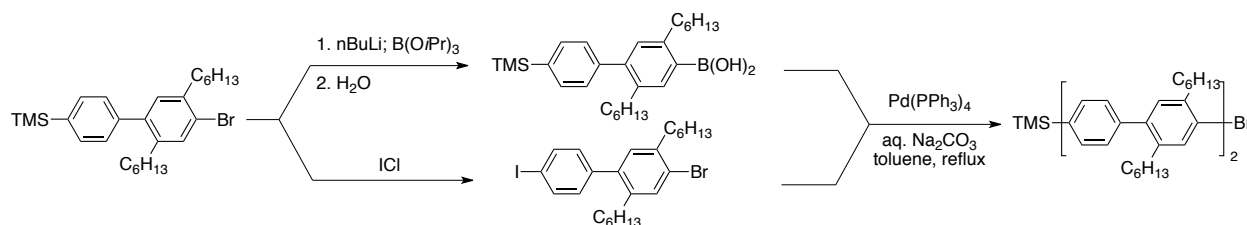
Scheme 1.6. Iterative oligophenylene synthesis with silyl masking groups.
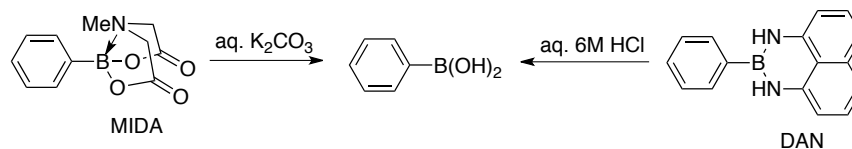
Scheme 1.7. Boronic acid protecting groups and deprotection conditions.

R = ―≡―〈 〉―OC$_{12}$H$_{25}$

R' = OMe
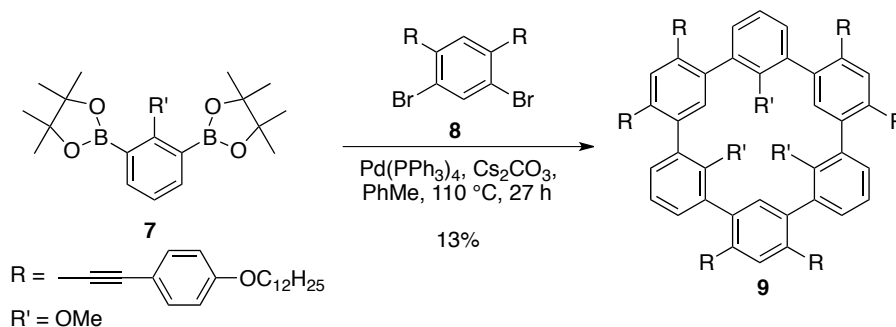
Scheme 1.8. One-pot formation of a cyclohexa-*m*-phenylene.
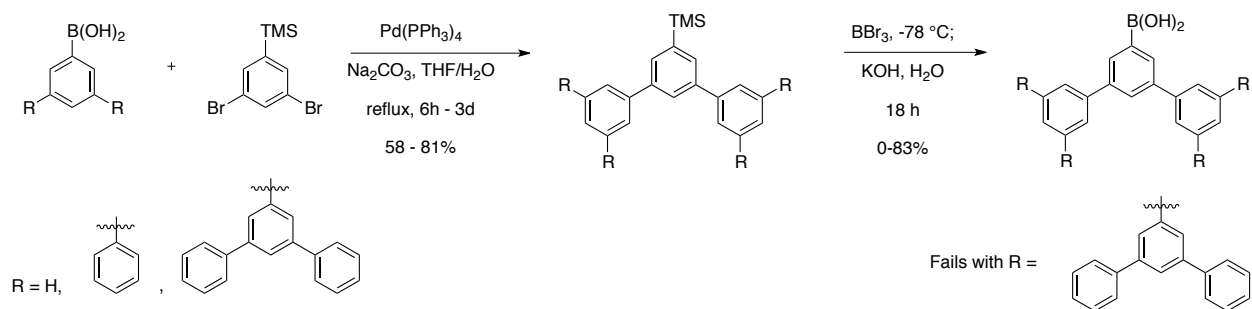
Scheme 1.9. Miller and Neenan's general method for 1,3,5-polyphenylene dendrimer growth.
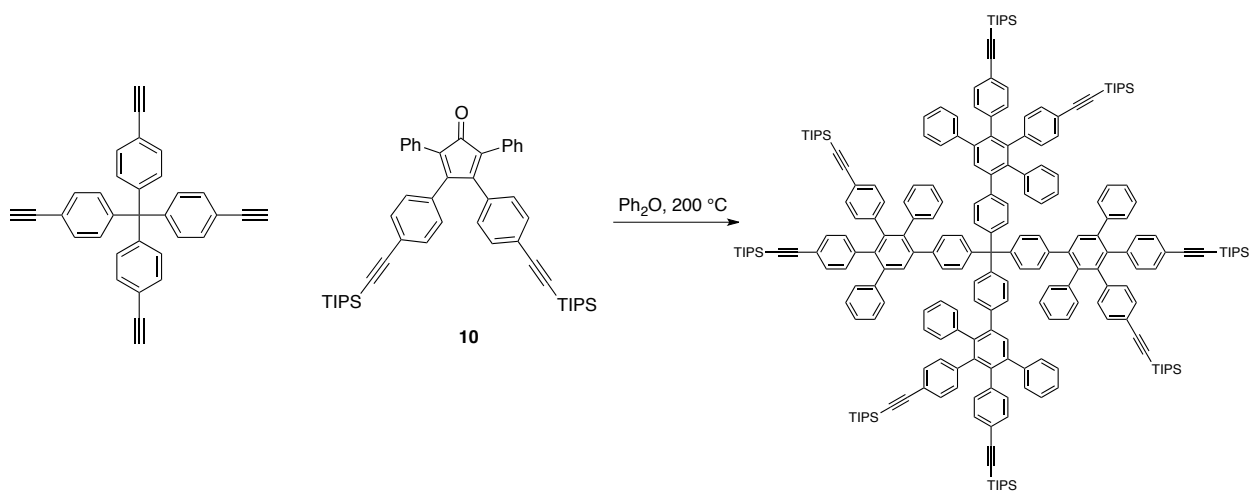
Scheme 1.10. Müllen's Diels-Alder approach to polyphenylene dendrimers.
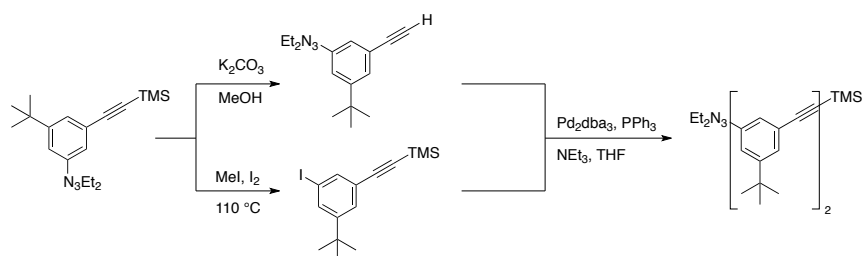
Scheme 1.11. General schematic for the preparation of arylene-ethynylene oligomers.
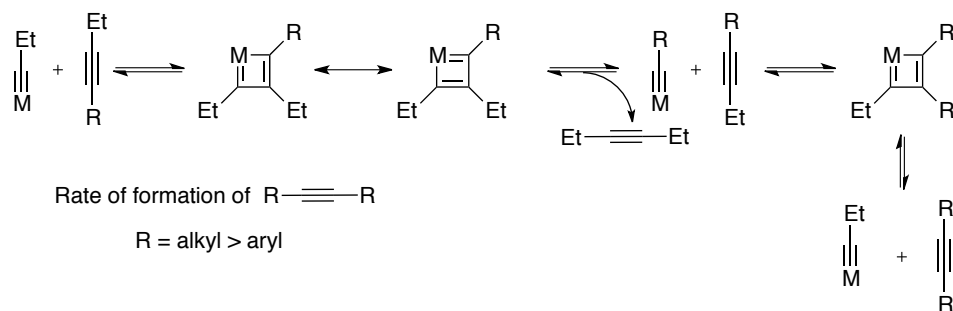
Scheme 1.12. Mechanism of alkyne metathesis proceeds *via* a metallacyclobutadiene intermediate.
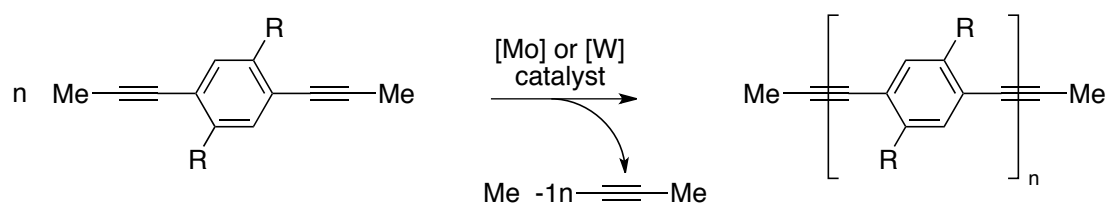
Scheme 1.13. General schematic of ADIMET polymerization.
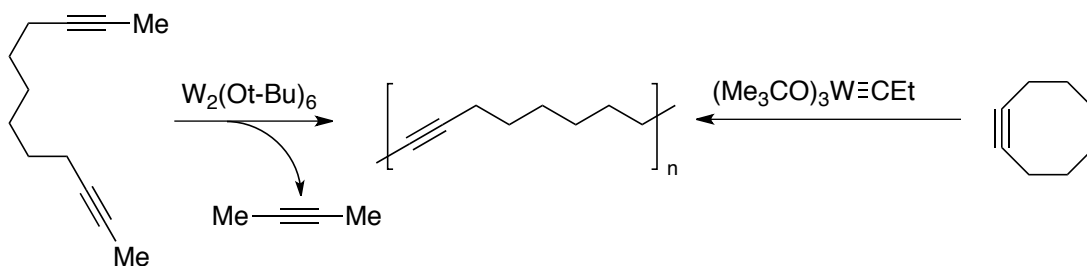
Scheme 1.14. Ring-opening and acyclic polymerization of aliphatic alkynes.
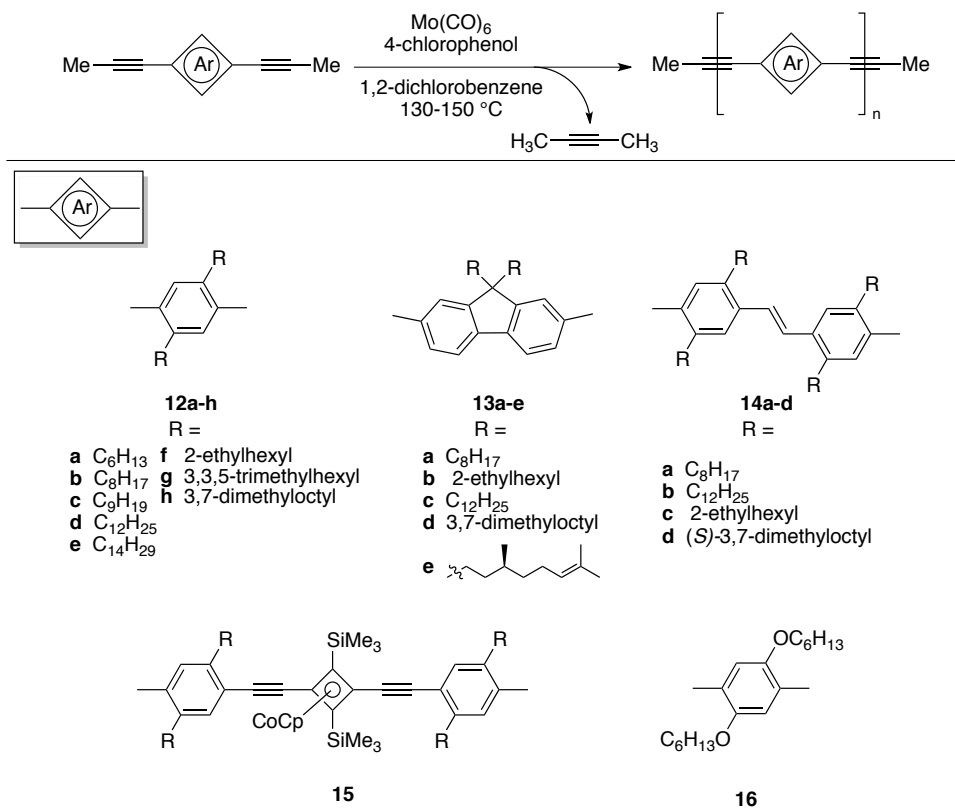
Scheme 1.15. PPE-containing architectures generated with the Mortreux $Mo(CO)_6$ / 4-chlorophenol system.
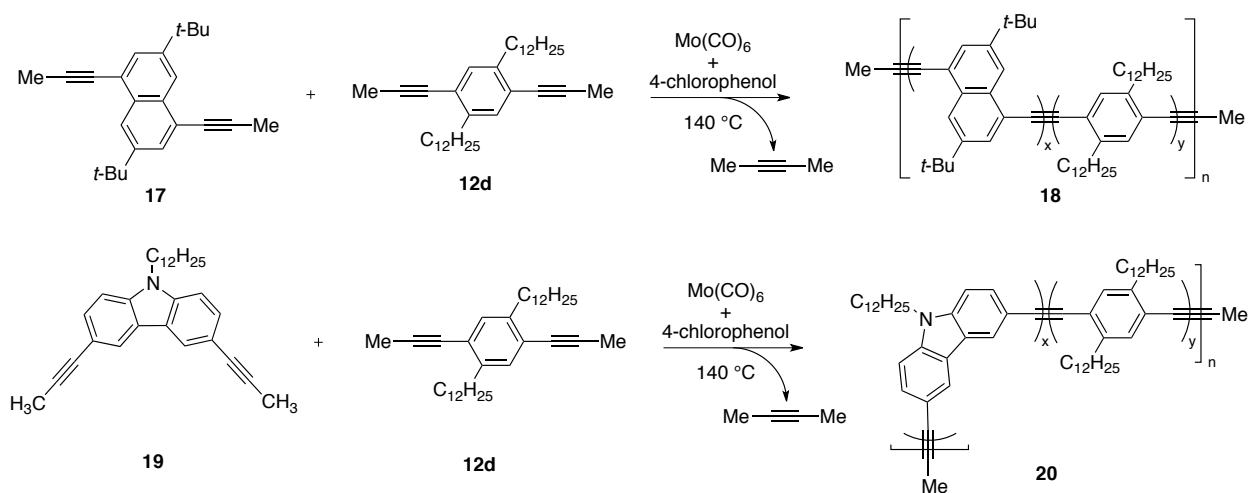
Scheme 1.16. Copolymers generated with the Mortreux catalyst system.

27
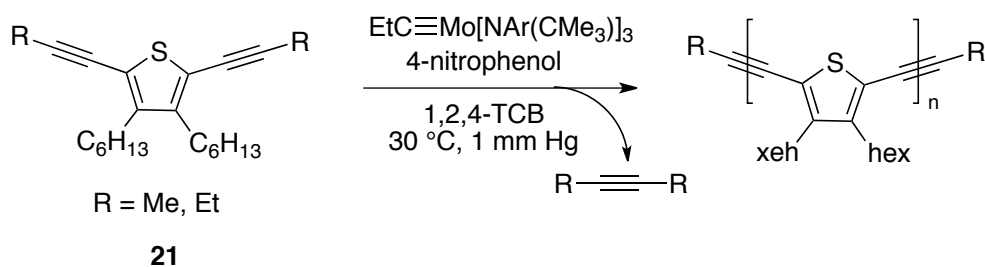
Scheme 1.17. Preparation of poly(thienylene ethynylene)s with a well-defined Mo catalyst.
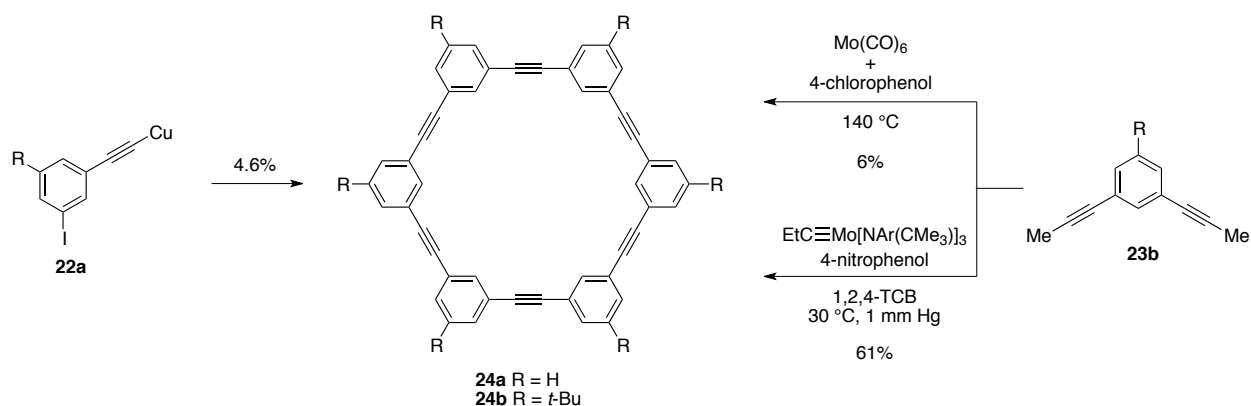
Scheme 1.18. Comparison of kinetic (Stephens-Castro, left) vs. thermodynamic control (ADIMAC, right) in the formation of [6]cycle **16**.
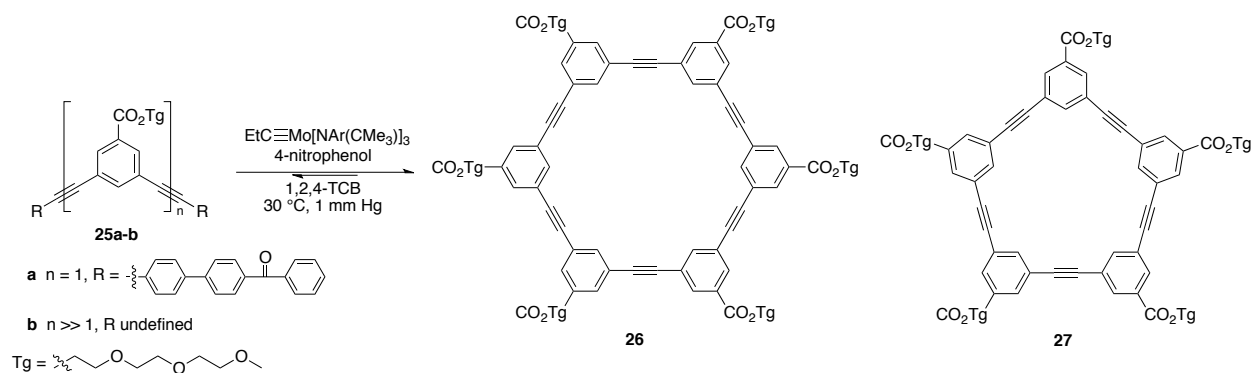
Scheme 1.19. Dynamic formation of [5-6]cycles *via* ADIMAC.
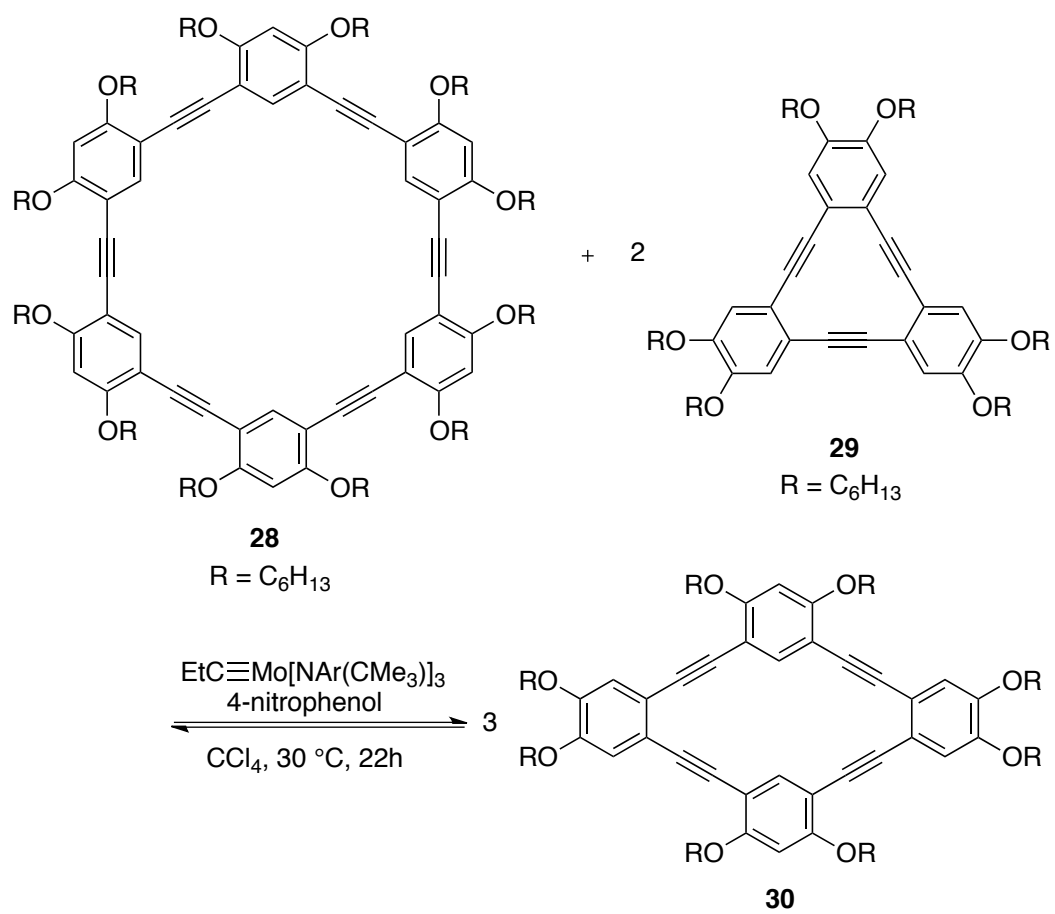
Scheme 1.20. Macrocycle equilibrium between macrocycles under dynamic metathesis conditions.
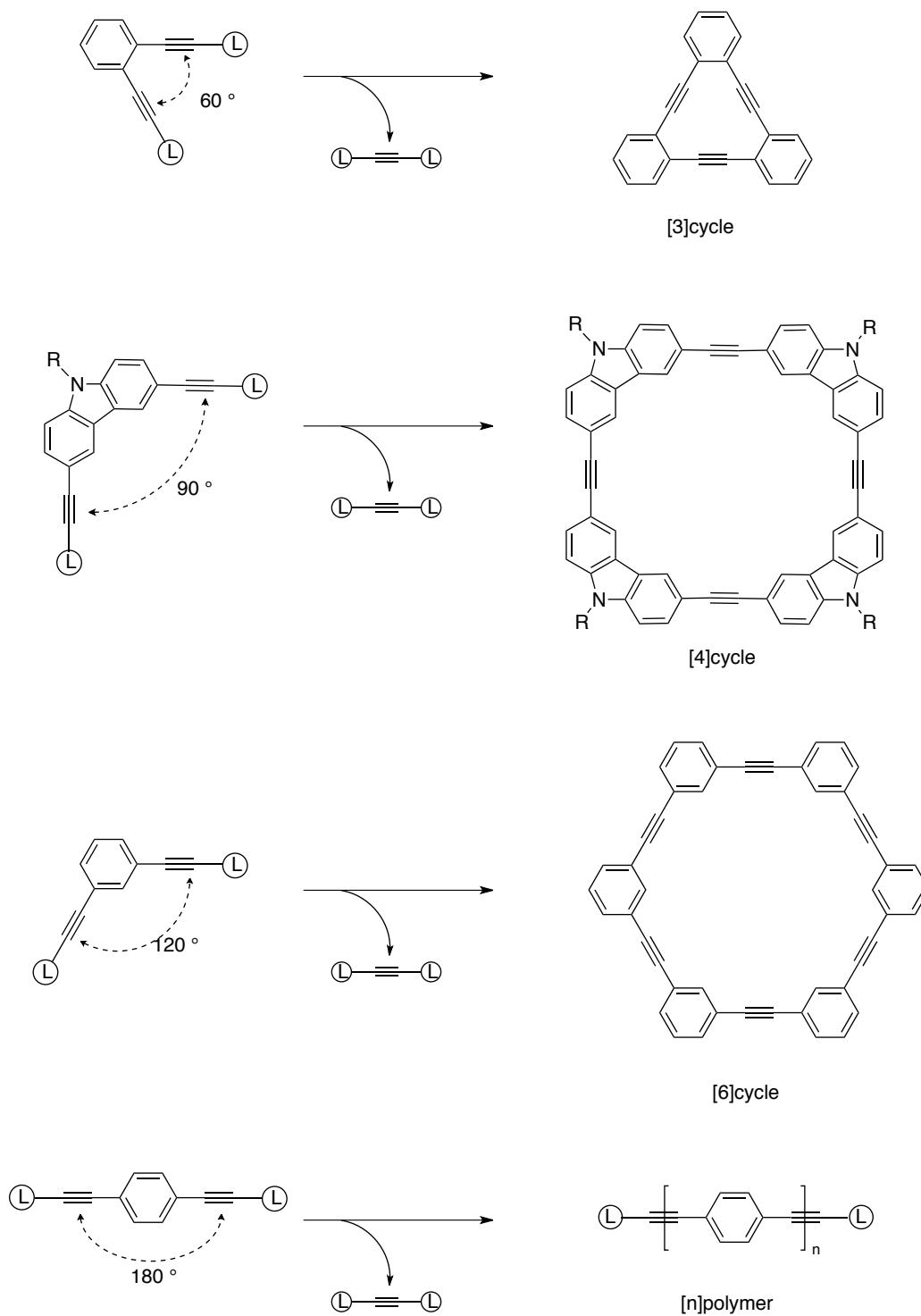
Scheme 1.21. General schematic of the angle-dependence on the dynamic formation of

AEMs under ADIMET.

31a: R$_1$ = R$_2$ = H (54%)
31b: R$_1$ = H, R$_2$ = Me (27%)
31c: R$_1$ = H, R$_2$ = OMe (28%)
31d: R$_1$ = H, R$_2$ = Br (12%)
31e: R$_1$ = R$_2$ = Me (0%)
31f: R$_1$ = Br, R$_2$ = H (0%)
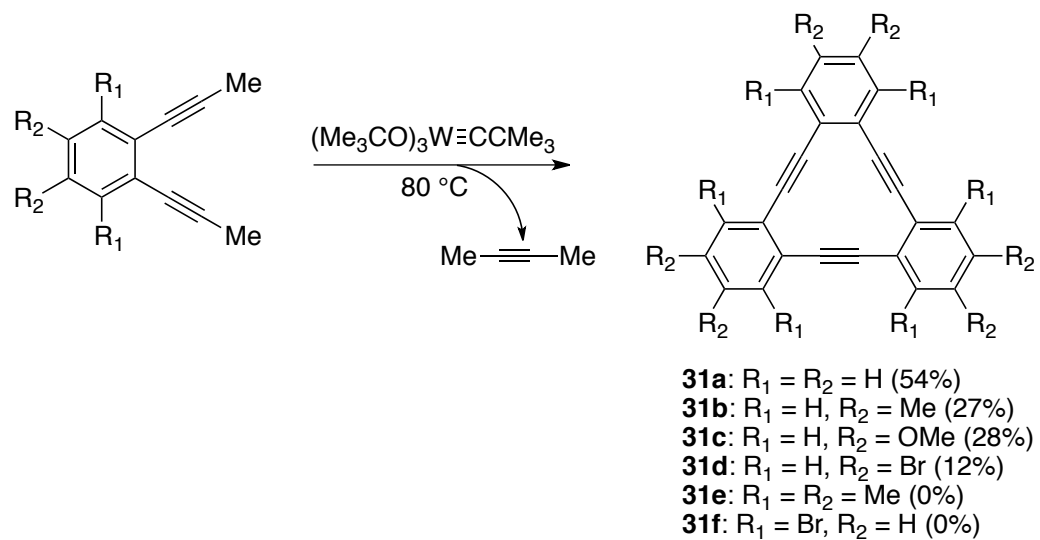
Scheme 1.22. [3]cycles from *o*-phenylene ethynylenes *via* alkyne metathesis.

32   **33** (14%)   **34** (18%)
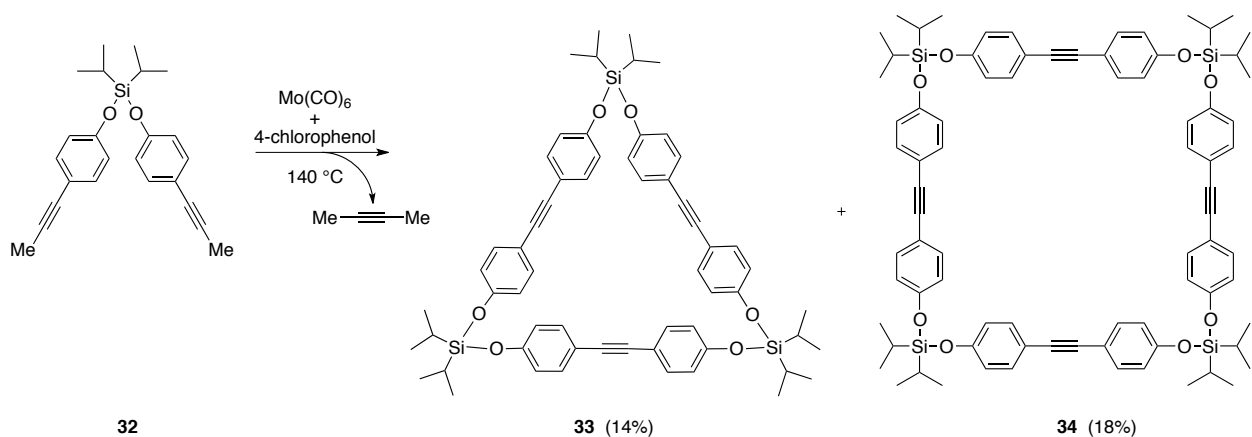
Scheme 1.23. Preparation of [3-4] cycles with the Mortreux system featuring a disiloxane hinge.

Reaction scheme (top): Starting material with R groups (R = C₁₀H₂₁) reacting under conditions:

EtC≡Mo[NAr(CMe₃)]₃
silanol-POSS

1,2,4-TCB
75 °C, 1 mm Hg

Me—≡—Me

to give **35** (77%)

R = C$_{10}$H$_{21}$

35 (77%)

Reaction scheme (bottom): Starting material with R₁ and R₂ groups reacting under conditions:

EtC≡Mo[NAr(CMe₃)]₃
silanol-POSS

1,2,4-TCB
75 °C, 1 mm Hg

Me—≡—Me

to give **36** (31%)

R$_1$ = C$_{14}$H$_{29}$
R$_2$ = C$_{10}$H$_{21}$

36 (31%)
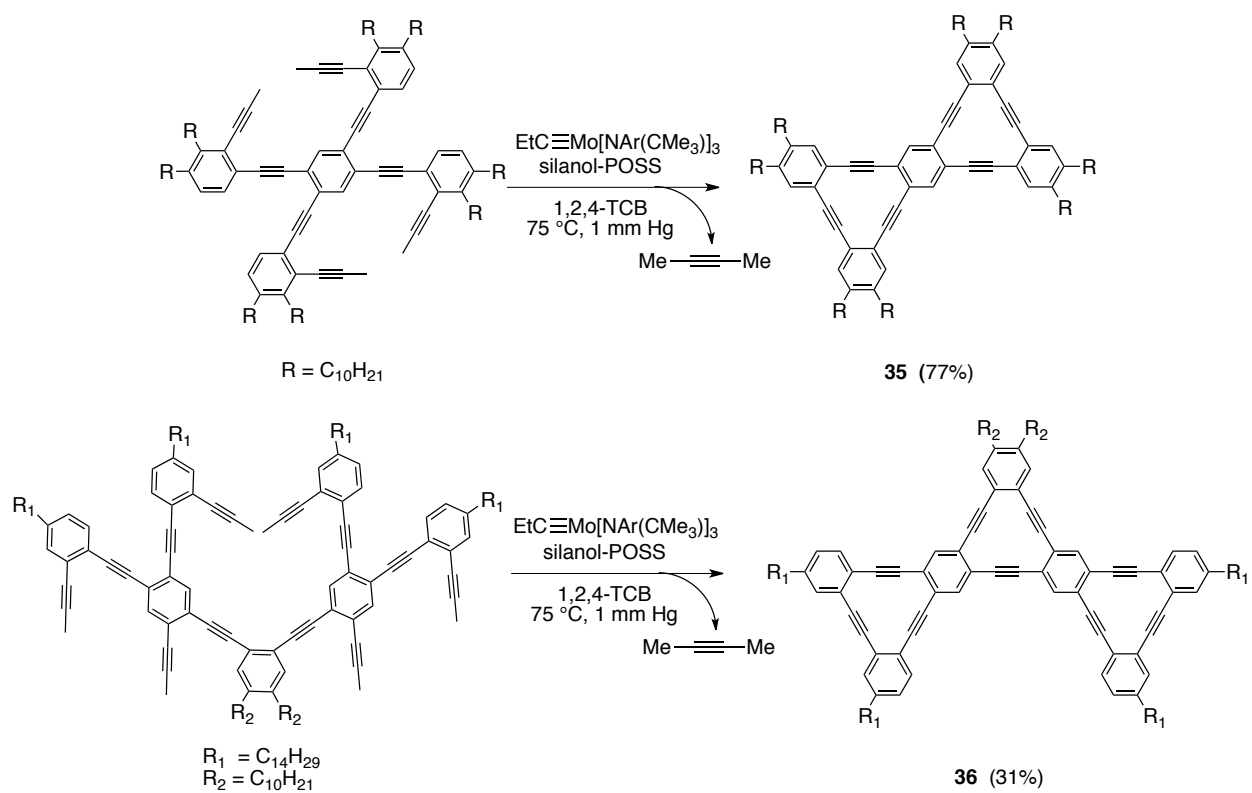
Scheme 1.24. Preparation of benzcyclynes based on *o*-phenylene ethynylenes.

Table 1.1. Summary of Catalyst Systems Utilized in Alkyne Metathesis Polymerization.

Entry	Catalyst system	Advantages	Challenges
1	$(Me_3CO)_3W≡CCMe_3$	• Commercially available • Good for dialkyl-PPEs	• Air- and moisture-sensitive • Low functional group tolerance
2	$Mo(CO)_6$ + 4-chlorophenol	• Inexpensive • Capable of forming very high MW polymers • Tolerant of alkenes, oxygen	• High temperatures required • Intolerant of Lewis basic atoms, sulfur
3	$EtC≡Mo(NArCMe_3)_3$ + 4-nitrophenol	• Extremely active catalyst • Highest functional group compatibility • Can undergo cyclooligomerization	• Not commercially available • Sensitive to air, moisture, N_2 • Limited shelf life

Table 1.2. **Effect of Catalyst on Polymerization of 11**.

Entry	Catalyst	Pressure (mm Hg)	Temp (°C)	Time (h)	Yield (%)	P_n (GPC)	M_w/M_n (GPC)
1	$(Me_3CO)_3W≡CCMe_3$ (2 mol%)	9.0	90	72	68	148	2.1
2	$Mo(CO)_6$ (5 mol %) 4-chlorophenol (100 mol %)	760 (N_2 stream)	150	overnight	>99	146	5.0
3	$Mo(C≡CEt)[N(Ar)(CMe_3)]$ (4 mol %) 4-nitrophenol (12 mol %)	1.0	30	22	93	52	2.1

1.6   References

[1]   Tour, J. M. *Chem. Rev.* **1996**, *96*, 537–554.
[2]   Martin, R. E.; Diederich, F. *Angew. Chem. Int. Ed.* **1999**, *38*, 1350-1377.
[3]   Lo, S. C.; Burn, P. L. *Chem. Rev.* **2007**, *107*, 1097-1116.
[4]   Zhang, W.; Moore, J. S. *Angew. Chem., Int. Ed.* **2006**, *45*, 4416-4439.
[5]   Marder, S. R.; Torruellas, W. E.; Blanchard-Desce, M.; Ricci, V.; Stegeman, G. I.; Gilmour, S.; Brédas, J.-L.; Li, J.; Bublitz, G. U.; Boxer, S. G. *Science* **1997**, *276*, 1233-1236.

[6]   Effenberger, F.; Schlosser, H. *Synthesis* **1990**, 1085-1094.

[7]   Effenberger, F.; Wolf, H. C. *New J. Chem.* **1991**, *15*, 117-123.

[8]   Duhamel, L.; Duhamel, P.; Plé, G.; Ramondenc, Y. *Tetrahedron Lett.* **1993**, *34*, 7399-7400.

[9]   Puccetti, G.; Blanchard-Desce, M.; Ledoux, I.; Lehn, J.-M.; Zyss, J. *J. Phys. Chem.* **1993**, *97*, 9385–9391.

[10]   Kiehl, A.; Eberhardt, A.; Adam, M.; Enkelmann, V.; Müllen, K. *Angew. Chem., Int. Ed. Engl.* **1992**, *31*, 1588-1591.

[11]   Stille, J. K.; Simpson, J. H. *J. Am. Chem. Soc.* **1987**, *109*, 2138-2152.

[12]   Knoll, K.; Schrock, R. R. *J. Am. Chem. Soc.* **1989**, *111*, 7989-8004.

[13]   Gorman, C. B.; Ginsburg, E. J.; Marder, S. R.; Grubbs, R. H. *Angew. Chem., Int. Ed.* **1989**, *28*, 1571-1574.

[14]   Norris, B. N.; Pan, T.; Meyer, T. Y. *Org. Lett.* **2010**, *12*, 5514–5517.

[15]   Lehmann, M.; Schartel, B.; Hennecke, M.; Meier, H. *Tetrahedron* **1999**, *55*, 13377-13394.

[16]   Pillow, J. N. G.; Halim, M.; Lupton, J. M.; Burn, P. L.; Samuel, I. D. W. *Macromolecules* **1999**, *32*, 5985-5993.

[17]   Kovacic, P.; Lange, R. M. *J. Org. Chem.* **1964**, *29*, 2416–2420.

[18]   Unroe, M. R.; Reinhardt, B. A. *Synthesis* **1987**, 981-986.

[19]   Liess, P.; Hensel, V.; Schlüter, A.-D. *Liebigs Ann.* **1996**, 1037-1040.

[20]   Wang, C.; Glorius, F. *Angew. Chem., Int. Ed.* **2009**, *48*, 5240-5244.

[21]   Gillis, E. P.; Burke, M. D. *J. Am. Chem. Soc.* **2007**, *129*, 6716-7.

[22]   Noguchi, H.; Hojo, K.; Suginome, M. *J. Am. Chem. Soc.* **2007**, *129*, 758-759.

[23]   Wren, E. J.; Wang, X.; Farlow, A.; Lo, S.; Burn, P. L.; Meredith, P. *Org. Lett.* **2010**, *12*, 4338-4340.

[24]   Nakao, Y.; Chen, J.; Tanaka, M.; Hiyama, T. *J. Am. Chem. Soc.* **2007**, *129*, 11694–11695.

[25]   Staab, H. A.; Binnig, F. *Chem. Ber.* **1967**, *100*, 293-305.

[26]   Fujioka, Y. *Bull. Chem. Soc. Jpn.* **1984**, *57*, 3494-3506.

[27]   Percec, V.; Okita, S. *J. Polym. Sci., Part A: Polym. Chem.* **1993**, *31*, 877-884.

[28]   Trueblood, K. N.; Knobler, C. B.; Maverick, E.; Helgeson, R. C.; Brown, S. B.; Cram, D. J. *J. Am. Chem. Soc.* **1981**, *103*, 5594-5596.

[29]   Cram, D. J.; Kaneda, T.; Helgeson, R. C.; Brown, S. B.; Knobler, C. B.; Maverick, E.; Trueblood, K. N. *J. Am. Chem. Soc.* **1985**, *107*, 3645-3657.

[30]   Cram, D. J.; Lein, G. M. *J. Am. Chem. Soc.* **1985**, *107*, 3657-3668.

[31]   Cram, D. J.; Carmack, R. A.; Helgeson, R. C. *J. Am. Chem. Soc.* **1988**, *110*, 571-577.

[32]   Hensel, V.; Lützow, K.; Jacob, J.; Gessler, K.; Saenger, W.; Schlüter, A.-D. *Angew. Chem., Int. Ed. Engl.* **1997**, *36*, 2654-2655.

[33]   Hensel, V.; Schluter, A. D. *Chem.-Eur. J.* **1999**, *5*, 421-429.

[34]   Chan, J. M. W.; Swager, T. M. *Tetrahedron Lett.* **2008**, *49*, 4912-4914.

[35]   Rahman, M. J.; Yamakawa, J.; Matsumoto, A.; Enozawa, H.; Nishinaga, T.; Kamada, K.; Iyoda, M. *J. Org. Chem.* **2008**, *73*, 5542–5548.

[36] Pisula, W.; Kastler, M.; Yang, C.; Enkelmann, V.; Mullen, K. *Chem.-Asian J.* **2007**, *2*, 51-56.

[37] Jasti, R.; Bhattacharjee, J.; Neaton, J. B.; Bertozzi, C. R. *J. Am. Chem. Soc.* **2008**, *130*, 17646-17647.

[38] Takaba, H.; Omachi, H.; Yamamoto, Y.; Bouffard, J.; Itami, K. *Angew. Chem., Int. Ed.* **2009**, *48*, 6112-6116.

[39] Yamago, S.; Watanabe, Y.; Iwamoto, T. *Angew. Chem., Int. Ed.* **2010**, *49*, 757-759.

[40] Miller, T. M.; Neenan, T. X. *Chem. Mater.* **1990**, *2*, 346-349.

[41] Miller, T. M.; Neenan, T. X.; Zayas, R.; Bair, H. E. *J. Am. Chem. Soc.* **1992**, *114*, 1018-1025.

[42] Lo, S.; Namdas, E.; Burn, P.; Samuel, I. *Macromolecules* **2003**, *36*, 9721-9730.

[43] Capitosti, G. J.; Guerrero, C. D.; Binkley, D. E.; Rajesh, C. S.; Modarelli, D. A. *J. Org. Chem.* **2003**, *68*, 247-261.

[44] Wiesler, U. M.; Weil, T.; Mullen, K. *Dendrimers III: Design, Dimension, Function* **2001**, *212*, 1-40.

[45] Ogliaruso, M. A.; Shadoff, L. A.; Becker, E. I. *J. Org. Chem.* **1963**, *28*, 2725-2728.

[46] Fieser, L. F. *Org. Synth.* **1966**, *46*, 44.

[47] Stille, J. K.; Rakutis, R. O.; Mukamal, H.; Harris, F. W. *Macromolecules* **1968**, *1*, 431-436.

[48] Andreitchenko, E. V.; Clark, C. G.; Bauer, R. E.; Lieser, G.; Müllen, K. *Angew. Chem., Int. Ed.* **2005**, *44*, 6348-54.

[49] Morgenroth, F.; Reuther, E.; Mullen, K. *Angew. Chem., Int. Ed. Engl.* **1997**, *36*, 631-634.

[50] Shifrina, Z. B.; Averina, M. S.; Rusanov, A. L.; Wagner, M.; Mullen, K. *Macromolecules* **2000**, *33*, 3525-3529.

[51] Liu, D. J.; De Feyter, S.; Cotlet, M.; Stefan, A.; Wiesler, U. M.; Herrmann, A.; Grebel-Koehler, D.; Qu, J. Q.; Mullen, K.; De Schryver, F. C. *Macromolecules* **2003**, *36*, 5918-5925.

[52] De Schryver, F. C.; Vosch, T.; Cotlet, M.; Van der Auweraer, M.; Mullen, K.; Hofkens, J. *Acc. Chem. Res.* **2005**, *38*, 514-522.

[53] Bernhardt, S.; Baumgarten, M.; Mullen, K. *Eur. J. Org. Chem.* **2006**.

[54] Bernhardt, S.; Kastler, M.; Enkelmann, V.; Baumgarten, M.; Müllen, K. *Chemistry (Weinheim an der Bergstrasse, Germany)* **2006**, *12*, 6117-28.

[55] Yin, M.; Shen, J.; Pflugfelder, G. O.; Mullen, K. *J. Am. Chem. Soc* **2008**, *130*, 7806-+.

[56] Wiesler, U. M.; Müllen, K. *Chem. Commun.* **1999**, 2293-2294.

[57] Bunz, U. H. F. *Chem. Rev.* **2000**, *100*, 1605-1644.

[58] Moore, J. S. *Acc. Chem. Res.* **1997**, *30*, 402-413.

[59] Moore, J. S.; Xu, Z. F. *Macromolecules* **1991**, *24*, 5893-5894.

[60] Zhang, J. S.; Moore, J. S.; Xu, Z. F.; Aguirre, R. A. *J. Am. Chem. Soc.* **1992**, *114*, 2273-2274.

[61] Xu, Z. F.; Moore, J. S. *Angew. Chem., Int. Ed. in English* **1993**, *32*, 246-248.

[62] Xu, Z. F.; Moore, J. S. *Angew. Chem., Int. Ed. in English* **1993**, *32*, 1354-1357.

[63] Xu, Z. F.; Kahr, M.; Walker, K. L.; Wilkins, C. L.; Moore, J. S. *J. Am. Chem. Soc.* **1994**, *116*, 4537-4550.

[64] Kawaguchi, T.; Walker, K. L.; Wilkins, C. L.; Moore, J. S. *J. Am. Chem. Soc.* **1995**, *117*, 2159-2165.

[65] Moore, J. S.; Weinstein, E. J.; Wu, Z. Y. *Tetrahedron Lett.* **1991**, *32*, 2465-2466.

[66] Elliott, E. L.; Ray, C. R.; Kraft, S.; Atkins, J. R.; Moore, J. S. *J. Org. Chem.* **2006**, *71*, 5282-5290.

[67] Katz, T. J.; McGinnis, J. *J. Am. Chem. Soc.* **1975**, *97*, 1592-1594.

[68] Wengrovius, J. H.; Sancho, J.; Schrock, R. R. *J. Am. Chem. Soc.* **1981**, *103*, 3932-3935.

[69] Sancho, J.; Schrock, R. R. *J. Mol. Catal.* **1982**, *15*, 75-79.

[70] Zhang, W.; Kraft, S.; Moore, J. S. *J. Am. Chem. Soc.* **2004**, *126*, 329-335.

[71] McCullough, L. G.; Listemann, M. L.; Schrock, R. R.; Churchill, M. R.; Ziller, J. W. *J. Am. Chem. Soc.* **1983**, *105*, 6729-6730.

[72] Coutelier, O.; Mortreux, A. *Adv. Synth. Catal.* **2006**, *348*, 2038-2042.

[73] Coutelier, O.; Nowogrocki, G.; Paul, J.-F.; Mortreux, A. *Adv. Synth. Catal.* **2007**, *349*, 2259- 2263.

[74] Carnes, M.; Buccella, D.; Siegrist, T.; Steigerwald, M. L.; Nuckolls, C. *J. Am. Chem. Soc.* **2008**, *130*, 14078-14079.

[75] Krouse, S. A.; Schrock, R. R.; Cohen, R. E. *Macromolecules* **1989**, *22*, 2569-2576.

[76] Zhang, X.-P.; Bazan, G. C. *Macromolecules* **1994**, *27*, 4627-4628.

[77] Weiss, K.; Michel, A.; Auth, E.-M.; Bunz, U. H. F.; Mangel, T.; Müllen, K. *Angew. Chem. Int. Ed.* **1997**, *36*, 506-509.

[78] Schrock, R. R.; Czekelius, C. *Adv. Synth. Catal.* **2007**, *349*, 55-77.

[79] Zhang, W.; Moore, J. S. *Adv. Synth. Catal.* **2007**, *349*, 93-120.

[80] Bunz, U. H. F. *Acc. Chem. Res.* **2001**, *34*, 998-1010.

[81] Fürstner, A.; Davies, P. W. *Chem. Commun.* **2005**, 2307-2320.

[82] Chabanas, M.; Baudouin, A.; Copéret, C.; Basset, J.-M. *J. Am. Chem. Soc.* **2001**, *123*, 2062-2063.

[83] Beer, S.; Hrib, C. G.; Jones, P. G.; Brandhorst, K.; Grunenberg, J.; Tamm, M. *Angew. Chem., Int. Ed.* **2007**, *46*, 8890-8894.

[84] Beer, S.; Brandhorst, K.; Grunenberg, J.; Hrib, C. G.; Jones, P. G.; Tamm, M. *Org. Lett.* **2008**, *10*, 981-984.

[85] Beer, S.; Brandhorst, K.; Hrib, C. G.; Wu, X.; Haberlag, B.; Grunenberg, J.; Jones, P. G.; Tamm, M. *Organometallics* **2009**, *28*, 1534-1545.

[86] Mortreux, A.; Blanchard, M. *J. Chem. Soc., Chem. Commun.* **1974**, 786-787.

[87] Mortreux, A.; Delgrange, J. C.; Blanchard, M.; Lubochinsky, B. *J. Mol. Catal.* **1977**, *2*, 73-82.

[88] Mortreux, A.; Petit, F.; Blanchard, M. *J. Mol. Catal.* **1980**, *8*, 97-106.

[89] Benchelck, A.; Petit, M.; Mortreux, A.; Petit, F. *J. Mol. Catal.* **1982**, *15*, 93-101.

[90] Kaneta, N.; Hikichi, K.; Uemura, M.; Mori, M. *Chem. Lett.* **1995**, 1055-1056.

[91] Fürstner, A.; Mathes, C.; Lehmann, C. W. *J. Am. Chem. Soc.* **1999**, *121*, 9453-9454.

[92] Zhang, W.; Kraft, S.; Moore, J. S. *Chem. Commun.* **2003**, 832-833.

[93] Zhang, W.; Lu, Y.; Moore, J. S. *Org. Synth.* **2007**, *84*, 173-176.

[94] Cummins, C. C. *Chem. Commun.* **1998**, 1777-1786.

[95] Laplaza, C. E.; Cummins, C. C. *Science* **1995**, *268*, 861-863.

[96] Laplaza, C. E.; Johnson, M. J. A.; Peters, J. C.; Odom, A. L.; Kim, E.; Cummins, C. C.; George, G. N.; Pickering, I. J. *J. Am. Chem. Soc.* **1996**, *118*, 8623–8638.

[97] Cho, H. M.; Weissman, H.; Wilson, S. R.; Moore, J. S. *J. Am. Chem. Soc.* **2006**, *128*, 14742-14743.

[98] Weissman, H.; Plunkett, K. N.; Moore, J. S. *Angew. Chem. Int. Ed.* **2006**, *45*, 585-588.

[99] Cho, H. M.; Weissman, H.; Moore, J. S. *J. Org. Chem.* **2008**, *73,* 4526-4528.

[100] Bunz, U. H. F. *Adv. Polym. Sci.* **2005**, *177*, 1-52.

[101] Liu, J.; Lam, J. W. Y.; Tang, B. Z. *Chem. Rev.* **2009**, *109*, 5799-5867.

[102] McQuade, D. T.; Pullen, A. E.; Swager, T. M. *Chem. Rev.* **2000**, *100*, 2537-2574.

[103] Thomas, S. W.; Joly, G. D.; Swager, T. M. *Chem. Rev.* **2007**, *107*, 1339-1386.

[104] Negishi, E.; Anastasia, L. *Chem. Rev.* **2003**, *103*, 1979-2017.

[105] Nguyen, P.; Yuan, Z.; Agocs, L.; Lesley, G.; Marder, T. B. *Inorg. Chim. Acta* **1994**, *220*, 289-296.

[106] Goodson, F. E.; Wallow, T. I.; Novak, B. M. *J. Am. Chem. Soc.* **1997**, *119*, 12441–12453.

[107] Kloppenburg, L.; Song, D.; Bunz, U. H. F. *J. Am. Chem. Soc.* **1998**, *120*, 7973-7974.

[108] Kloppenburg, L.; Jones, D.; Bunz, U. H. F. *Macromolecules* **1999**, *32*, 4194–4203.

[109] Zhang, W.; Moore, J. S. *Macromolecules* **2004**, *37*, 3973-3975.

[110] Bly, R. K.; Dyke, K. M.; Bunz, U. H. F. *J. Organomet. Chem.* **2005**, *690*, 825-829.

[111] Pschirer, N. G.; Bunz, U. H. F. *Macromolecules* **2000**, *33*, 3961-3963.

[112] Brizius, G.; Pschirer, N. G.; Steffen, W.; Stitzer, K.; zur Loye, H.-C.; Bunz, U. H. F. *J. Am. Chem. Soc.* **2000**, *122*, 12435-12440.

[113] Steffen, W.; Bunz, U. H. F. *Macromolecules* **2000**, *33*, 9518–9521.

[114] Steffen, W.; Köhler, B.; Altmann, M.; Scherf, U.; Stitzer, K.; zur Loye, H.-C.; Bunz, U. H. F. *Chem. Eur. J.* **2001**, *7*, 117-126.

[115] Sashuk, V.; Ignatowska, J.; Grela, K. *J. Org. Chem.* **2004**, *69*, 7748–7751.

[116] Brizius, G.; Bunz, U. H. F. *Org. Lett.* **2002**, *4*, 2829-2831.

[117] Pschirer, N. G.; Miteva, T.; Evans, U.; Roberts, R. S.; Marshall, A. R.; Neher, D.; Myrick, M. L.; Bunz, U. H. F. *Chem. Mater.* **2001**, *13*, 2691–2696.

[118] Pschirer, N. G.; Marshall, A. R.; Stanley, C.; Beckham, H. W.; Bunz, U. H. F. *Macromol. Rapid Commun.* **2000**, *21*, 493-495.

[119] Brizius, G.; Kroth, S.; Bunz, U. H. F. *Macromolecules* **2002**, *35,* 5317-5319.

[120] Zang, L.; Che, Y.; Moore, J. S. *Acc. Chem. Res.* **2008**, *41*, 1596-1608.

[121] Rowan, S. J.; Cantrill, S. J.; Cousins, G. R. L.; Sanders, J. K. M.; Stoddart, J. F. *Angew. Chem. Int. Ed.* **2002**, *41*, 898-952.

[122] Zhang, W.; Moore, J. S. *J. Am. Chem. Soc.* **2004**, *126*, 12796-12796.

[123] Zhang, W.; Brombosz, S. M.; Mendoza, J. L.; Moore, J. S. *J. Org. Chem.* **2005**, *70*, 10198-10201.

[124] Zhang, W.; Cho, H. M.; Moore, J. S. *Org. Synth.* **2007**, *84*, 177-191.

[125] Ge, P.-H.; Fu, W.; Herrmann, W. A.; Herdtweck, E.; Campana, C.; Adams, R. D.; Bunz, U. H. F. *Angew. Chem. Int. Ed.* **2000**, *39*, 3607-3610.

[126] Zhang, W.; Moore, J. S. *J. Am. Chem. Soc.* **2005**, *127*, 11863-11870.

[127] Naddo, T.; Che, Y.; Zhang, W.; Balakrishnan, K.; Yang, X.; Yen, M.; Zhao, J.; Moore, J. S.; Zang, L. *J. Am. Chem. Soc.* **2007**, *129*, 6978-6979.

[128] Naddo, T.; Yang, X.; Moore, J. S.; Zang, L. *Sens. Act. B: Chemical* **2008**, *134*, 287-291.

[129] Miljanic, O. S.; Vollhardt, K. P. C.; Whitener, G. D. *Synlett* **2003**, 29-34.

[130] Pschirer, N. G.; Fu, W.; Adams, R. D.; Bunz, U. H. F. *Chem. Commun.* **2000**, 87-88.

[131] Johnson, C. A.; Lu, Y.; Haley, M. M. *Org. Lett.* **2007**, *9*, 3725-3728.

Chapter 2

Polyphenylene Dendrons *via* Iridium-Catalyzed C–H Activation[†]

2.1   Introduction

Dendrimers containing 1,3,5-polyphenylene linkages (Fig. 2.1) constitute one of the simplest, yet lesser-utilized rigid dendritic architectures. Since their first reports nearly twenty years ago, dendrimers of this class have been used in several photophysical studies,[1] and perhaps most notably in the incorporation of highly efficient organic light-emitting diodes.[2] While the optoelectronic properties of these dendrimers are attractive, their preparation and synthetic manipulation are not ideal. Typically limited to convergent methods, the preparation of 1,3,5-polyphenylene dendrons has almost exclusively relied upon the elucidation of a "masked" boronic acid at the focal point prior to Suzuki-Miyaura coupling[3] with an aryl halide and mask-containing branching unit.[4]

The convergent approach to dendrimer synthesis requires that focal point reactivity be installed or unveiled prior to each generation-building step. The first synthetic method for the preparation of 1,3,5-polyphenylene dendrimers outlined by Miller and Neenan in 1990 was a convergent approach; polyphenylene dendrons with a boronic acid focal point were coupled to 1,3,5-tribromobenzene *via* a Suzuki-Miyaura coupling (Scheme 2.1). Critical to this approach is the use of a trimethylsilyl "mask" for the boronic acid focal point in the preparation of dendrons; displacement of the silyl group with BBr_3 followed by hydrolysis gives the boronic acid allowing for further

---

[†] Parts of this chapter were published: Finke, A. D.; Moore, J. S. *Org. Lett.* **2008**, *10*, 4851-4854.

displacement. It is worth noting that, in the 20 years since it was first introduced, while the materials and the procedures for unmasking focal point reactivity have changed, *the overall method has not.*[5]

Herein we describe a new method for the iterative assembly of 1,3,5-polyphenylene dendrons containing 3,5-di-*tert*-butyl-phenylene containing peripheral groups. The method requires no "masked" focal point; instead, direct and selective borylation of an aryl C-H bond via iridium-catalyzed C-H activation generates the reactive pinacolboronate ester at the focal point. The dendron can then undergo Suzuki-Miyaura coupling with an inexpensive, commercially available 1,3-dihalobenzene to build the higher generations. We show that the process can be iterated to build a third-generation polyphenylene dendron in good yield. Utilizing highly efficient Suzuki-Miyaura coupling conditions dramatically decreases reaction times and inhibits byproduct formation.

The borylation of aromatic compounds via iridium-catalyzed C-H bond activation has been extensively studied since initial reports by Smith,[6] Hartwig, Ishiyama and Miyaura.[7] This reaction is unique with respect to other aromatic substitution reactions because regioselectivity is predominantly controlled by sterics rather than electronics.[8] Under these reaction conditions, a 1,3-disubstituted arene preferentially borylates *meta* to both substituents and typically in excellent yields. This methodology has been extended to the borylation of substituted arenes and aromatic heterocycles,[9] but the borylation of larger aromatics has been limited to porphyrins[10] and simple polycyclic aromatics such as naphthalene, pyrene and perylene.[11] The implementation of this

transformation into iterative methods for the preparation of novel materials has been limited to date, and to our knowledge there are no examples of the Ir-catalyzed borylation of oligoarenes.

2.2 Preparation of 1,3,5-Polyphenylene Dendrons

The preparation of third-generation dendron **6** occurs in good yield from 1,3-di-*tert*-butylbenzene (Scheme 2.2). The borylation of 1,3-di-*tert*-butylbenzene with bis(pinacolato)diboron (B_2pin_2) as the borylating reagent to form boronate ester **1** occurs in good yield in cyclohexane at 80 °C. It was found that, for all boronate esters in this work, column chromatography on silica gel depreciated the yields considerably, likely due to decomposition of the product on silica gel. A short plug of silica gel was sufficient to remove the catalyst, excess B_2pin_2 and boron-containing byproducts, without apparent product decomposition. The crude product, which typically contained small amounts (< 5%) of starting material and B_2pin_2, was taken on without further purification, and with no detriment to subsequent transformations or purification.

In most previous preparations of 1,3,5-polyphenylene dendrons, Suzuki-Miyaura coupling was undertaken with the standard palladium catalyst $Pd(PPh_3)_4$. However, coupling of **1** with 1,3-diiodobenzene or 1,3-dibromobenzene to form **2** was very slow and tended to give significant amounts of byproducts, including homocoupled[12] and deboronated pinacolboronate esters. Effective methods of converting the relatively unreactive pinacolboronate esters to more reactive boronic acids and aryltrifluoroborate salts are available;[13] however, extra synthetic steps are undesirable. Instead, more efficient catalyst systems were screened. The phosphine ligand 2-

dicyclohexylphosphino-2',6'-dimethoxybiphenyl (S-phos) developed by Buchwald[14] is highly active toward Suzuki-Miyaura cross-couplings and is particularly effective in the coupling of sterically-hindered boronic acids and aryl halides. The syntheses of dendrons **2**, **4** and **6** from boronate esters **1**, **3**, and **5** using 5 mol% $Pd(OAc)_2$ and 10 mol% S-phos and aqueous NaOH in THF proceeded rapidly at 60 °C. All three are readily purified by flash chromatography on silica gel, eluting with hexane/dichloromethane mixtures. Analytical GPC of **2, 4** and **6** give narrow bands with PDI values below 1.03.

The ^{1}H NMR of **6** was taken in both $CDCl_3$ and benzene-d_6 (Figure 2.2). The aromatic proton chemical shifts have a high degree of solvent dependence, as better dispersion of the aromatic protons can be achieved with benzene as solvent, while in $CDCl_3$ there is significant overlap of many peaks. Most notably, the peripheral aromatic groups are fully resolved in benzene, but in $CDCl_3$, both resonances convolute to appear as a singlet. (It should be noted that the ^{13}C NMR spectra was taken in $CDCl_3$ due to significant overlap of the solvent peaks in C_6D_6.) While K_3PO_4 is most commonly used as a base with this ligand system, significant amounts of deboronated starting material was generated in the syntheses of **4** and **6** if aqueous K_3PO_4 or K_2CO_3 was used. Homocoupling of the pinacolboronate esters was detrimental to the purification of **4** and **6**, as homocoupled **3** and **5** were difficult to isolate from the desired product by most purification methods. It was found that switching the base to aqueous NaOH and using no more than 2 equiv of **3** or **5** attenuated homocoupling and deboronation, while

only marginally lowering the yield.[15] Furthermore, switching to the more reactive 1,3-diiodobenzene for the syntheses of **4** and **6** also decreased byproduct formation.

2.3   Optimization of Borylation of Dendrons

Initial attempts to borylate dendrons **2** and **4** were slow and did not proceed to complete conversion, even with extended heating and high catalyst loadings. Extensive GC studies on the borylation of **2** were performed (Table 2.1). Interestingly, it was found that using low catalyst loadings and sequential addition of a pre-made catalyst stock solution containing [Ir(COD)(OMe)]$_2$, 4,4'-di-*tert*-butyl-2,2'-bipyridine (dtbpy), and pinacolborane (HBpin) (Table 2.1, Entry 3) gave higher conversions than using higher initial catalyst loadings (Table 2.1, Entry 6).[16] Addition of excess B$_2$pin$_2$ after 4 h slightly enhanced conversion (Table 2.1, Entry 4).

Previous studies on the effects of steric inhibition of borylation by peripheral, non-*ortho* substituents are limited. Borylation of N-(triisopropylsilyl)pyrrole occurs at the 3 position, in contrast to unsubstituted pyrrole, which borylates at the 2 position.[17] Elegant studies by Hata demonstrated that a *m*-phenylene-linked Zn-tetraarylporphyrin dimer borylates quantitatively at the focal point, but a similar dimer with peralkylated porphyrins does not undergo borylation.[10] To investigate the role of sterics, dendron **7**, which is less sterically hindered than **2**, was prepared and subsequently borylated (Table 2.1, Entry 7). It was found that no additional catalyst was needed to get high conversions for the borylation of **7** unlike dendron **2**, indicating that steric hindrance from distal moieties plays an important role in the efficiency of borylation. Likewise, dendron **4** also required sequential addition of catalyst to achieve full conversion. At present, we

cannot understand why sequential addition of low catalyst loadings led to more effective borylation of sterically hindered arenes. However, these data suggest a complex mechanistic pathway for decomposition of the catalyst that is competitive with C-H activation; the details will be investigated further in subsequent studies.

2.4   **Physical Characterization of Dendrons**

The potential of these polyphenylene dendrons for use in optoelectronic materials led us to characterize the thermal and photophysical properties of **2**, **4**, and **6**. Like previously synthesized 1,3,5-polyphenylene dendrimers, all three exhibit high thermal stability (Figure 2.3). TGA studies run under N_2 show that **4** and **6** are stable up to nearly 500 °C (Figure 2.4). Interestingly, DSC studies run under N_2 showed no melting for **4** and **6** up to 400 °C. Dendron **6** displays two glass transitions at 230 °C and 330 °C. Not surprisingly, absorbance and emission spectra of the dendrons (Figure 2.5) show evidence for disrupted conjugation between phenyl rings. Absorbance spectra of the dendrons indicate a slight redshift in the λ_{max} from 250 nm for **2** to 255 nm for **4** to 257 nm for **6**. Fluorescence quantum yields measured for **4** (Φ = 0.16) and **6** (Φ = 0.15) in methylcyclohexane upon excitation at 250 nm show low fluorescence efficiencies. However, low fluorescence quantum yields do not preclude efficient energy transfer upon covalent attachment of an acceptor moiety.

Crystals suitable for X-ray analysis were grown from slow evaporation of solutions of **1** and **4**. Crystals of **1** were grown from evaporation of a solution in DCM (Fig. 2.6) **1** crystallizes in the orthorhombic space group Pnma (Figure 2.6). The pinacolboronate ester in **1** is disordered about a mirror plane that cuts through the

benzene ring. Crystals of **4** were grown from slow evaporation of a THF/ether mixture (Figure 2.7). The high degree of biaryl twist in **4** is indicative of low pi-overlap between benzene rings, confirmed by the relative lack of redshift in the absorbance spectra with increasing generation of dendron. From these data, we conclude that the cross-conjugated benzene rings in these dendrons are essentially behaving as individual chromophores.

2.5   Conclusion

In summary, we have developed a novel method for the preparation of 1,3,5-polyphenylene dendrons with 3,5-di-*tert*-butylphenyl peripheral groups. To our knowledge, this is the first example of an iterative synthetic method that utilizes the direct C-H activation of an arene. For larger generations of dendrons, sequential addition of the iridium catalyst is necessary for high turnovers, presumably due in part to steric hindrance caused by the peripheral *tert*-butyl groups. While it is efficient for this particular example with 3,5-di-*tert*-butyl peripheral groups, this method is generally limited to the construction of 1,3,5-polyphenylene dendrons with peripheral groups unreactive to borylation. Dendrons containing unsubstituted arenes, alkynes, alkenes, nitro groups, phenols and primary or secondary amines are thus unsuitable. Future work will demonstrate the versatility of this iterative approach, with the preparation of novel architectures that would otherwise be extremely difficult to synthesize.

2.6   Experimental Procedures

2.6.1. General Procedures

Materials. Unless otherwise stated, all starting materials and reagents were purchased from commercial sources and used without further purification. 1,3-di-*tert*-butylbenzene was purchased from ChemSampCo. Bis(pinacolato)diboron and 4-*tert*-butylphenylboronic acid were purchased from Frontier Scientific. di-*mu*-methoxobis(1,5-cyclooctadiene)diiridium(I) ([Ir(COD)(OMe)]$_2$) was purchased from Strem and stored in a dry box under argon. Pd(OAc)$_2$ was purchased from Strem. 1,3-dibromobenzene, 1,3-diiodobenzene, S-phos, and 4,4'-di-*tert*-butyl-2,2'-bipyridine (dtbpy) were purchased from Aldrich. THF was distilled from sodium benzophenone ketyl. Cyclohexane (ACS spectrophotometric grade, Aldrich) was degassed with three consecutive freeze-pump-thaw cycles and stored over 4Å molecular sieves under argon.

Reaction Setup. For reactions on a 2 mmol scale or lower, the reaction vessels used were 20 mL I-Chem vials fitted with PTFE/silicone septa, purchased from VWR. For larger-scale reactions, 40 mL I-Chem vials fitted with PTFE/silicone septa purchased from VWR, or heavy-walled round-bottom flasks with o-ring fitted Teflon screwcaps were used. All glassware was oven- or flame-dried before use. All reactions were prepared in an argon-filled dry box. Reactions were monitored by thin layer chromatography (Merck silica gel F254, 0.25 mm) and visualized under UV irradiation at 254 nm. Flash chromatography was performed using silica gel (Silicycle, 60 Å, 230-400 mesh).

Physical Characterization. Melting points were obtained either using an electrothermal melting temperature apparatus (Mel-Temp, Model 1001) or by DSC; melting points obtained by DSC are defined as the onset point of the melting endotherm. ^{1}H and ^{13}C NMR were taken on a Varian Unity 400, Varian Unity 500 or a Varian VXR 500 NMR. Spectra were referenced to residual solvent peaks. Chemical shifts are expressed in parts per million (δ). Splitting constants (J) are expressed in Hz. Splitting patterns are designated as s, singlet; d, doublet; t, triplet; dd, doublet of doublets; td, triplet of doublets; m, multiplet. In ^{13}C NMR, carbons bearing boron substituents were not observed due to quadrupolar relaxation. Low-resolution matrix-assisted laser desorption ionization (MALDI) mass spectra were obtained using a Voyager-DE STR spectrometer using 7,7,8,8-tetracyanoquinodimethane (TCNQ) as matrix.[1] Other mass spectrometric methods were performed by the Mass Spectrometry Center at the University of Illinois, Urbana-Champaign. Analytical gel permeation chromatography (GPC) was performed with a Waters 515 HPLC pump, a Viscotek TDA Model 300 triple detector array, a Thermo separations Trace Series AS100 autosampler, and series of three Viscotek Viscogel columns (7.8 x 300 mm, 2 GMHHRM17392 and 1 GMHHRH17360) in THF (spectrophotometric grade, inhibitor-free) at 30 °C. The GPC was calibrated with monodisperse polystyrene standards. Differential scanning calorimetry (DSC) was performed on a Mettler-Toledo DSC821^e and traces were run under an N_2 atmosphere at a temperature rate of 10 °C/min. Thermogravimetric analysis (TGA) was performed on a Mettler-Toledo TGA/SDTA851^e and traces were run under an N_2 atmosphere at a temperature rate of 10 °C/min. UV

experiments were performed using a Shimadzu UV-2401PC equipped with a temperature controlled cell holder. Quartz cells with a path length of 1 cm, and volumes of 1.0 mL were used. Fluorescence spectra were recorded on a Photon Technology International PTI QM-1 fluorometer. Fluorescence quantum yields were measured against a quinine sulfate standard in 0.1 N H_2SO_4 (Φ = 0.54). Elemental analysis was performed at the Microanalysis Laboratory at the University of Illinois using an Exeter, Inc. CE-440 elemental analyzer. Data are reported as percentages. Infrared (IR) spectra were acquired on a Nicolet Nexus 670 FT-IR spectrometer; values are reported as wavenumbers. Analytical gas chromatography (GC) was performed using a Hewlett-Packard 5890 Gas Chromatograph fitted with a flame ionization detector. GC samples were injected onto a Hewlett-Packard HP5 (30 m x 0.32 mm) capillary column. The injector temperature was 250 °C and the detector temperature was 280 °C with a H_2 carrier gas flow of 16 mL/min. The column temperature program was as follows: 120 °C to 320 °C at 50 °C/min, then hold for 6 min for a total run time of 10.00 min. Retention times (t_R) were obtained using Agilent Chemstation software.

2.6.2 Synthesis
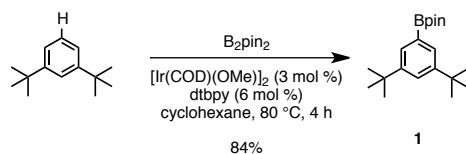
2-(3,5-di-*tert*-butylphenyl)-4,4,5,5-tetramethyl-1,3,2-dioxaborolane (1). The catalyst solution was prepared and transferred into the reaction flask in an Ar-filled dry box. A flame-dried vial was charged with, in order, [Ir(COD)(OMe)]₂ (0.188 g, 0.283 mmol, 0.01

equiv), cyclohexane (3 mL), HBpin (0.75 g, 5.86 mmol, 0.2 equiv) and dtbpy (0.152 g, 0.566 mmol, 0.02 equiv). The solution was agitated for 20 seconds to produce a dark red solution. An oven-dried heavy-walled round-bottom flask with o-ring fitted Teflon screwcap and stirbar was charged with 1,3-di-*tert*-butylbenzene (5.41 g, 28.4 mmol, 1 equiv), bis(pinacolato)diboron (7.22 g, 28.4 mmol, 1 equiv), and cyclohexane (40 mL). The catalyst solution was added to the flask, then the flask was sealed and heated to 80 °C for 4 h. The solution was passed through a pad of silica gel and eluted with CH_2Cl_2 (500 mL). The resulting brown solid was dissolved in CH_2Cl_2 (50 mL) passed again through silica gel and eluted with CH_2Cl_2 to give **1** as a white solid (7.54 g, 84% yield). mp (Mel-Temp)195-198 °C. ^{1}H NMR (500 MHz, CDCl$_3$) δ 7.66 (d, J = 2 Hz, 2H), 7.55 (t, J = 2 Hz, 1H), 1.34-1.35 (m, 30H). ^{13}C NMR (125 MHz; CDCl$_3$) δ 149.8, 128.8, 125.5, 83.5, 34.8, 31.5, 24.9. LRMS (EI+, 70 eV) *m/z* 316.3 (15), 301.2 (100), 217.2 (8), 201.2 (10), 57 (18). HRMS (EI+) Calc'd for $C_{20}H_{33}BO_2$: 316.2574, found: 316.2575. Anal. Calc'd for $C_{20}H_{33}BO_2$: C 75.95, H 10.52, B 3.42, found: C 75.65, H 10.92, B 3.45. IR (thin film) 3050, 2988, 2698, 1590, 1419, 1361, 1147, 964, 902, 847.
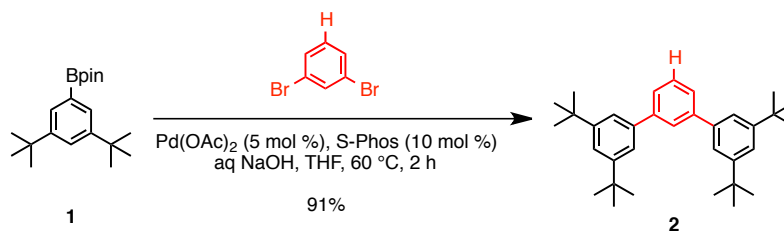
4-cascade:benzene[2-1,3]:(1,3,5-phenylene):isobutane (2).[18] In an Ar-filled dry box, a flame-dried vial with stirbar was charged with Pd(OAc)$_2$ (47 mg, 0.209 mmol, 0.05 equiv) and S-phos (174 mg, 0.423 mmol, 0.10 equiv) and THF (5 mL) and the solution

stirred under Ar for 30 minutes at room temperature. To a flame-dried 40 mL I-Chem

vial was added **1** (3.22 g, 10.2 mmol, 2.4 equiv). The vial was introduced into the dry

box and THF (20 mL), aq 5M NaOH (6.0 mL, 30.0 mmol, 7.1 equiv), the catalyst

solution prepared above, and 1,3-dibromobenzene (1.00 g, 4.24 mmol, 1.0 equiv) was

added. The vial was sealed and heated to 60 °C for 2 h. The solution was cooled and

partitioned between Et$_2$O (50 mL) and water (50 mL). The aqueous layer was extracted

with Et$_2$O (2 x 150 mL), the combined organic layers were washed with water and brine,

and dried over anhydrous MgSO$_4$. Column chromatography on silica gel eluting with

20:1 hexane:CH$_2$Cl$_2$ gave **2** as a white solid (1.76 g, 91% yield). mp (DSC) 198 °C. [1]H-

NMR (500 MHz; C$_6$D$_6$) δ 8.13 (m, 1H), 7.68-7.64 (m, 6H), 7.57 (m, 2H), 7.40 (t, J = 7.6

Hz, 1H), 1.31 (s, 36H). ^{13}C NMR (125 MHz; CDCl$_3$) δ 151.2, 143.0, 140.9, 128.8, 126.9,

126.3, 121.9, 121.5, 35.0, 31.5. LRMS (EI+, 70 eV) m/z 454.4 (100), 439.4 (70), 378.4

(16), 363.3 (16), 212.2 (20), 57.0 (64). HRMS (EI+) Calc'd for C$_{34}$H$_{46}$: 454.3600, found:

454.3597. Anal. Calc'd for C$_{34}$H$_{46}$: C 89.80, H 10.20, found: C 89.93, H 10.38. IR (thin

film) 3050, 2992, 2964, 2918, 2840, 1587, 1419, 1369, 1143, 1018, 890.
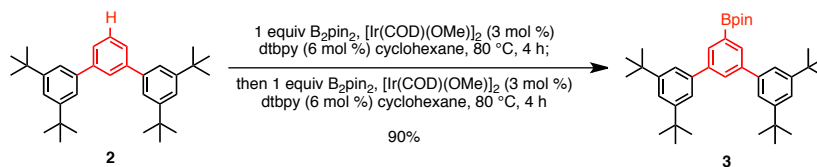
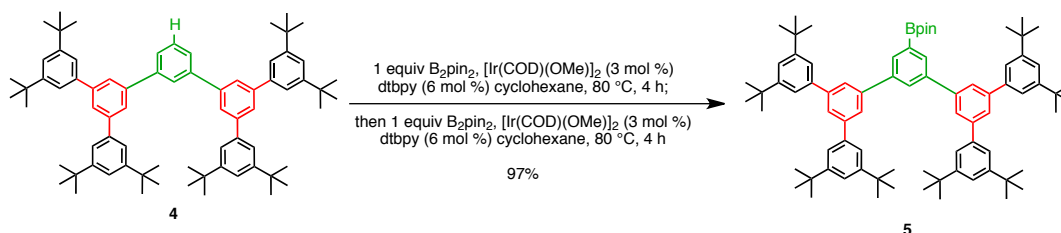**4-cascade:phenylboronic acid pinacol ester[2-3,5]:(1,3,5-phenylene):isobutane**

(3). In an Ar-filled dry box, a flame-dried vial with stirbar was charged with **2** (0.996 g,

2.19 mmol, 1 equiv), bis(pinacolato)diboron (0.417 g, 1.64 mmol, 0.75 equiv),

[Ir(COD)(OMe)]$_2$ (43 mg, 0.064 mmol, 0.03 equiv), dtbpy (35 mg, 0.13 mmol, 0.06

equiv), and cyclohexane (10 mL). The vial was sealed, taken out of the dry box, and heated to 80 °C for 4 h. The vial was cooled, reintroduced into the dry box, and bis(pinacolato)diboron (0.417 g, 1.64 mmol, 0.75 equiv), [Ir(COD)(OMe)]$_2$ (43 mg, 0.064 mmol, 0.03 equiv), dtbpy (35 mg, 0.13 mmol, 0.06 equiv) were added. The vial was sealed, taken out of the glove box, and heated overnight. The solution was passed through a thin pad of silica and eluted with hexane to remove residual starting material, then with CH$_2$Cl$_2$ to isolate **3** as a white solid (1.14 g, 90 % yield). This material was used without further purification. mp (DSC) 252 °C. ^{1}H-NMR (400 MHz; CDCl$_3$) δ 7.96 (d, J = 1.9 Hz, 2H), 7.85 (t, J = 1.9 Hz, 1H), 7.45-7.44 (m, 6H), 1.37 (m, 48H). ^{13}C NMR (126 MHz; CDCl$_3$) δ 151.2, 142.7, 141.1, 132.7, 130.3, 122.2, 121.6, 84.0, 77.4, 77.2, 76.9, 35.2, 25.0. LRMS (EI+, 70 eV) m/z 580.5 (100), 565.5 (24), 454.4 (24), 439.4 (18), 377.4 (20), 275.2 (18), 152.2 (12), 84.1 (35), 57.0 (55). HRMS (EI+) m/z Calc'd for C$_{40}$H$_{57}$O$_2$B: 580.4452, found: 580.4453. Anal. Calc'd for C$_{40}$H$_{57}$O$_2$B: C 82.73, H 9.89, B 1.86, found: C 82.53, H 10.21, B 1.56. IR (thin film) 3046, 2984, 2956, 1602, 1474, 1419, 1376, 1306.
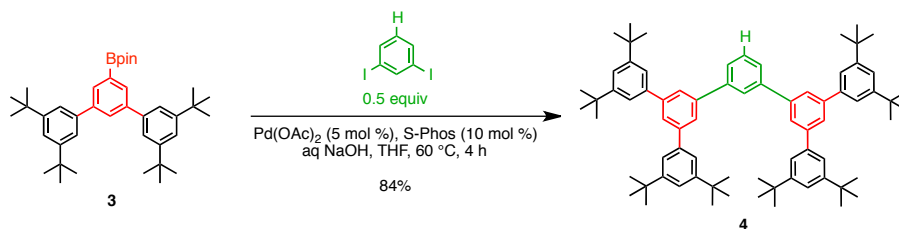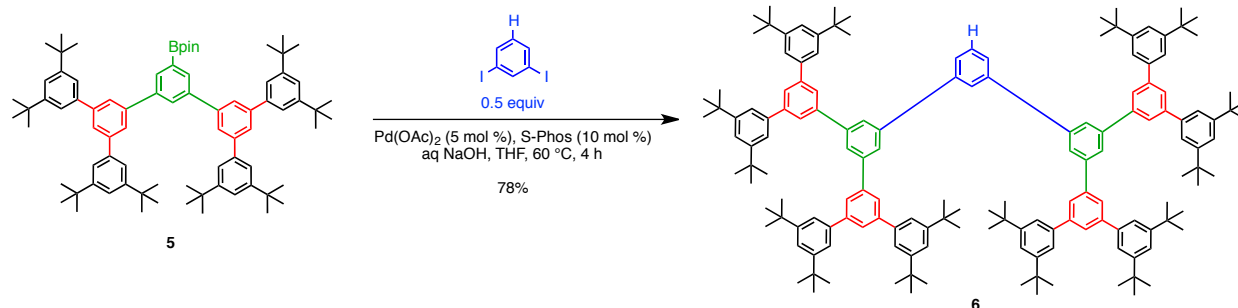

8-cascade:benzene[2-1,3]:(1,3,5-phenylene)^2:isobutane (4). In an Ar-filled dry box, a flame-dried vial was charged with Pd(OAc)$_2$ (5.1 mg, 0.023 mmol, 0.05 equiv), S-phos (19 mg, 0.046 mmol, 0.10 equiv) and THF (1 mL). The solution was stirred for 30 min at

rt. Another flame-dried vial with stirbar was charged with **3** (0.53 g, 0.916 mmol, 2.0 equiv), 1,3-diiodobenzene (0.15 g, 0.458 mmol, 1.0 equiv), aq 5M NaOH (0.6 mL, 3 mmol, 6 equiv) and THF (4 mL). The catalyst solution prepared above was added. The vial was sealed and heated to 40 °C for 6 h. The solution was cooled to room temperature, partitioned between Et$_2$O (50 mL) and water (50 mL), and the aqueous later extracted with Et$_2$O (2 x 50 mL). The organic layers were combined and washed with water and brine, and dried over anhydrous MgSO$_4$. Column chromatography on silica gel using the solvent gradient 20:1 hexane:CH$_2$Cl$_2$ → 15:1 hexane:CH$_2$Cl$_2$ gave **4** as a white crystalline solid (378 mg, 84 %). mp (DSC) > 400 °C (dec. 453 °C). ^{1}H-NMR (500 MHz; C$_6$D$_6$) δ 8.18 (t, J = 1.6 Hz, 1H), 8.12 (t, J = 1.5 Hz, 2H), 8.04 (d, J = 1.6 Hz, 4H), 7.71 (d, J = 1.8 Hz, 8H), 7.60-7.58 (m, 6H), 7.28 (t, J = 7.7 Hz, 1H), 1.30 (s, 72H). ^{13}C NMR (126 MHz; CDCl$_3$) δ 151.4, 144.0, 142.4, 142.2, 141.0, 129.6, 127.0, 126.8, 126.5, 125.7, 122.2, 121.8, 35.2. MALDI-TOF MS (TCNQ) m/z Calc'd for C$_{74}$H$_{94}$: 982.73, found: 981.22. HR-ESI [M + H]$^+$ Calc'd for C$_{74}$H$_{95}$: 983.7434, found: 983.7418. Anal. Calc'd for C$_{74}$H$_{94}$: C 90.37, H 9.63, found: C 90.56, H 9.88. IR (thin film) 3050, 2984, 1575, 1423, 894.


8-cascade:phenylboronic acid pinacol ester[2-3,5]:(1,3,5-phenylene)^2:isobutane (5). In an Ar-filled dry box, a flame-dried vial with stirbar was charged with **4** (0.301 g,

0.306 mmol, 1.0 equiv), bis(pinacolato)diboron (58 mg, 0.230 mmol, 0.75 equiv), [Ir(COD)(OMe)]$_2$ (6 mg, 9.05 μmol, 0.03 equiv), dtbpy (5 mg, 18.6 μmol, 0.06 equiv) and cyclohexane (3 mL). The vial was sealed and heated to 80 °C for 4 h. The solution was cooled to rt and bis(pinacolato)diboron (58 mg, 0.230 mmol, 0.75 equiv), [Ir(COD)(OMe)]$_2$ (6 mg, 9.05 μmol, 0.03 equiv), dtbpy (5 mg, 18.6 μmol, 0.06 equiv) were added. The vial was resealed and heated to 80 °C for 4 h. The cooled solution was diluted with CH$_2$Cl$_2$ and passed through a thin pad of silica gel eluting with CH$_2$Cl$_2$. Removal of solvent gave a white solid (330 mg, 97%) which was used without further purification. mp (DSC) 341 °C. ^{1}H-NMR (500 MHz; CDCl$_3$) δ 8.17-8.16 (m, 2H), 8.08 (s, 1H), 7.81-7.79 (m, 4H), 7.74 (s, 2H), 7.48 (s, 13H), 7.37 (t, J = 0.6 Hz, 1H), 1.38 (s, 72H), 1.35 (s, 12H). ^{13}C NMR (126 MHz; CDCl$_3$) δ 151.4, 144.0, 142.2, 141.8, 141.1, 133.3, 129.6, 128.5, 126.5, 125.9, 122.2, 121.8, 84.1, 35.2, 31.7, 25.0. MALDI-TOF MS (TCNQ) m/z Calc'd for C$_{80}$H$_{105}$BO$_2$: 1108.82, found: 1108.64. Anal. Calc'd for C$_{80}$H$_{105}$BO$_2$: C 86.60, H 9.54, B 0.97, found: C 86.21, H 9.86, B 0.63. IR (thin film) 3054, 2694, 2906, 2863, 1583, 1423, 1388, 1334, 1143, 894, 867.

16-cascade:benzene[2-1,3]:(1,3,5-phenylene)^3:isobutane (6). A catalyst stock solution was prepared for small-scale reactions. In an Ar-filled dry box, a flame-dried vial

was charged with Pd(OAc)$_2$ (6 mg, 27 μmol), S-phos (20 mg, 48 μmol), and THF (1 mL). The solution was stirred at rt for 30 min. Another flame-dried vial with stirbar was charged with **5** (108 mg, 97 μmol, 2.2 equiv), 1,3-diiodobenzene (15 mg, 45 μmol, 1 equiv), THF (1 mL), and aq 5M NaOH (60 μL, 0.300 mmol, 6.6 equiv). In the dry box, the catalyst stock solution (0.1 mL; corresponding to 0.05 equiv Pd(OAc)$_2$ and 0.10 equiv S-phos) was added, the vial was sealed and heated to 60 °C for 4 h. The vial was cooled, Et$_2$O (10 mL) was added and the solution dried over MgSO$_4$. Column chromatography on silica gel using the solvent gradient 20:1 hexane:CH$_2$Cl$_2$ → 10:1 hexane:CH$_2$Cl$_2$ gave **6** as a white crystalline solid (73 mg, 78% yield). mp > 400 °C (dec. 501 °C). ^{1}H-NMR (500 MHz; C$_6$D$_6$) δ 8.15 (m, 6H), 8.10 (d, J = 1.6 Hz, 8H), 8.01 (d, J = 1.6 Hz, 4H), 7.98 (m, 1H), 7.72 (d, J = 1.8 Hz, 16H), 7.59 (t, J = 1.8 Hz, 8H), 7.51 (dd, J = 7.8, 1.7 Hz, 2H), 7.27-7.24 (m, 1H), 1.30 (s, 144H). ^{13}C NMR (126 MHz; CDCl$_3$) δ 151.4, 144.1, 143.0, 142.4, 142.06, 141.94, 141.0, 126.80, 126.66, 126.2, 125.8, 122.1, 121.8, 35.1, 31.71, 31.67. MALDI-TOF MS (TCNQ) m/z Calc'd for C$_{154}$H$_{190}$: 2039.48, found: 2039.17. Anal. Calc'd for C$_{154}$H$_{190}$: C 90.62, H 9.38, found: C 90.06, H 9.42. IR (thin film) 3058, 2949, 2902, 2859, 1785, 1583, 1478, 1392, 1361, 1096, 863.
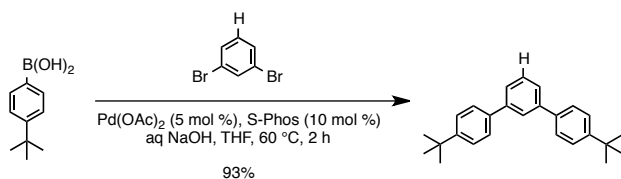
4,4''-di-*tert*-butyl-m-terphenyl (7). In an Ar-filled dry box, a flame-dried vial with stirbar was charged with Pd(OAc)$_2$ (13 mg, 57 μmol, 0.05 equiv) and S-phos (48 mg, 116 μmol, 0.10 equiv) and THF (1 mL) and the resulting solution was stirred under Ar for 30

minutes at room temperature. To a flame-dried 20 mL I-Chem vial was added 4-*tert*-butylphenylboronic acid (0.500 g, 2.81 mmol, 2.4 equiv). The vial was introduced into the dry box and THF (9 mL), aq 1M NaOH (5.6 mL, 5.6 mmol, 4.8 equiv), the catalyst solution prepared above, and 1,3-dibromobenzene (0.276 g, 1.17 mmol, 1.0 equiv) was added. The vial was sealed and heated to 60 °C overnight. The solution was cooled to rt and extracted twice with Et_2O (50 mL). The organic extracts were combined and washed with water (2 x 100 mL) and brine (100 mL), and dried over anhydrous $MgSO_4$. Column chromatography on silica gel (99:1 hexane:EtOAc) gave **7** as a white solid (0.374 g, 93%). mp (DSC) 150 °C. ^{1}H-NMR (500 MHz; C_6D_6)δ 7.95 (td, J = 1.8, 0.4 Hz, 1H), 7.56-7.53 (m, 4H), 7.51 (dd, J = 7.7, 1.8 Hz, 2H), 7.34-7.29 (m, 5H), 1.23 (s, 18H). ^{13}C NMR (126 MHz; C_6D_6) δ 150.4, 142.4, 139.1, 129.6, 127.4, 126.5, 126.21, 126.10, 34.5, 31.5. LRMS (EI+, 70 eV) *m/z* 342.2 (50), 327.2 (100), 251.2 (16), 156.1 (16), 128.1 (16), 57.0 (18). HRMS (EI+) *m/z* Calc'd for $C_{26}H_{30}$: 342.23475, found: 342.23436. Anal. Calc'd for $C_{26}H_{30}$: C 91.17, H 8.83, found: C 90.86, H 8.91.IR (thin film) 3050, 2988, 2960, 2898, 2859, 1602, 1481, 1419, 898, 843, 800.

General Procedure for GC Studies of the Borylation of 2 and 7. The water content of cyclohexane used in the GC experiments (Karl Fisher titration) was 13.5 μg/mL. Reactions were prepared in an Ar-filled dry box. The stock solution was prepared according to the protocol outlined by Smith.[19] To an oven-dried vial, [Ir(COD)(OMe)]$_2$ (14.6 mg, 22 μmol) and cyclohexane (2 mL) were added. HBpin (56 mg, 0.44 mmol) was added and the solution was mixed to form a dark brown solution. Last, dtbpy (11.8 mg, 44 μmol) was added to the solution. 100 μL aliquots of the solution correspond to

1.1 μmol [Ir(COD)(OMe)]$_2$ (0.01 equiv), 21.9 μmol HBpin (0.2 equiv), and 2.2 μmol dtbpy (0.02 equiv). The solution was kept under rigorous air- and moisture-free conditions. To oven-dried vials with stirbars, **2** or **7** (0.110 mmol, 1.0 equiv) and B$_2$pin$_2$ (0.110 mmol, 1.0 equiv; for Entry 5, 0.220 mmol or 2.0 equiv) were added and dissolved in cyclohexane (1.0 mL). The catalyst stock solution was added (100 μL; for Entry 6, 300 μL was added) and the mixture heated to 80 °C. After 4 h, the solutions were analyzed by GC, and in an Ar-filled dry box, any extra reagents or catalyst stock solution were added. The solutions were heated to 80 °C for 4 h, and analyzed by GC.

t$_R$ for **2** : 6.27 min

t$_R$ for **3** : 8.62 min

t$_R$ for **7** : 5.56 min

t$_R$ for borylated **7** : 8.78 min

2.6.3. Crystal Structure Data

Low-temperature diffraction data were collected on a Bruker-AXS Apex CCD detector with graphite-monochromated Mo Kα radiation (λ = 0.71073 Å), performing phi and omega scans. All structures were solved by direct methods and refined against F^2 on all data by full-matrix least squares with SHELXL-97 (Sheldrick, G. M. *SHELXL 97*; Universität Göttingen: Göttingen, Germany, 1997). All non-hydrogen atoms were refined anisotropically. All hydrogen atoms were included in the model at geometrically calculated positions and refined using a riding model. The isotropic displacement

parameters of the hydrogen atoms were fixed to 1.2 times the U value of the atoms they are linked to (1.5 U for methyl groups). Crystals of **4** contained a highly disordered ether solvent molecule. Since positions for the solvate molecules were poorly determined a second structural model was refined with contributions from the solvate molecules removed from the diffraction data using the bypass procedure in PLATON.[20] No positions for the host network differed by more than two su's between these two refined models. The electron count from the "squeeze" model converged in satisfactory agreement with the number of solvate molecules predicted by the complete refinement. The "squeeze" data are reported here.

Crystal Data for 1: $C_{20}H_{33}BO_2$, M = 316.27, orthorhombic, space group *Pnma*, a = 11.0312(12) Å, b = 16.3017(17) Å, c = 10.8502(12) Å , V = 1951.2(4) Å^3, Z = 4, D_c = 1.077 g cm^{-3}, μ(Mo-K) = 0.066 mm^{-1}, $F(000)$ = 696, T = 193 K. $R(F)^{\ddagger}$ = 0.0442, $R_w(F^2)^{\S}$ = 0.1232 for 24256 independent reflections with a goodness-of-fit of 1.072.

Crystal Data for 4: $C_{74}H_{94}$, M = 983.49, triclinic, space group *P*-1, a = 15.1083(8) Å, b = 16.5046(8) Å, c = 16.7776(9) Å , α = 81.808(3)°, β = 78.842(3)°, γ = 70.258(3)°, V = 3849.8(4) Å^3, Z = 2, D_c = 0.848 g cm^{-3}, μ(Mo-K) = 0.047 mm^{-1}, $F(000)$ = 1076, T = 193 K. $R(F)^a$ = 0.0691, $R_w(F^2)^b$ = 0.1693 for 44521 independent reflections with a goodness-of-fit of 0.815.

[‡] $R(F) = \Sigma ||F_o| - |F_c||/\Sigma |F_o|$ for $F_o^2 > 2\sigma(F_o)^2$.
[§] $R_w(F_o^2) = [\Sigma w(F_o^2 - F_c^2)^2/\Sigma wF_o^4]^{1/2}$, $w^{-1} = \sigma^2(F_o) + [M(F_o^2)]^2 + [N(F_o^2 + 2F_c^2)/3]$ for $F_o^2 \geq 0$; $w^{-1} = \sigma^2(F_o^2)$ for $F_o^2 < 0$. **1**: M = 0.0498; N = 0.6675. **4**: M = 0.0654; N = 0.
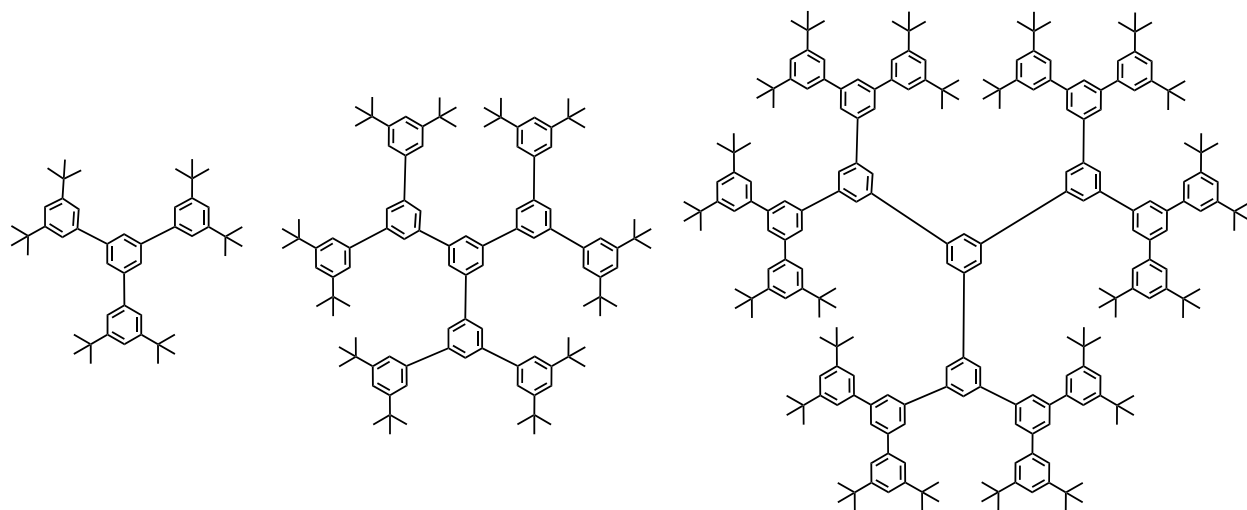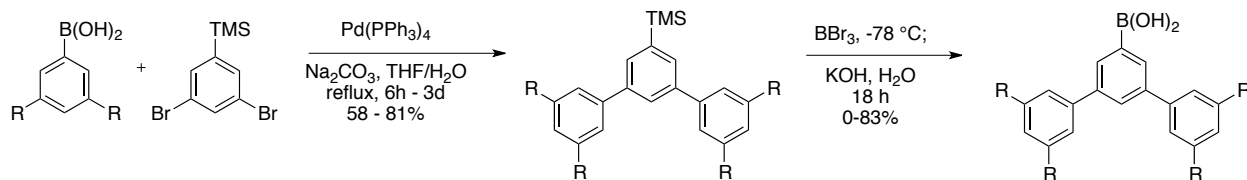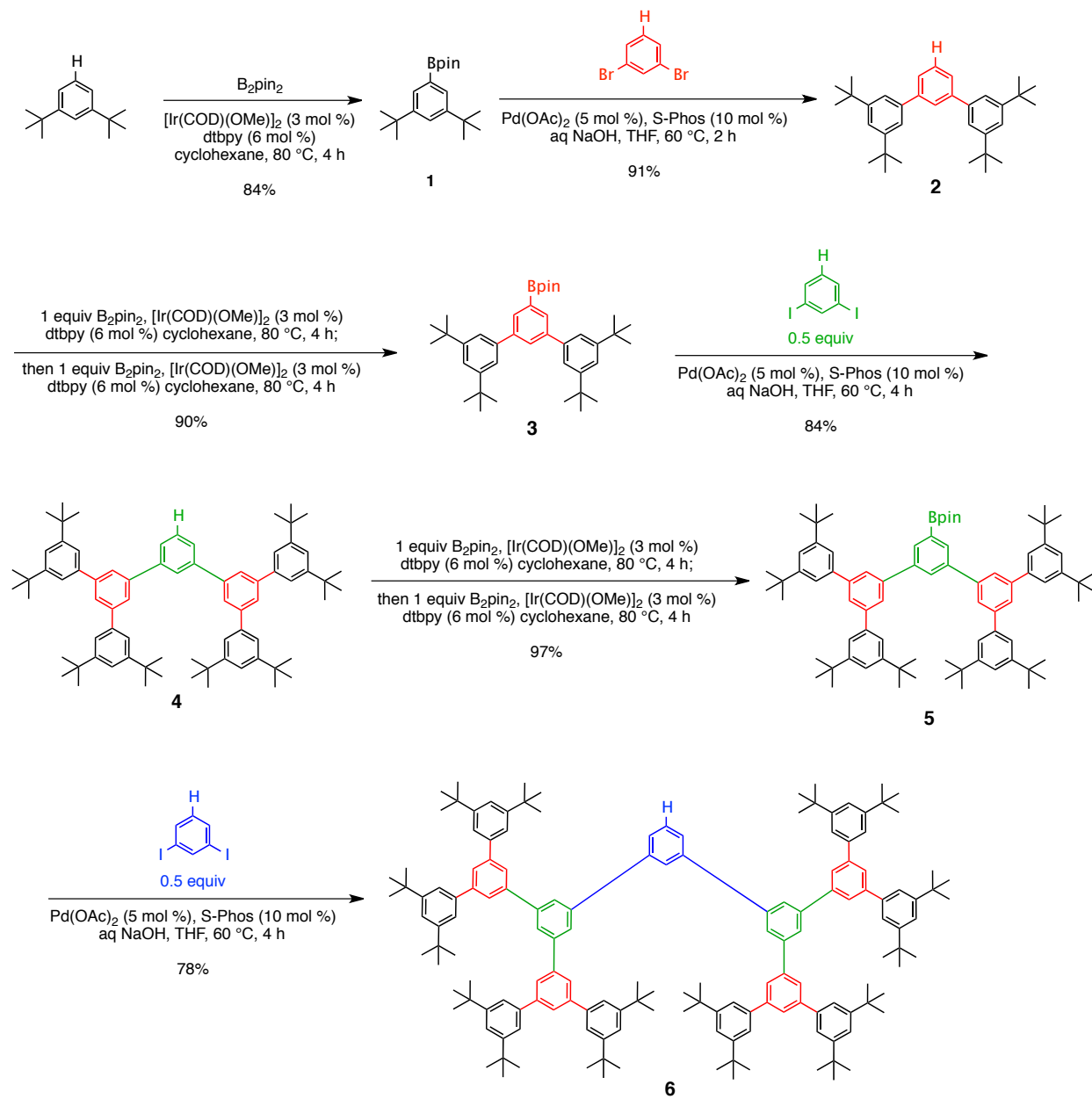
2.7 Figures and Schemes

Figure 2.1. Left to right: first, second and third-generation 1,3,5-polyphenylene dendrimers.

Scheme 2.1. Miller And Neenan's original approach to "unmasking" focal point reactivity in convergent dendron synthesis.

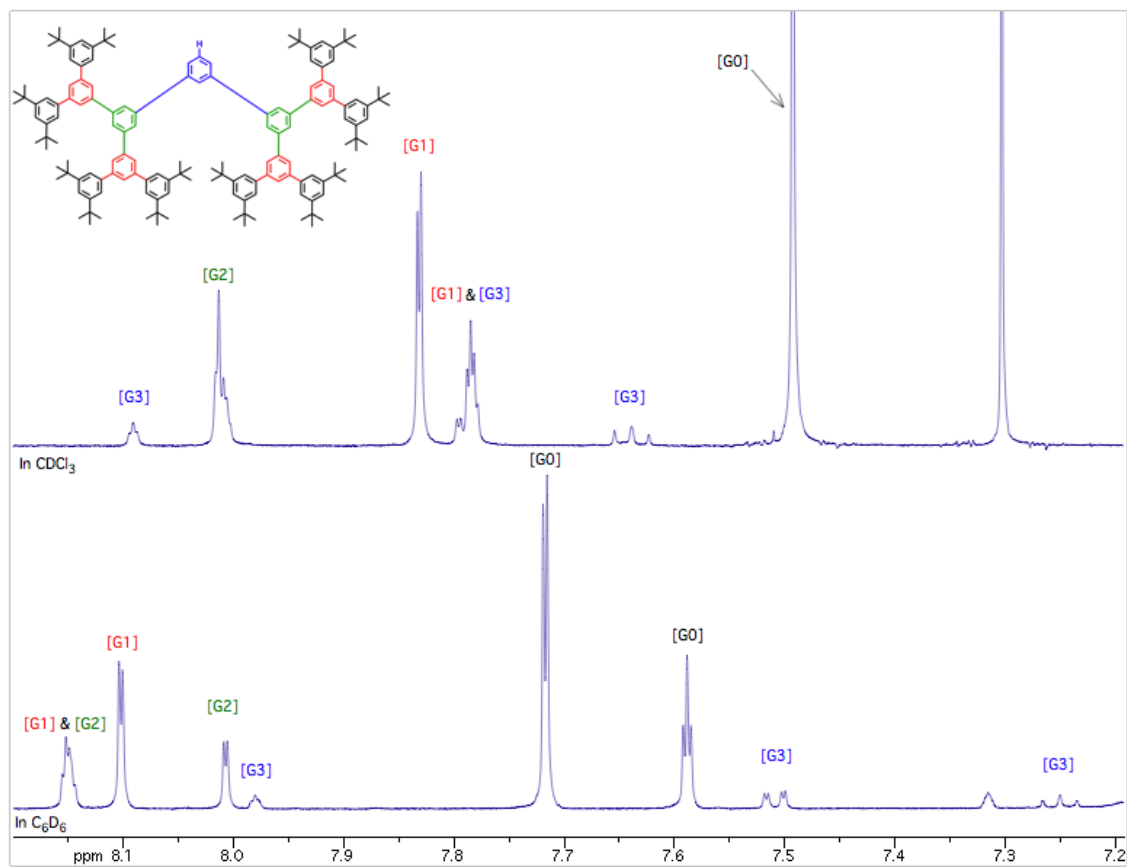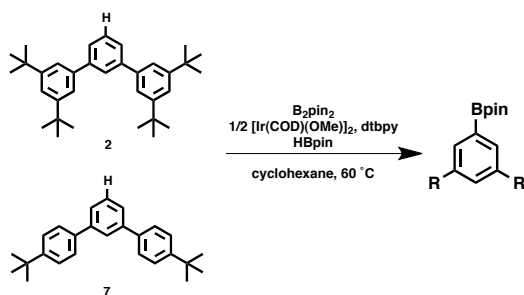**Scheme 2.2.** Synthesis of 1,3,5-polyphenylene dendrons.

Figure 2.2. ^{1}H NMR of the aromatic region of **6** in CDCl$_3$ (top) and C$_6$D$_6$ (bottom).

Table 2.1. Borylation of Sterically-Hindered *m*-terphenyls

		Initial	Added After 4 h		% conv. (GC)	
Entry	Arene	Catalyst[b]	B$_2$pin$_2$	Catalyst [b]	4 h	8 h
1	**2**	2 mol %	n/a[d]	n/a[d]	70	74
2	**2**	2 mol %	1 equiv	n/a[d]	70	77
3	**2**	2 mol %	n/a[d]	2 mol %	68	91
4	**2**	2 mol %	1 equiv	2 mol %	67	95
5[c]	**2**	2 mol %	n/a[d]	n/a[d]	70	75
6	**2**	6 mol %	n/a[d]	n/a[d]	nd[e]	91
7	**7**	2 mol %	n/a[d]	n/a[d]	nd[e]	91

[a] Reactions were carried out with 1.0 equiv arene, 1.0 equiv B$_2$pin$_2$, 20 mol% HBpin, and the specified amount of catalyst. [b] mol% 1/2[Ir(COD)(OMe)]$_2$ and dtbpy added. [c] 2 equiv B$_2$pin$_2$ initally added. [d] Nothing added. [e] Conversion not determined.
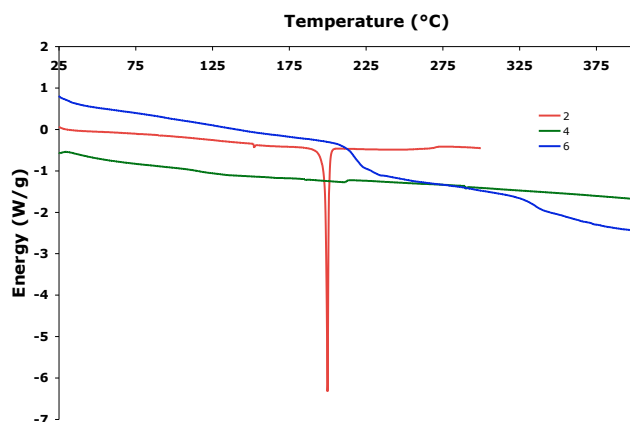
Figure 2.3. DSC of Dendrons **2**, **4** and **6** (25-400 °C, N$_2$, 10 °C/min).

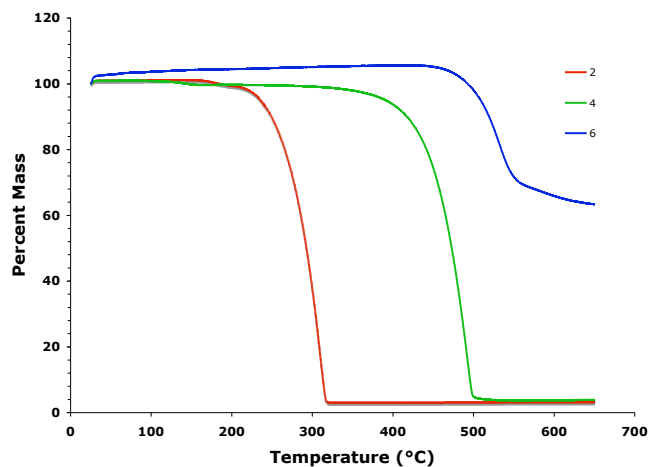**Figure 2.4.** TGA of Dendrons 2, 4 and 6 (25-650 °C, N_2, 10 °C/min).
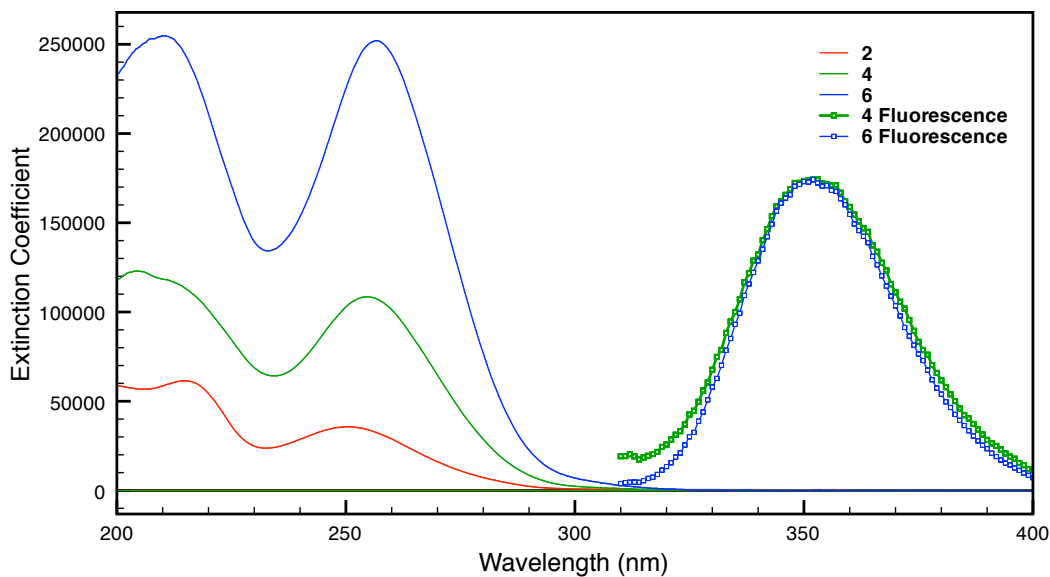

Figure 2.5. Absorbance and fluorescence spectra of **2**, **4**, and **6**. Fluorescence units are arbitrary.
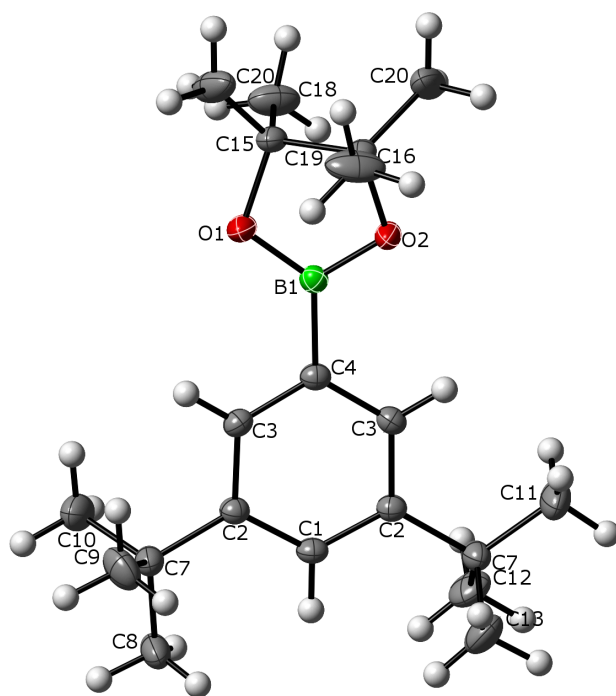
Figure 2.6. Thermal ellipsoid representation of **4**. Ellipsoids at 35% probability.
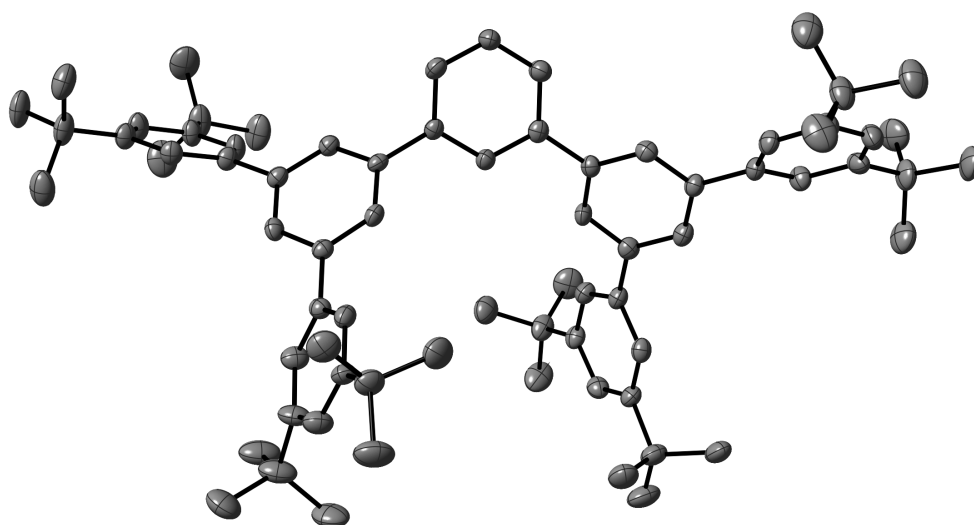

Figure 2.7. Thermal ellipsoid representation of **4**. Ellipsoids at 35% probability. Hydrogens omitted for clarity.

2.8   References

[1] (a) Gong, L.; Pu, L. *Tetrahedron Lett.* **2001**, *42,* 7337. (b) Gong, L.Z.; Hu, Q.S.; Pu, L. *J. Org. Chem.* **2001**, *66,* 2358. (c) Kimura, M.; Shiba, T.; Muto, T.; Hanabusa, K.; Shirai, H. *Macromolecules* **1999**, *32,* 8237. (d) Kimura, M.; Shiba, T.; Muto, T.; Hanabusa, K.; Shirai, H. *Chem. Commun.* **2000**, 11. (e) Kimura, M.; Shiba, T.; Yamazaki, M.; Shirai, H.; Kobayashi, N. *J. Am. Chem. Soc.* **2001**, *123,* 5636. (f) Zhao, L.; Li, C.; Zhang, Y.; Zhu, X.H.; Peng, J.B.; Cao, Y. *Macromol. Rapid Commun.* **2006**, *27,* 914. (g) Capitosti, G.J.; Guerrero, C.D.; Binkley, D.E.; Rajesh, C.S.; Modarelli, D.A. *J. Org. Chem.* **2003**, *68,* 247.

[2] Burn, P.L.; Lo, S.C.; Samuel, I.D.W. *Adv. Mater. (Weinheim, Ger.)* **2007**, *19,* 1675.

[3] Miyaura, N.; Suzuki, A. *Chem. Rev.* **1995**, *95,* 2457.

[4] (a) Miller, T.M.; Neenan, T.X. *Chem. Mater.* **1990**, *2,* 346. (b) Miller, T.M.; Neenan, T.X.; Zayas, R.; Bair, H.E. *J. Am. Chem. Soc.* **1992**, *114,* 1018. (c) Lo, S.; Namdas, E.; Burn, P.L.; Samuel, I. *Macromolecules* **2003**, *36,* 9721.

[5] Wren, E. J.; Wang, X.; Farlow, A.; Lo, S.; Burn, P. L.; Meredith, P. *Org. Lett.* **2010**, *12*, 4338-4340.

[6] Cho, J.Y.; Tse, M.K.; Holmes, D.; Maleczka, R.E.; Smith, M.R. *Science* **2002**, *295,* 305.

[7] (a) Ishiyama, T.; Takagi, J.; Hartwig, J.F.; Miyaura, N. *Angew. Chem., Int. Ed.* **2002**, *41,* 3056. (b) Ishiyama, T.; Takagi, J.; Ishida, K.; Miyaura, N.; Anastasi, N.R.; Hartwig, J.F. *J. Am. Chem. Soc.* **2002**, *124,* 390.

[8] (a) Ishiyama, T.; Miyaura, N. *J. Organomet. Chem.* **2003**, *680,* 3. (b) Boller, T. M.; Murphy, J. M.; Hapke, M.; Ishiyama, T.; Miyaura, N.; Hartwig, J. F. *J. Am. Chem. Soc.* **2005**, *127*, 14263. (c) Chotana, G. A.; Rak, M. A.; Smith, M. R. *J. Am. Chem. Soc.* **2005**, *127*, 10539.

[9] (a) Paul, S.; Chotana, G. A.; Holmes, D.; Reichle, R. C.; Maleczka, R. E.; Smith, M. R. *J. Am. Chem. Soc.* **2006**, *128*, 15552. (b) Chotana, G. A.; Kallepalli, V. A.; Maleczka, R. E.; Smith, M. R. *Tetrahedron* **2008**, *64*, 6103. (c) Mkhalid, I. A. I.; Coventry, D. N.; Albesa-Jove, D.; Batsanov, A. S.; Howard, J. A. K.; Perutz, R. N.; Marder, T. B. *Angew. Chem., Int. Ed.* **2006**, *45*, 489.

[10] Hata, H.; Yamaguchi, S.; Mori, G.; Nakazono, S.; Katoh, T.; Takatsu, K.; Hiroto, S.; Shinokubo, H.; Osuka, A. *Chem.-Asian J.* **2007**, *2,* 849.

[11] Coventry, D.N.; Batsanov, A.S.; Goeta, A.E.; Howard, J.A.K.; Marder, T.B.; Perutz, R.N. *Chem. Commun.* **2005**, 2172.

[12] Moreno-Manas, M.; Perez, M.; Pleixats, R. *J. Org. Chem.* **1996**, *61,* 2346.

[13] Murphy, J.M.; Tzschucke, C.C.; Hartwig, J.F. *Org. Lett.* **2007**, *9,* 757.

[14] (a) Barder, T.E.; Walker, S.D.; Martinelli, J.R.; Buchwald, S.L. *J. Am. Chem. Soc.* **2005**, *127,* 4685. (b) Martin, R.; Buchwald, S.L. *Acc. Chem. Res.* **2008**, *41*, 1461-1473.

[15] It is known that strong bases promote coupling of sterically-hindered boronic acids: Watanabe, T.; Miyaura, N.; Suzuki, A. *Synlett* **1992**, 207.

[16] The formation of the active trisboryl-iridium catalyst is accelerated by addition of HBpin, but the use of HBpin is unnecessary. HBpin is an impractical reagent due to its extreme moisture susceptibility. Sequential addition of the precatalyst, ligand and B$_2$pin$_2$

without HBpin gave similar results. Thus, HBpin was not used in the synthesis of **3** and **5**.

[17] Beck, E.M.; Hatley, R.; Gaunt, M.J. *Angew. Chem., Int. Ed.* **2008**, *47,* 3004.

[18] Dendron nomenclature is based on Newkome's method: Neokome, G.R.; Baker, G.R.; Young, J.K.; Traynham, J.G. *J. Polym. Sci., Part A: Polym. Chem.* **1993**, *31*, 641.

[19] Chotana, G. A.; Kallepalli, V. A.; Maleczka, R. E.; Smith, M. R. *Tetrahedron* **2008**, *64*, 6103-6114.

[20] Spek, A. L. *J. Appl. Cryst.* **2003**, *36*, 7-13.

Chapter 3

Zinc Chloride-Promoted Aryl Bromide-Alkyne Cross-Coupling Reactions at Room Temperature[†]

3.1. Introduction

The Pd- and CuI-catalyzed cross-coupling reaction of aryl and vinyl halides with terminal alkynes, known as the Sonogashira or Hagihara-Sonogashira reaction,[123] is one of the most widely-used and reliable methods of alkyne functionalization. Nonetheless, Cu-mediated homodimerization of alkynes and the requirement of elevated temperatures for the coupling of aryl bromides present a challenge to the efficient preparation of acetylene-containing molecular scaffolds free of chemical defects. [4,5] Recently, there have been significant advancements in overcoming the above limitations through two general strategies: the utilization of novel, highly active Pd catalysts;[6] and developing methodologies that are active in the absence of copper co-catalyst.[7] However, while "copper-free" Sonogashira conditions prevent CuI-mediated homocoupling,[8] they can suffer from lower rates compared to reactions promoted by CuI.[9] Alternative co-catalysts that do not display this side reactivity are thus highly desirable. In this chapter, we describe conditions for aryl bromide-alkyne cross coupling reactions at room temperature, which utilize substoichiometric amounts of inexpensive $ZnCl_2$ in the presence of an active Pd catalyst.[10]

3.2. Results

The yields for the room temperature coupling of the relatively unreactive 4-bromoanisole with phenylacetylene, both in the absence and presence of $ZnCl_2$, for selected Pd precatalyst systems are described in Table 3.1. Many of these Pd catalysts have been reported previously for aryl bromide-alkyne cross-couplings. Gratifyingly, most of these catalysts, in the presence of 10 mol% $ZnCl_2$, are effective at promoting cross-coupling at room temperature, with high yields after 1 h. The less reactive $Pd(PPh_3)_4$ (Table 3.1, entry 2) is an ineffective catalyst at room temperature. Pd(I) dimer **1** (Table 3.1, entry 6)[11] displays the highest activity in aryl bromide-alkyne cross-coupling of the catalyst systems studied. Complex **1** is a highly active catalyst that is more air-stable than other previously reported $Pd/P(t-Bu)_3$ precatalysts.

The necessity of a co-catalyst for rapid couplings, even in the presence of a highly active Pd catalyst, is illustrated in Table 3.1, entries 1 and 2. Pd catalysts which displayed high activity in the presence of $ZnCl_2$ were far less active in the absence of $ZnCl_2$ (Table 3.1, entries 3-7). Coupling in the presence of 1 mol % CuI (Table 3.2, entry 6) is complete in 2 h, but forms a significant amount of diyne byproduct. We attribute the low yield of the CuI-promoted coupling after 15 min to the solubility of CuI, which is less soluble in the reaction mixture than zinc halides.

The effect of zinc halide salts in alkyne cross-coupling reactions is well documented but underutilized.[12] Anastasia and Negishi reported that stoichiometric $ZnBr_2$ promoted room temperature coupling of alkynes with aryl iodides in the presence

---

of Pd(PPh$_3$)$_4$.[13] Notably, they were able to couple the typically unreactive methyl propiolate with iodobenzene at elevated temperatures.[14] Furthermore, they demonstrated the relative inertness of zinc halide promoted alkyne cross-couplings to air and moisture.[15]

The coupling of 4-bromoanisole with phenylacetylene with 1 mol % **1** in THF/HN(*i*-Pr)$_2$ was performed in the presence of 10 mol % of various zinc halides (Table 3.2, entries 2-5). Using only 10 mol % of a zinc halide salt promotes rapid cross-coupling at room temperature, indicating that stoichiometric quantities are not needed. All Zn salts display significant conversion after only 15 min. Strong inorganic bases such as Cs$_2$CO$_3$ and NaOt-Bu, when used in lieu of HN(*i*-Pr)$_2$, lead to no product formation at room temperature. Furthermore, deliberate addition of 20 mol% of a chloride source (LiCl or Bu$_4$NCl) leads to no noticeable rate enhancement.

The scope of the optimized conditions described above is summarized in Table 3.3. A variety of aryl bromides couple with alkynes rapidly with low catalyst loadings and at room temperature.[16] The reaction conditions tolerate many functional groups, including esters, aldehydes, and nitro groups (Table 3.3, entries 9-11, respectively). Heteroaryl bromides such as 2-bromothiophene are tolerated (Table 3.3, entry 15). Moderately hindered aryl bromides such as 2-bromotoluene couple rapidly at room temperature (Table 3.3, entries 6 and 12, respectively). However, very hindered aryl bromides such as 2-bromomesitylene and 9-bromoanthracene do not couple as rapidly at room temperature (Table 3.3, Entries 11 and 14, respectively) but still give acceptable yields. Aryl chlorides are unreactive at room temperature. Both 3- and 4-

bromophenyltriflate exclusively couple with the bromide over the triflate under the standard reaction conditions, rapidly and in good yield (Table 3.3, entries 17-18).[17] No triflate coupling products are detectable by GC. This orthogonal reactivity has the potential for the rapid, iterative preparation of unsymmetrical, conjugated architectures.

It has been noted recently that trace copper in commercially available iron salts are the active catalyst in those transformations and not the iron salt.[18] To address the possibilty that trace copper in our zinc salts is responsible for the rate enhancement in our reactions, trace metal copper analysis was performed by ICP-MS. The amounts of Cu (in ppm) of the zinc salts we used were as follows: $ZnCl_2$ (0.97 ppm); $ZnBr_2$ (1.10 ppm); ZnI_2 (1.23 ppm); $Zn(OTf)_2$ (0.62 ppm). The coupling of 4-bromoanisole with phenylacetylene in the presence of trace amounts of CuI (0.005 mol %, 50 ppm) was compared to the use of 10 mol% $ZnCl_2$; the results are summarized in Table 3.4. To our surprise, even small amounts of CuI can enhance the rate of coupling (Table 3.4, Entry 2). However, couplings were faster in the presence of 10 mol % $ZnCl_2$ (Table 3.4, Entry 4) which, after accounting for trace Cu contaminants in $ZnCl_2$, contains $1/100^{th}$ the amount of Cu compared to Entries 3 and 4. There does not appear to be a significant rate enhancement when trace CuI is added in the presence of 10 mol% $ZnCl_2$. Thus, we conclude that trace copper does not appear to be the active catalyst.

Amine identity appears to be crucial for hindered aryl bromides. The coupling of hindered 2-bromomesitylene was screened for optimal bases (Table 3.5). Diisopropylamine and DABCO were optimal, whereas triethylamine and Hünig's base

were less reactive. Interestingly, piperidine, known to be an excellent base for the coupling of aryl iodides, leads to only trace coupling at room temperature.

Alkyne oligomerization is possible with Pd/P(*t*-Bu)$_3$ systems (see below). While diyne products were not observed, in the case of the coupling of 2-bromoanisole with phenylacetylene to form 2-methoxytolan, a byproduct which could not be identified was present. This impurity was highly fluorescent and difficult to separate by conventional column chromatography. HPLC analysis of impure product (Fig. 3.1) indicates that the impurity is more conjugated than the product, as evidenced by the higher absorption of the impurity at 325 nm versus 280 nm. We tentatively assign this impurity as an enyne as the result of multiple alkyne addition. Such an impurity has been reported once before, in the Sonogashira coupling of haloporphyrins with TMS-acetylene; it is presumed to add *via* Heck-type carbopalladation, and this double alkyne addition appears to be more prevalent when a more electron-rich ligand for Pd is used.[19]

3.3 Mechanistic Studies

The exact role of the zinc halide salt is unknown at this time. However, previous mechanistic studies under similar conditions propose an in-situ zinc acetylide formation *via* "soft" deprotonation of a zinc halide-alkyne complex.[20] We have been unable to replicate these experiments; under the literature conditions as well as our own conditions, no alkyne deprotonation occurs by IR or ^{1}H NMR. "Soft" deprotonation of alkynes is possible with dialkylzinc complexes, but no trace of alkylzinc complexes under these reaction conditions has been found. A second possibility for the role of zinc

halide is the abstraction of halide from the intermediate Pd(II) aryl bromide; halide abstraction products have been shown for Ni(II)-benzyl halides.[21] To test the effect of zinc halide addition, the oxidative addition intermediate (t-Bu$_3$P)Pd(Ph)(Br) was prepared and subjected to phenylacetylene with and without the presence of ZnBr$_2$. The Pd(I) dimer [(t-Bu$_3$P)Pd(μ-Br)]$_2$ is known to rapidly polymerize terminal alkynes. In the absence of ZnBr$_2$, rapid polymerization of phenylacetylene occurs as evidenced by the rapid color change from orange to dark red. ^{31}P NMR indicates conversion of the starting material (δ 63.5 ppm) to [(t-Bu$_3$P)Pd(μ-Br)]$_2$ (δ 87.5 ppm); the presence of peaks at 100.1 and 94.1 ppm in the ^{31}P NMR are also observed, indicating alkyne polymerization. By contrast, the addition of zinc appears to inhibit polymerization: color change to red is slower. The major peak at 63.5 ppm is significantly broadened, and the peak at 87.5 ppm is minor. This indicates that the ZnBr$_2$ may be in equilibrium with (t-Bu$_3$P)Pd(Ph)(Br), inhibiting alkyne polymerization.

Zinc halides do react with (t-Bu$_3$P)Pd(Ph)(Br) by themselves. Addition of ZnCl$_2$ to a solution of (t-Bu$_3$P)Pd(Ph)(Br) results in a color change from yellow to green, the color of [(t-Bu$_3$P)Pd(μ-Br)]$_2$. Two new peaks appear in the ^{31}P NMR at 87.5 ppm (corresponding to [(t-Bu$_3$P)Pd(μ-Br)]$_2$) and 49.1 ppm. The latter peak cannot be identified; it is likely the result of cyclometalation.

In the presence of amines, formation of Zn halide-amine complexes form. This was verified by the addition of DABCO to a solution of ZnCl$_2$ in THF. Precipitation of [DABCO·ZnCl$_2$]$_n$ was immediate and irreversible. Nevertheless, DABCO is still a good base for these reactions (Table 3.5, Entry 4).

71

In conclusion, we have developed optimized conditions for a general and convenient aryl bromide-alkyne cross-coupling method in which rates of coupling are significantly enhanced by addition of catalytic $ZnCl_2$, without promoting diyne byproduct formation. These conditions present a superior alternative to other "copper-free Sonogashira" cross-couplings, by enhancing the rate of coupling *via* addition of an inexpensive co-catalyst that is less susceptible to alkyne homocoupling.

3.4   Experimental Section

Materials. Unless otherwise stated, all starting materials and reagents were purchased from commercial sources and used without further purification. THF was distilled from sodium benzophenone ketyl. Diisopropylamine was stored under Ar gas. $ZnCl_2$ (ACS grade, 97%, Strem), $ZnBr_2$ (98%, Strem), ZnI_2 (98%, Aldrich), and $Zn(OTf)_2$ (98%, Strem) were used as received and stored in a dessicator. No further drying of the zinc salts was undertaken. CuI (99.999%, PURATREM grade, Strem) was stored under Ar gas.

General Methods. All reactions were prepared in an argon-filled glove box and run under an inert atmosphere. The reaction vessels used, unless otherwise specified, were 20 mL vials fitted with PTFE/silicone septa. All glassware was oven-dried before use. Reactions were monitored by thin layer chromatography (Merck silica gel F254, 0.25 mm) and visualized under UV irradiation at 254 nm. Flash chromatography was performed using silica gel (60 Å, 230-400 mesh). Reaction yields shown in Table 3.3 of

the main text are an average of two runs; the following procedures are representative and the yields may differ from the Table 3.. Procedures and yields for the preparation of **1**, 4-bromophenyl triflate, and 3-bromophenyl triflate are based on a single run.

Physical Characterization. Melting points were obtained using an electrothermal melting temperature apparatus. ^{1}H and ^{13}C NMR spectra were referenced to residual solvent peaks or TMS (δ = 0 ppm). ^{19}F NMR was calibrated using $CFCl_3$ (δ = 0 ppm) as an external standard. ^{31}P NMR is referenced to H_3PO_4 (δ = 0 ppm). Chemical shifts (δ) are expressed in parts per million (ppm). Splitting constants (J) are expressed in Hz. Splitting patterns are designated as s, singlet; d, doublet; t, triplet; dd, doublet of doublets; td, triplet of doublets; m, multiplet. GC samples (using dodecane as an internal standard) were injected onto a capillary column. The injector temperature was 250 °C and the detector temperature was 280 °C with a H_2 carrier gas flow of 16 mL/min. The column temperature program was as follows: 100 °C for 3 min, ramp to 300 °C at 40 °C/min, then hold for 3 min for a total run time of 11.00 min.

Synthetic Procedures

Preparation and handling of Pd(I) Dimer 1. [22] A solution of tri-*tert*-butyl phosphine (639 mg, 3.02 mmol) in 20 mL of MeOH was added to a stirred suspension of [(2-methylallyl)PdCl]$_2$ (560 mg, 1.51 mmol) in 40 mL of MeOH under argon, immediately followed by addition of NaOH (60.5 mg, 1.51 mmol) in 20 mL MeOH. The solution turned yellow and was stirred at room temperature for 1h. **1** was obtained as a yellow

precipitate. The precipitate was washed with a small amount of methanol, dissolved in benzene and passed through a PTFE filter (pore size 0.45 μm) to remove residual Pd black. The filtrate was lyophilized to give 1.06 g (91% yield) of pure complex **1** as a yellow powder. The ^{1}H NMR and ^{13}C NMR corresponded to the values reported in the literature for this compound. Single crystals suitable for X-ray diffraction were obtained by slow evaporation of a benzene solution.[23] **1** can be handled in ambient atmosphere for short periods of time (up to a week) but should be stored under inert gas when not in use. When appropriately stored, **1** has a shelf life of ~1 year before noticeable decomposition occurs. Over time, the canary yellow solid develops a green tinge. Impure **1** can be purified via trituration of a THF solution of **1** into pentane.

4-bromophenyl triflate.[24] An oven-dried 250 mL 2-necked flask under an atmosphere of nitrogen was charged with 4-bromophenol (5.19 g, 30 mmol, 1 equiv), dry CH_2Cl_2 (60 mL) and pyridine (7.2 mL, 90 mmol, 3 equiv), and cooled to 5 °C in a water bath. Trifluoromethanesulfonic anhydride (6.05 mL, 36 mmol, 1.2 equiv) was added dropwise to the solution. The resulting red solution was stirred for 4 h at room temperature. The solution was then passed through a plug of SiO_2 (50 g), and eluted with 200 mL of a solution of 1:1 hexane:CH_2Cl_2. The solvent was evaporated, and the resulting oil was dissolved in 100 mL Et_2O, washed with saturated aq. $CuSO_4$ twice (to remove excess pyridine) and brine, and then dried over $MgSO_4$. The solvent was evaporated, and the crude material was purified further via Kugelrohr distillation to give 4-bromophenyl

triflate as a slightly yellow oil (7.33 g, 80% yield). NMR and MS data match that of the literature. The product was stored in a desiccator under nitrogen gas.

3-bromophenyl triflate.[25] The same procedure for the preparation of 4-bromophenyl triflate described above was used with 3-bromophenol (5.19 g, 30 mmol) to give 3-bromophenyl triflate as a colorless oil (7.54 g, 82% yield). NMR and MS data match that of the literature. The product was stored in a desiccator under nitrogen gas.

General Procedure for the Preparation of Substituted Alkynes with Catalytic ZnCl$_2$. The following general procedure was used for the preparation of substrates in Table 3.3. In a glove box, a 20 mL vial with stirbar and PTFE/silicone septum-lined cap was charged with, in order, the aryl bromide (3 mmol, 1 equiv), ZnCl$_2$ (41 mg, 0.3 mmol, 0.1 equiv), THF (7 mL), HN(i-Pr)$_2$ (3 mL), and Pd(I) dimer **1** (21 mg, 0.03 mmol, 0.01 equiv). The solution was stirred to dissolve the solids, and then the alkyne (3 mmol, 1 equiv) was added. (*NOTE: the alkyne must be added last to avoid catalyst decomposition and excess alkyne addition byproduct formation*). The vial was capped, removed from the glove box, and stirred at room temperature for the specified amount of time. The solution was diluted with EtOAc, and passed through a plug of silica gel (10 g) and eluted with 100 mL EtOAc to remove H$_2$N(i-Pr$_2$)Br and Zn salt. The solution was evaporated, and the residue was purified by column chromatography on silica gel.
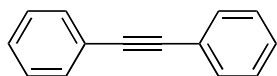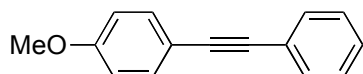
Table 3.3, Entry 1. Diphenylacetylene.[26] The General Procedure was utilized above, Reaction stirred at room temperature for 1 hour. Purification by column chromatography (99:1 hexane:EtOAc) gave the product in 93% yield (0.495 g). White solid. mp 59-60 °C (lit. 58-61 °C).

^{1}H NMR (500 MHz; CDCl$_3$): δ 7.59-7.54 (m, 4H), 7.41-7.33 (m, 6H).

^{13}C NMR (126 MHz; CDCl$_3$): δ 131.7, 128.48, 128.40, 123.4, 89.5.

Table 3.3, Entry 2. 4-methoxydiphenylacetylene.[27] The General Procedure was utilized above, Reaction stirred at room temperature for 1 hour. Purification by column chromatography (6:1 hexane:CH$_2$Cl$_2$) gave the product in 90% yield (0.562 g). Pale yellow solid. mp 58-59 °C (lit. 58-61 °C).

^{1}H NMR (500 MHz; CDCl$_3$): δ 7.53-7.51 (m, 2H), 7.50-7.47 (m, 2H), 7.36-7.32 (m, 3H), 6.90-6.88 (m, 2H), 3.83 (s, 3H).

^{13}C NMR (126 MHz; CDCl$_3$): δ 159.7, 133.2, 131.6, 128.4, 128.1, 123.7, 115.5, 114.1, 89.5, 88.2, 55.4.
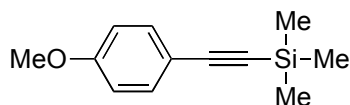

Table 3.3, Entry 3.(2-(4-methoxyphenyl)ethynyl)trimethylsilane.[28] The General Procedure was utilized above, Reaction stirred at room temperature for 2 hours.

Purification by column chromatography (10:1 hexane:CH_2Cl_2 with 3% NEt_3) gave the product in 89% yield (0.551 g). Yellow oil.

^{1}H NMR (500 MHz; CDCl$_3$): δ 7.40 (d, J = 8.8 Hz, 2H), 6.82 (d, J = 8.8 Hz, 2H), 3.80 (s, 3H), 0.24 (s, 9H).

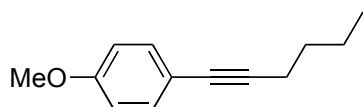^{13}C NMR (126 MHz; CDCl$_3$): δ 159.8, 133.6, 115.4, 113.9, 105.3, 92.5, 55.4, 0.2.

Table 3.3, Entry 4. 1-(4-methoxyphenyl)-1-hexyne.[29] The General Procedure was utilized above, Reaction stirred at room temperature for 2 hours. Purification by column chromatography (99:1 hexane:EtOAc) gave the product in 91% yield (0.512 g). Yellow oil.

^{1}H NMR (400 MHz; CDCl$_3$): δ 7.34 (d, J = 8.9 Hz, 2H), 6.81 (d, J = 8.9 Hz, 2H), 3.79 (s, 3H), 2.39 (t, J = 7.0 Hz, 2H), 1.60-1.54 (m, 2H), 1.50-1.44 (m, 2H), 0.94 (t, J = 7.3 Hz, 3H).

^{13}C NMR (101 MHz; CDCl$_3$): δ 159.1, 133.0, 116.4, 113.9, 88.9, 80.3, 55.4, 31.1, 22.2, 19.3, 13.8.
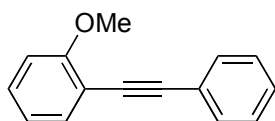

Table 3.3, Entry 5. 2-methoxydiphenylacetylene.[30] A modification to the General Procedure was used. The alkyne (as a solution in 1 mL THF) was added dropwise over

2 hours, then stirred at room temperature for an additional two hours. Purification by column chromatography (hexane → 10:1 hexane:CH_2Cl_2) gave the product in 83% yield (0.521 g). Yellow oil.

^{1}H NMR (500 MHz; CDCl_3): δ 7.60-7.57 (m, 2H), 7.53 (dd, J = 7.6, 1.8, Hz, 1H), 7.38-7.30 (m, 4H), 6.96 (td, J = 7.5, 1.0 Hz, 1H), 6.93-6.91 (m, 1H), 3.94 (s, 3H).

^{13}C NMR (126 MHz; CDCl_3): δ 160.2, 133.8, 131.9, 130.0, 128.50, 128.37, 123.8, 120.7, 112.7, 110.9, 93.7, 86.0, 56.1.
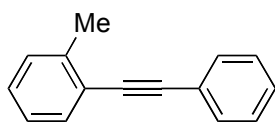

Table 3.3, Entry 6. 2-methyldiphenylacetylene.[3] The General Procedure was utilized above, Reaction stirred at room temperature for one hour. Purification by column chromatography (40:1 hexane: CH_2Cl_2) gave the product in 94% yield (0.519 g). Colorless oil.

^{1}H NMR (500 MHz; CDCl_3): δ 7.56 (dd, J = 7.9 Hz, 1.8 Hz, 2H), 7.52 (d, J = 7.5 Hz, 1H), 7.36 (m, 3H), 7.25 (m, 2H), 7.19 (m, 1H), 2.54 (s, 3H).

^{13}C NMR (125 MHz; CDCl_3): δ 140.3, 132.0, 131.7, 129.6, 128.50, 128.45, 128.32, 125.7, 123.7, 123.2, 93.5, 88.5, 20.9.
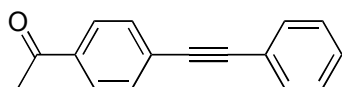

Table 3.3, Entry 7. 4-acetyldiphenylacetylene.[31] The General Procedure was utilized above, Reaction stirred at room temperature for 20 minutes. Purification by column

chromatography (9:1 hexane:EtOAc) gave the product in 95% yield (0.628 g). Pale yellow solid. mp 100-101 °C (lit. 97-103 °C).

^{1}H NMR (500 MHz; CDCl$_3$): δ 7.94 (d, J = 8.6 Hz, 2H), 7.61 (d, J = 8.6 Hz, 2H), 7.55 (m, 2H), 7.37 (m, 3H), 2.62 (s, 3H).

^{13}C NMR (126 MHz; CDCl$_3$): δ 197.5, 136.3, 131.87, 131.83, 128.9, 128.58, 128.40, 128.33, 122.8, 92.8, 88.7, 26.8.
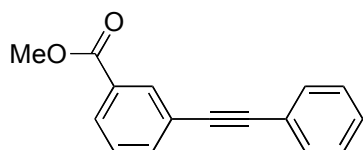

Table 3.3, Entry 8. Methyl 3-(phenylethynyl)benzoate.[32] The General Procedure was utilized above, Reaction stirred at room temperature for 30 minutes. Purification by column chromatography (10:1 hexane:EtOAc) gave the product in 99% yield (0.703 g). Yellow solid. mp 76-78 °C (lit. 77-79 °C).

^{1}H NMR (500 MHz; CDCl$_3$): δ 8.21 (s, 1H), 8.00 (d, J = 7.9 Hz, 1H), 7.71 (d, J = 7.7 Hz, 1H), 7.56-7.53 (m, 2H), 7.44 (t, J = 7.8 Hz, 1H), 7.38-7.36 (m, 3H), 3.94 (s, 3H).

^{13}C NMR (126 MHz; CDCl$_3$): δ 166.6, 135.8, 132.9, 131.8, 130.6, 129.3, 128.70, 128.64, 128.55, 123.9, 123.0, 90.4, 88.4, 52.4.
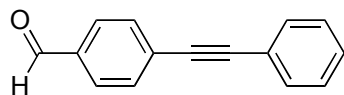

Table 3.3, Entry 9. 4-(phenylethynyl)benzaldehyde.[33] The General Procedure was utilized above, Reaction stirred at room temperature for 20 minutes. Purification by

column chromatography (1:1 hexane:CH$_2$Cl$_2$) gave the product in 93% yield (0.574 g).

Yellow solid. mp 98-100 °C (lit. 98-100 °C).

^{1}H NMR (500 MHz; CDCl$_3$): δ 10.02 (s, 1H), 7.88-7.85 (m, 2H), 7.68 (d, J = 8.1 Hz, 2H), 7.57-7.54 (m, 2H), 7.41-7.35 (m, 3H).

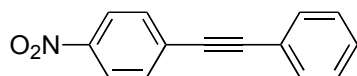^{13}C NMR (126 MHz; CDCl$_3$): δ 191.5, 135.5, 132.2, 131.9, 129.7, 129.1, 128.6, 122.6, 93.6, 88.6.

Table 3.3, Entry 10. 4-nitrodiphenylacetylene.[34] The General Procedure was utilized above, Reaction stirred at room temperature for 20 minutes. Purification by column chromatography (10:1 hexane:EtOAc) gave the product in 99% yield (0.668 g). Yellow solid. mp 119-121 °C (lit. 121-123 °C).

^{1}H NMR (500 MHz; CDCl$_3$): δ 8.24-8.21 (m, 3H), 7.68-7.66 (m, 3H), 7.58-7.55 (m, 3H), 7.41-7.37 (m, 5H).

^{13}C NMR (126 MHz; CDCl$_3$): δ 147.1, 132.4, 132.0, 130.4, 129.4, 128.7, 123.8, 122.2, 94.8, 87.7.
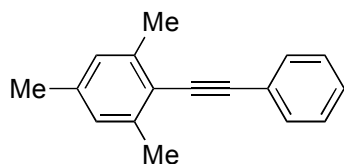

Table 3.3, Entry 11. 2,4,6-trimethyldiphenylacetylene.[35] The General Procedure was utilized above, Reaction stirred at room temperature for 16 hours. Purification by column

chromatography (hexane → 10:1 hexane:CH$_2$Cl$_2$) gave the product in 73% yield (0.481 g). White solid. mp 36-38 °C (lit. 36-37 °C).

^{1}H NMR (500 MHz; CDCl$_3$): δ 7.55-7.54 (m, 2H), 7.38-7.31 (m, 3H), 6.91 (s, 2H), 2.49 (s, 6H), 2.31 (s, 3H).

^{13}C NMR (126 MHz; CDCl$_3$): δ 140.1, 137.7, 131.3, 128.3, 127.9, 127.6, 124.0, 119.9, 97.0, 87.3, 21.3, 21.0.
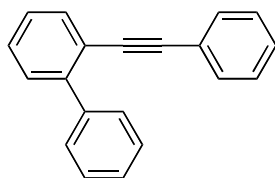

Table 3.3, Entry 12. 2-(phenylethynyl)biphenyl.[36] The General Procedure was utilized above, Reaction stirred at room temperature for 2 hours. Purification by column chromatography (hexane → 10:1 hexane:CH$_2$Cl$_2$) gave the product in 92% yield (0.699 g). Pale yellow oil.

^{1}H NMR (499 MHz; CDCl$_3$): δ 7.74-7.70 (m, 3H), 7.53-7.31 (m, 11H).

^{13}C NMR (126 MHz; CDCl$_3$): δ 144.0, 140.6, 132.9, 131.4, 129.57, 129.49, 128.6, 128.34, 128.19, 128.0, 127.6, 127.1, 123.5, 121.7, 92.3, 89.5.
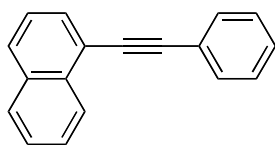

Table 3.3, Entry 13.1-(phenylethynyl)naphthalene.[37] The General Procedure was utilized above, Reaction stirred at room temperature for 1 hour. Purification by column

chromatography (99:1 hexane:EtOAc) gave the product in 94% yield (0.609 g). Colorless oil.

^{1}H NMR (500 MHz; CDCl$_3$): δ 8.49 (d, *J* = 8.4 Hz, 1H), 7.88 (dd, *J* = 12.6, 8.2 Hz, 2H), 7.80 (dd, *J* = 7.1, 1.0 Hz, 1H), 7.69 (dt, *J* = 8.0, 1.9 Hz, 2H), 7.63 (ddd, *J* = 8.3, 6.9, 1.3 Hz, 1H), 7.56 (ddd, *J* = 8.0, 6.9, 1.2 Hz, 1H), 7.49 (dd, *J* = 8.2, 7.2 Hz, 1H), 7.45-7.38 (m, 3H).

^{13}C NMR (126 MHz; CDCl$_3$): δ 133.40, 133.35, 131.8, 130.5, 128.9, 128.57, 128.52, 128.44, 126.9, 126.6, 126.4, 125.4, 123.5, 121.0, 94.5, 87.7.
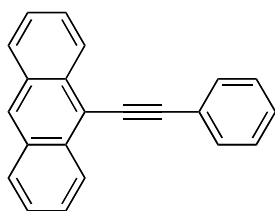

Table 3.3, Entry 14. 9-(phenylethynyl)anthracene.[38] The General Procedure was utilized above, Reaction stirred at room temperature for 5 hours. Purification by column chromatography (hexane → 10:1 hexane:CH$_2$Cl$_2$) gave the product in 86% yield (0.718 g). Highly fluorescent, yellow solid. mp 110-112 °C.

^{1}H NMR (500 MHz; CDCl$_3$): δ 8.69 (d, *J* = 8.7 Hz, 2H), 8.44 (s, 1H), 8.03 (d, *J* = 8.4 Hz, 2H), 7.82-7.80 (m, 2H), 7.64-7.61 (m, 2H), 7.53 (t, *J* = 7.5 Hz, 2H), 7.50-7.42 (m, 3H).

^{13}C NMR (126 MHz; CDCl$_3$): δ 132.6, 131.6, 131.1, 128.65, 128.48, 128.44, 127.7, 126.72, 126.56, 125.6, 123.6, 117.2, 100.7, 86.3.
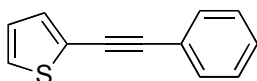
Table 3.3, Entry 15. 2-(phenylethynyl)thiophene.[39] The General Procedure was utilized above, Reaction stirred at room temperature for 1 hour. Purification by column chromatography (99:1 hexane:EtOAc) gave the product in 91% yield (0.516 g). White solid. mp 50-51 °C (lit. 49-51 °C).

^{1}H NMR (500 MHz; CDCl$_3$): δ 7.55-7.52 (m, 2H), 7.39-7.35 (m, 3H), 7.30 (d, J = 4.1 Hz, 2H), 7.04-7.02 (m, 1H).

^{13}C NMR (126 MHz; CDCl$_3$): δ 132.0, 131.5, 128.54, 128.50, 127.38, 127.22, 123.4, 123.0, 93.2, 82.7.
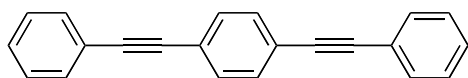

Table 3.3, Entry 16. 1,4-bis(phenylethynyl)benzene.[40] The General Procedure was utilized above, Reaction stirred at room temperature for 2 hours. The reaction was run with 2 equiv phenylacetylene (0.612 g, 6 mmol). Purification by column chromatography (10:1 hexane:CH$_2$Cl$_2$) gave the product in 88% yield (0.545 g). White to pale yellow solid. mp 181-184 °C (lit. 183 °C).

^{1}H NMR (500 MHz; CDCl$_3$): δ 7.54 (m, 4H), 7.52 (s, 4H), 7.36 (m, 6H).

^{13}C NMR (125 MHz; CDCl$_3$): δ 131.6, 131.5, 128.5, 128.4, 123.1, 123.0, 91.2, 89.1.

Table 3.3, Entry 17. 4-(2-phenylethynyl)phenyl trifluoromethanesulfonate.[41] This reaction was performed on a 1 mmol scale with 2 mL THF and 1 mL HN(i-Pr)$_2$. The

General Procedure was utilized above, Reaction stirred at room temperature for 20 minutes. Purification by column chromatography (10:1 hexane:CH_2Cl_2) gave the product in 89% yield (0.89 mmol, 0.290 g). Colorless solid. mp 61-62 °C.

^{1}H NMR (400 MHz; CDCl$_3$): δ 7.59-7.55 (m, 2H), 7.52-7.48 (m, 2H), 7.35-7.32 (m, 3H), 7.25-7.21 (m, 2H).

^{13}C NMR (101 MHz; CDCl$_3$): δ 149.1, 133.6, 131.9, 129.0, 128.6, 124.2, 122.7, 121.7, 118.3 (q, J = 318 Hz), 91.4, 87.5.
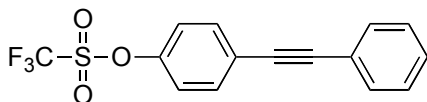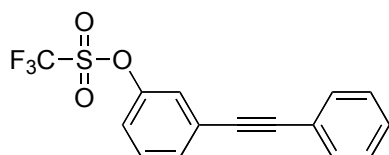
^{19}F NMR (376 MHz; CDCl$_3$): δ -74.0.

Table 3.3, Entry 18. 3-(2-phenylethynyl)phenyl trifluoromethanesulfonate. This reaction was performed on a 1 mmol scale with 2 mL THF and 1 mL HN(*i*-Pr)$_2$. The General Procedure was utilized above, Reaction stirred at room temperature for 20 minutes. Purification by column chromatography (10:1 hexane:CH_2Cl_2) gave the product in 89% yield (0.290 g). Yellow oil.

^{1}H NMR (400 MHz; CDCl$_3$): δ 7.54-7.51 (m, 3H), 7.42-7.34 (m, 5H), 7.23-7.21 (m, 1H).

^{13}C NMR (100 MHz; CDCl$_3$): δ 149.4, 131.7, 130.3, 129.1, 128.6, 126.0, 124.3, 122.4, 121.3, 118.9 (q, J = 321 Hz), 91.7, 87.2.

^{19}F NMR (376 MHz; CDCl$_3$): δ -73.1.

IR (film, cm^{-1}): 3081, 2217, 1952, 1882, 1803, 1695, 1607, 1570, 1495, 1424, 1213, 1140, 943, 848, 754.

MS (EI+): 326.0 (98), 262.0 (10), 165.1 (100), 139.0 (10), 115.0 (5), 69.0 (10).

HRMS (EI+): Calc'd for $C_{15}H_9F_3O_3S$: 326.02246; Found 326.02198.

Anal. Calc'd for $C_{15}H_9F_3O_3S$: C 55.21, H 2.78; Found: C 55.00, H 2.75.

Procedure for Cross-Coupling in the Presence of ZnCl$_2$ and/or Trace CuI (Table 3.4). All manipulations were performed in an argon-filled glove box. CuI (1.0 mg, 0.0052 mmol) was added to a 100 mL volumetric flask. Dry, degassed THF (95 mL) and HN(*i*-Pr)$_2$ (5 mL) were added, then the flask was sealed, removed from the glove box, and sonicated for 10 minutes. The flask was returned to the glove box. In a 20 mL vial with septum-lined cap and stirbar was added, in order, 4-bromoanisole (0.187 g, 1 mmol), dodecane (20 μL), THF (9 mL), HN(*i*-Pr)$_2$ (3 mL), ZnCl$_2$ (14 mg, 0.1 mmol) 1.0 mL of the CuI solution (5.2 × 10^{-5} mmol), **1** (7 mg, 0.01 mmol), and phenylacetylene (120 μL, 1.1 mmol). The solutions were stirred under Ar at room temperature and analyzed by GC.
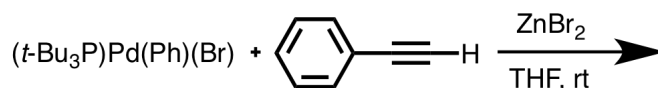
Reaction of phenylacetylene in the presence and absence of ZnBr$_2$.

With ZnBr$_2$: (*t*-Bu$_3$P)Pd(Ph)(Br) (10 mg, 0.021 mmol) was dissolved in 1 mL THF. ZnBr$_2$ (7 mg, 0.031 mmol) was added. Phenylacetylene (50 μL, 0.526 mmol, 25 equiv) was added. The yellow color slowly changed to red after 1 hour at room temperature. ^{31}P{^{1}H} NMR: δ 87.51, 63.48 (br s, major), 48.93, 40.20.

Without ZnBr$_2$: (*t*-Bu$_3$P)Pd(Ph)(Br) (10 mg, 0.021 mmol) was dissolved in 1 mL THF. Phenylacetylene (50 μL, 0.526 mmol, 25 equiv) was added. The yellow color rapidly

changed to red upon addition, and was allowed to stir for 1 h at room temperature. $^{31}P\{^1H\}$ NMR: δ 100.07, 94.10, 87.51 (major), 82.79, 63.53.

$$(t\text{-Bu}_3P)Pd(Ph)(Br) \xrightarrow[\text{THF, -30 °C}]{\text{ZnCl}_2}$$
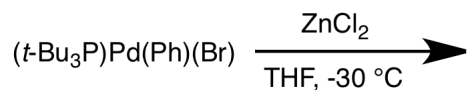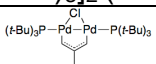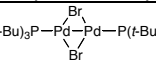
Reaction of ZnCl$_2$. A solution of (t-Bu$_3$P)Pd(Ph)(Br) (50 mg, 0.107 mmol) was dissolved in 5 mL THF and cooled to -30 °C. ZnCl$_2$ (0.214 mL of a 0.5M solution in THF, 0.107 mmol) was added and allowed to sit at -30 °C for 3 hours. The reaction mixture turned green over that time. $^{31}P\{^1H\}$ NMR: δ 87.53, 66.58, 49.09.

3.5 Figures and Schemes

Table 3.1. Scope of Palladium Sources With and Without ZnCl$_2$
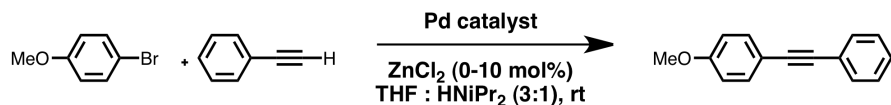
Entry	Pd catalyst (mol %)	% convn, 1 h[a] no added ZnCl$_2$[b]	% convn, 1 h[a] with 10 mol % ZnCl$_2$[c]
1	--[d]	0	0
2	Pd(PPh$_3$)$_4$ (2 mol %)	0	0
3[6g]	[allylPdCl]$_2$ (1 mol %) P(t-Bu)$_3$ (2 mol %)	28	37
4[6d]	Pd$_2$dba$_3$ (1 mol %) P(t-Bu)$_3$ · HBF$_4$ (2 mol %)	26	85
5	Pd[P(t-Bu)$_3$]$_2$ (2 mol %)	27	90
6 [8]	(t-Bu)$_3$P—Pd—Pd—P(t-Bu)$_3$ **1** (1 mol%)	25	96
7[42]	(t-Bu)$_3$P—Pd—Pd—P(t-Bu)$_3$ (1 mol%)	25	75

[a]Conversions by GC. [b]Reaction conditions: 4-bromoanisole (1.0 mmol), phenylacetylene (1.0 mmol), Pd catalyst (0.02 mmol), THF (1.0 mL), HN(i-Pr)$_2$ (0.5 mL), rt. [c]Reaction conditions: 4-bromoanisole (1.0 mmol), phenylacetylene (1.0 mmol), Pd catalyst (0.02 mmol Pd), ZnCl$_2$ (0.1 mmol), THF (1.0 mL), HN(i-Pr)$_2$ (0.5 mL), rt. [d]No Pd catalyst added.

Table 3.2. Efficacy of Zinc Halides in Promotion of Cross-Coupling[a]
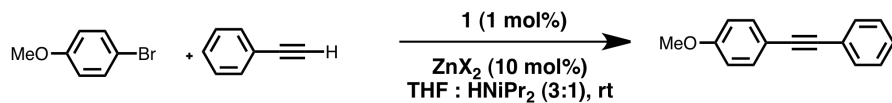
Entry	ZnX$_2$	Cost[b] ($ / mol)	% yield[c] 15 min	% yield[c] 24 h	% yield of diyne[c] 24 h
1	none	--	2	84	< 1
2	ZnCl$_2$	$29.71	87	100	0
3	ZnBr$_2$	$84.22	88	100	0
4	ZnI$_2$	$142.36	48	79	0
5	Zn(OTf)$_2$	$1076.05	85	100	0
6	CuI[d]	$48.52	< 1[e]	99	3

[a]Reaction conditions: 4-bromoanisole (1.0 mmol), phenylacetylene (1.0 mmol), **1** (0.01 mmol), zinc halide (0.1 mmol), THF (1.0 mL), HN(*i*-Pr)$_2$ (0.5 mL), rt. [b]Cost for reagent-grade salts (as of July 2009), Aldrich Chemical Co. [c]GC yields. [d]1 mol % CuI used in lieu of zinc halide (see text). [e]Reaction is complete after 2 h.

Table 3.3. Aryl Bromide-Alkyne Cross-Couplings Promoted By Catalytic ZnCl$_2$[a]

R–Br + R'$\equiv$H $\xrightarrow[\substack{\text{ZnCl}_2\ (0\text{-}10\ \text{mol\%}) \\ \text{THF : HNiPr}_2\ (3\text{:}1),\ \text{rt}}]{\text{Pd catalyst}}$ R$\equiv$R'
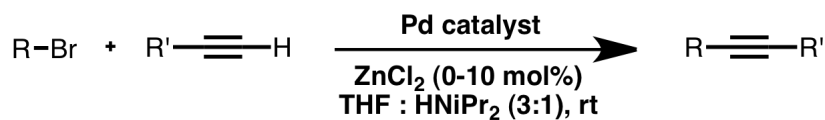
Entry	R	R'	Time	Yield (%)[b]
1	H	Ph	30 min	93
2	4-OMePh	Ph	1 h	86
3	4-OMePh	TMS	2 h	89
4	4-OMePh	Bu	2 h	88
5[c]	2-OMePh	Ph	2 h	83
6	2-MePh	Ph	1 h	92
7	4-COMePh	Ph	20 min	94
8	3-(COOMe)Ph	Ph	30 min	97
9	4-CHOPh	Ph	20 min	94
10	4-NO$_2$Ph	Ph	20 min	96
11	2,4,6-(Me)$_3$Ph	Ph	16 h	76 (90)
12	2-PhPh	Ph	2 h	93
13	1-naphthyl	Ph	1 h	94
14	9-anthracyl	Ph	5 h	86
15	2-thienyl	Ph	1 h	91
16[d]	4-BrPh	Ph	3 h	88
17	4-OTfPh	Ph	30 min	92
18	3-OTfPh	Ph	30 min	93

[a]Reaction conditions: aryl bromide (3.0 mmol), alkyne (3.0 mmol), **1** (0.03 mmol), ZnCl$_2$ (0.3 mmol), THF (7.0 mL), HN(i-Pr)$_2$ (3 mL), rt. [b]Yields are an average of two runs. Yields in parentheses are GC yields. [c]The alkyne was added over 2 h and stirred at rt for an additional 2 h. [d]2.0 equiv (6.0 mmol) phenylacetylene was used. The product is 1,4-bis(2-phenylethynyl)benzene.
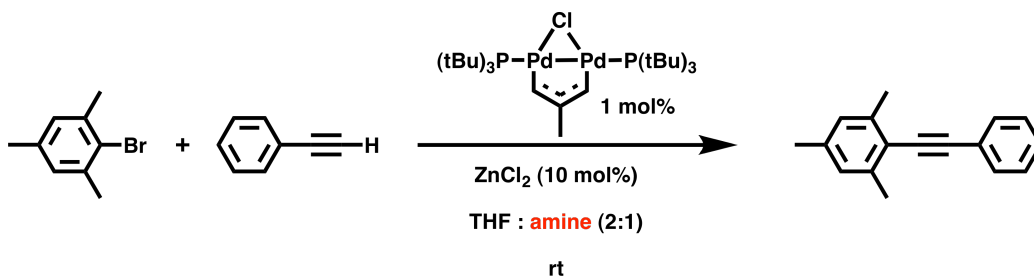
Table 3.4. Effects of Trace CuI in Cross-Coupling[a]
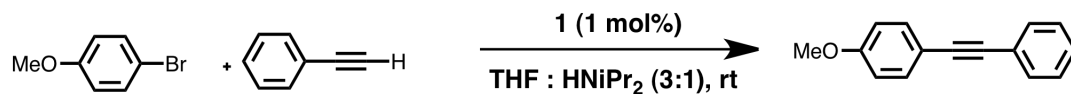
Entry	ZnCl$_2$ (mol %)	CuI (mol %)	% yield[b] 1 h	% yield[b] 2 h	% yield[b] 24 h
1	--[c]	--[c]	2	5	19
2	--[c]	0.005	5	10	56
3	10	0.005	24	56	100
4	10	--[c]	30	58	100

[a]Reaction conditions: 4-bromoanisole (1.0 mmol), phenylacetylene (1.1 mmol), **1** (0.01 mmol), zinc halide (0.1 mmol) and/or CuI (5 × 10^{-5} mmol), THF (10.0 mL), HN(*i*-Pr)$_2$ (3.0 mL), rt. [b]GC yields, average of two runs. [c]Not added.

Table 3.5. Amine Screen[a]

Entry	Amine	Convn (%)[b] 30 min	Convn (%)[b] 4 h (GC)	Convn (%)[b] 24 h (GC)
1	None	0	0	0
2	NEt$_3$	16	36	54
3	HN(iPr)$_2$	23	57	73
4	DABCO	14	65	77
5	EtN(iPr)$_2$	trace	20	27
6	Piperidine	trace	trace	trace

[a]Reaction conditions: 2-bromomesitylene (1.0 mmol), phenylacetylene (1.1 mmol), **1** (0.01 mmol), zinc chloride (0.1 mmol), THF (2.0 mL), amine (1.0 mL), rt. [b]GC yields, average of two runs.
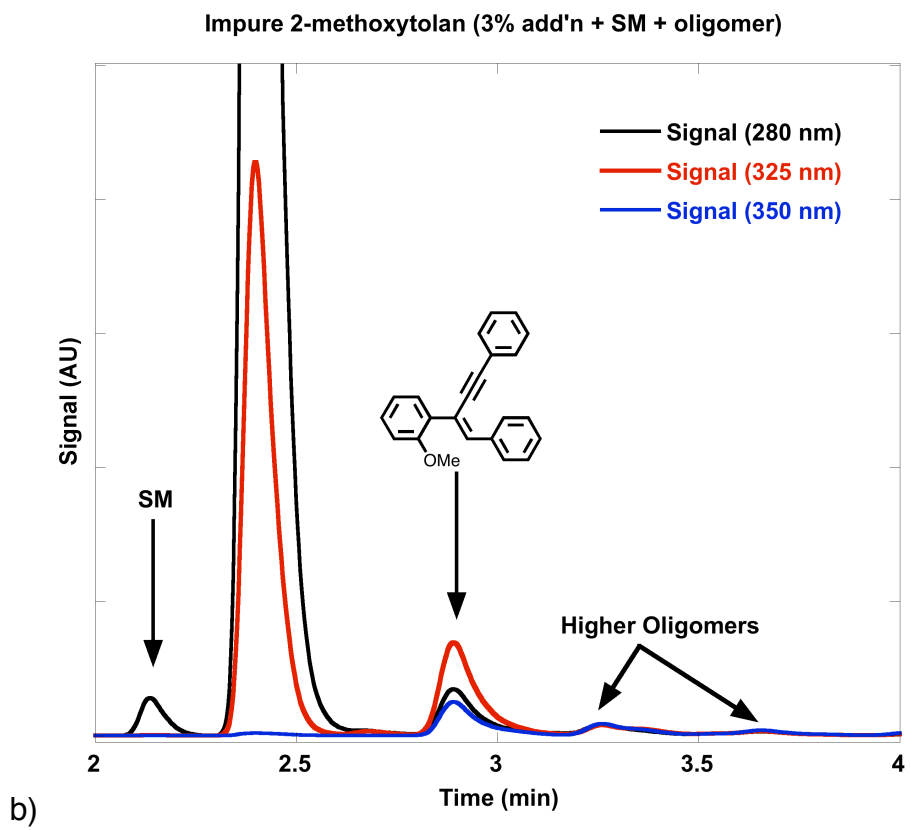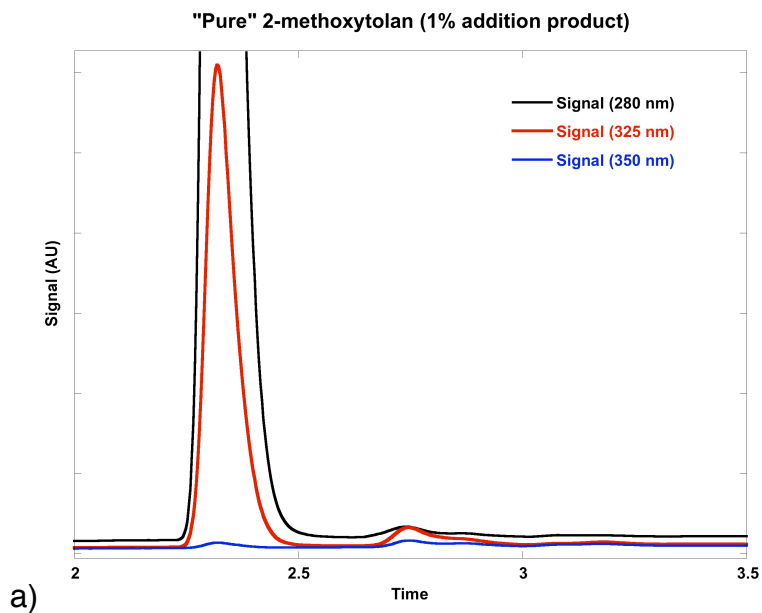
Figure 3.1. HPLC traces at multiple wavelengths for (a) pure and (b) impure 2-methoxytolan.

3.6 References

[1] Marsden, J. A.; Haley, M. M. In *Metal-Catalyzed Cross-Coupling Reactions*; 2nd ed.; de Meijre, A., Diederich, F., Eds.; Wiley-VCH: Weinheim, 2004, p 317-394.

[2] Negishi, E.; Anastasia, L. *Chem. Rev.* **2003**, *103*, 1979-2017.

[3] Sonogashira, K.; Tohda, Y.; Hagihara, N. *Tetrahedron Lett.* **1975**, 4467-4470.

[4] Selected reviews on synthesis and applications of acetylene scaffolds: (a) *Poly(arylene ethynylene)s: From Synthesis to Application*; Weder, C. Ed.; Springer: Berlin / Heidelberg, 2005; Vol. 177. (b) Bunz, U. H. F. *Chem. Rev.* **2000**, *100*, 1605-1644. (c) McQuade, D. T.; Pullen, A. E.; Swager, T. M. *Chem. Rev.* **2000**, *100*, 2537-2574. (d) Thomas, S. W.; Joly, G. D.; Swager, T. M. *Chem. Rev.* **2007**, *107*, 1339-1386. (e) Hill, D. J.; Mio, M. J.; Prince, R. B.; Hughes, T. S.; Moore, J. S. *Chem. Rev.* **2001**, *101*, 3893-4011. (f) Moore, J. S. *Acc. Chem. Res.* **1997**, *30*, 402-413. (g) Martin, R. E.; Diederich, F. *Angew. Chem. Int. Ed.* **1999**, *38*, 1350-1377.

[5] Previous work from our group on applications of arylene ethynylene scaffolds: (a) Hartley, C. S.; Elliott, E. L.; Moore, J. S. *J. Am. Chem. Soc.* **2007**, *129*, 4512. (b) Smaldone, R. A.; Moore, J. S. *Chem.-Eur. J.* **2008**, *14*, 2650-2657. (c) Zang, L.; Che, Y.; Moore, J. S. *Acc. Chem. Res.* **2008**, *41*, 1596-1608. (d) Zhang, W.; Moore, J. S. *Angew. Chem., Int. Ed.* **2006**, *45*, 4416-4439.

[6] Selected recent reports on utilizing active ligands for Pd-catalyzed cross-coupling of aryl halides with alkynes:
(a) Bohm, V. P. W.; Herrmann, W. A. *Eur. J. Org. Chem.* **2000**, 3679-3681. (b) Hundertmark, T.; Littke, A. F.; Buchwald, S. L.; Fu, G. C. *Org. Lett.* **2000**, *2*, 1729-1731. (c) McGuinness, D. S.; Cavell, K. J. *Organometallics* **2000**, *19*, 741-748. (d) Netherton, M. R.; Fu, G. C. *Org. Lett.* **2001**, *3*, 4295–4298. (e) Gelman, D.; Buchwald, S. L. *Angew. Chem., Int. Ed.* **2003**, *42*, 5993-5996. (f) Kollhofer, A.; Pullmann, T.; Plenio, H. *Angew. Chem., Int. Ed.* **2003**, *42*, 1056-1058. (g) Soheili, A.; Albaneze-Walker, J.; Murry, J. A.; Dormer, P. G.; Hughes, D. L. *Org. Lett.* **2003**, *5*, 4191-4194. (h) Feuerstein, M.; Berthiol, F.; Doucet, H.; Santelli, M. *Org. Biomol. Chem.* **2003**, *1*, 2235-2237. (i) Datta, A.; Ebert, K. Plenio, H. *Organometallics* **2003**, *22*, 4685-4691. (j) Hierso, J. C.; Fihri, A.; Amardeil, R.; Meunier, P.; Doucet, H.; Santelli, M.; Ivanov, V. V. *Org. Lett.* **2004**, *6*, 3473-3476. (k) Adjabeng, G.; Brenstrum, T.; Frampton, C. S.; Robertson, A. J.; Hillhouse, J.; McNulty, J.; Capretta, A. *J. Org. Chem.* **2004**, *69*, 5082-5086. (l) Cheng, J.; Sun, Y.; Wang, F.; Guo, M.; Xu, J.; Pan, Y.; Zhang, Z. *J. Org. Chem.* **2004**, *69*, 5428-5432. (m) Anderson, K. W.; Buchwald, S. L. *Angew. Chem., Int. Ed.* **2005**, *44*, 6173-6177. (n) Kollhofer, A.; Plenio, H. *Adv. Synth. Catal.* **2005**, *347*, 1295-1300. (o) Shirakawa, E.; Kitabata, T.; Otsuka, H.; Tsuchimoto, T. *Tetrahedron* **2005**, *61*, 9878-9885.

[7] For a review of recent advances in aryl halide-alkyne cross-coupling: Doucet, H.; Hierso, J. C. *Angew. Chem., Int. Ed.* **2007**, *46*, 834-871. (b) For a critical review on alternative metal-catalyzed cross-couplings of aryl halides and alkynes: Plenio, H. *Angew. Chem., Int. Ed.* **2008**, *47*, 6954-6956.

[8] Alkynes in the presence of CuI, amine, and a stoichiometric oxidant (Pd(II) or air) rapidly and quantitatively homocouple. This is the generally accepted mechanism for

reduction of some Pd(II) precatalysts in the Sonogashira reaction. See: Nguyen, P.; Yuan, Z.; Agocs, L.; Lesley, G.; Marder, T. B. *Inorg. Chim. Acta* **1994**, *220*, 289-296 and refs. therein.

[9] In our experience, this observation is true for couplings that utilize amines as base. However, Buchwald et al. have reported that for certain coupling conditions which utilize inorganic bases, CuI inhibits reactivity (see Ref. 6e).

[10] This is an optimization of a method we previously reported. Elliott, E. L.; Ray, C. R.; Kraft, S.; Atkins, J. R.; Moore, J. S. *J. Org. Chem.* **2006**, *71*, 5282-5290.

[11] (a) Werner, H.; Kühn, A. *J. Organomet. Chem.* **1979**, *179*, 439-445. (b) Denmark, S. E.; Baird, J. D. *Org. Lett.* **2006**, *8*, 793-795. (c) Denmark, S. E.; Baird, J. D.; Regens, C. S. *J. Org. Chem.* **2008**, *73*, 1440-1455. (d) Denmark, S. E.; Baird, J. D. *Tetrahedron* **2009**, *65*, 3120-3129.

[12] Pioneering studies on effects of Zn salts on aryl halide-alkyne cross-couplings: (a) Crisp, G. T.; Turner, P. D.; Stephens, K. A. *J. Organomet. Chem.* **1998**, *570*, 219-224. (b) Eberhard, M. R.; Wang, Z. H.; Jensen, C. M. *Chem. Commun.* **2002**, 818-819. For implementation of Zn-promoted aryl halide-alkyne cross-couplings,: (a) Boydston, A. J.; Pagenkopf, B. L. *Angew. Chem. Int. Ed.* **2004**, *43*, 6336-6338. (b) Grube, G. H.; Elliott, E. L.; Steffens, R. J.; Jones, C. S.; Baldridge, K. K.; Siegel, J. S. *Org. Lett.* **2003**, *5*, 713-716. (c) Crisp, G. T.; Turner, P. D. *Tetrahedron* **2000**, *56*, 407-415.

[13] Anastasia, L.; Negishi, E. *Org. Lett.* **2001**, *3*, 3111-3113.

[14] Reactions with methyl propiolate under our conditions lead only to decomposition/polymerization of the alkyne, regardless of the amine used. We observe that this occurs in the absence of Pd catalyst or Zn salt, indicating that even amine bases incapable of conjugate addition are capable of promoting alkyne decomposition. The method reported here is thus unsuitable for cross-couplings of propiolate esters.

[15] Our reaction conditions are insensitive to moisture, and drying of the hygroscopic zinc salts is unnecessary. However, the air sensitivity of the Pd catalysts requires these reactions be run under inert atmosphere with degassed solvents.

[16] "Room temperature" in this context refers to the absence of *external* heating. In reality, many of these reactions, particularly with electron-poor aryl bromides, can be quite exothermic.

[17] (a) For examples of reverse selectivity (triflates preferential to halides), see: Kamikawa, T.; Hayashi, T. *J. Org. Chem.* **1998**, *63*, 8922-8925. Espino, G.; Kurbangalieva, A.; Brown, J. M. *Chem. Commun.* **2007**, 1742-1744. (b) Pd/P(*t*-Bu)$_3$ is selective for aryl chlorides over aryl triflates in Suzuki cross-couplings: Littke, A. F.; Dai, C. Y.; Fu, G. C. *J. Am. Chem. Soc.* **2000**, *122*, 4020-4028.

[18] See Ref. 7b and Buchwald, S.L; Bolm, C. *Angew. Chem. Int. Ed.* **2009**, *48*, 5586-5587.

[19] Chen, Y. J.; Lee, G. H.; Peng, S. M.; Yeh, C. Y. *Tetrahedron Lett.* **2005**, *46*, 1541-1544.

[20] Fassler, R.; Tomooka, C. S.; Frantz, D. E.; Carreira, E. M. *Proc. Natl. Acad. Sci. U.S.A.* **2004**, *101*, 5843-5845.

[21] Anderson, T. J.; Vicic, D. A. *Organometallics* **2004**, *23*, 623-625.

[22] CAS No. 62586-36-1. Werner, H.; Kühn, A. *J. Organomet. Chem.* **1979**, *179*, 439-445. Procedure adapted from Elliott, E. L.; Ray, C. R.; Kraft, S.; Atkins, J. R.; Moore, J. S. *J. Org. Chem.* **2006**, *71*, 5282-5290.

[23] CCDC 285926 contains the supplementary crystallographic data for this paper. These data can be obtained free of charge from The Cambridge Crystallographic Data Centre via www.ccdc.cam.ac.uk/data_request/cif.

[24] CAS No. 66107-30-0. Kamikawa, T.; Hayashi, T. *J. Org. Chem.* **1998**, *63*, 8922-8925.

[25] CAS No. 66107-31-1. Espino, G.; Kurbangalieva, A. Brown, J. M. *Chem. Commun.* **2007**, 1742-1744.

[26] CAS No. 501-65-5. Nakagawa, K.; Onoue, H.; Minami, K. *Chem. Commun.* **1966**, 730-731.

[27] CAS No. 7380-78-1. Colacino, E.; Daich, L.; Martinez, J.; Lamaty, F. *Synlett* **2007**, 1279-1283.

[28] CAS No. 3989-14-8. Sakai, N.; Annaka, K.; Konakahara, T. *Org. Lett.* **2004**, *6*, 1527-1530.

[29] Xie, C.; Liu, L.; Zhang, Y.; Xu, P. *Org. Lett.* **2008**, *10*, 2393.

[30] CAS No. 41398-67-8. Yue, D.; Yao, T.; Larock, R. C. *J. Org. Chem.* **2005**, *70*, 10292-10296.

[31] CAS No. 1942-31-0. Komaromi, A.; Tolnai, G. L.; Novak, Z. *Tetrahedron Lett.* **2008**, *49*, 7294-7298.

[32] CAS No. 207845-32-7. Sorensen, U. S.; Pombo-Villar, E. *Tetrahedron* **2005**, *61*, 2697-2703.

[33] CAS No. 57341-98-7. Elangovan, A.; Wang, Y.; Ho, T. *Org. Lett.* **2003**, *5*, 1841-1844.

[34] CAS No. 1942-30-9. Kakusawa, N.; Yamaguchi, K.; Kurita, J. *J. Organomet. Chem.* **2005**, *690*, 2956-2966.

[35] CAS No. 29778-31-2. Huggins, J. M.; Bergman, R. G. *J. Am. Chem. Soc.* **1981**, *103*, 3002-11.

[36] CAS No. 10271-65-5. Moon, J.; Jeong, M.; Nam, H.; Ju, J.; Moon, J. H.; Jung, H. M.; Lee, S. *Org. Lett.* **2008**, *10*, 945-948.

[37] CAS No. 4044-57-9. Elangovan, A.; Wang, Y.; Ho, T. *Org. Lett.* **2003**, *5*, 1841-1844.

[38] CAS No. 87337-07-3. Dang, H.; Garcia-Garibay, M. A. *J. Am. Chem. Soc.* **2001**, *123*, 355-356.

[39] CAS No. 4805-17-8. Katritzky, A. R.; Abdel-Fattah, A. A. A.; Wang, M. *J. Org. Chem.* **2002**, *67*, 7526-7529.

[40] CAS No. 1849-27-0. Lydon, D. P.; Porres, L.; Beeby, A.; Marder, T. B.; Low, P. J. *New J. Chem.* **2005**, *29*, 972-976.

[41] CAS No. 166663-45-2. Kamikawa, T.; Hayashi, T. *J. Org. Chem.* **1998**, *63*, 8922-8925.

[42] Stambuli, J. P.; Kuwano, R.; Hartwig, J. F. *Angew. Chem., Int. Ed.* **2002**, *41*, 4746-4748.

Chapter 4

Lewis Acid Activation of Molybdenum Nitrides for Alkyne Metathesis

4.1. Introduction

Alkyne metathesis, once the underutilized cousin of olefin metathesis, has undergone a resurgence in the past ten years.[1] One major advance in this field has been the development of well-defined alkyne metathesis precatalysts based on molybdenum alkylidynes.[2,3] The preparation of Mo-alkylidynes is not straightforward; highly air- and moisture-sensitive precursors and difficult multistep syntheses complicate facile preparation. The Mo-nitrides, by contrast,[4] are much easier to prepare from commercially-available precursors.[5,6] In a seminal report, Johnson et al. reported that molybdenum nitrides could metathesize with aliphatic alkynes to generate the Mo-alkylidyne and an alkylnitrile irreversibly.[5,6] The kinetic barrier for this reaction is high, as with many *N*-transfer reactions, and occurs slowly at elevated temperatures. Nevertheless, recently-reported precatalysts based on Mo-nitrides have demonstrated excellent activity for ring-closing metathesis of aliphatic alkynes.[7]

    Herein, we describe the activation of Mo-nitrides toward metathesis with alkynes *via N*-ligation of a Lewis acid. Activation of MoO_x precatalysts with oxophilic trialkylaluminiums for alkyne metathesis is well-known;[8,9] however, the effects of Lewis acid addition to Mo-nitrides in alkyne metathesis has not been reported. The nitrogen atom in Mo-nitrides has sufficient nucleophilic character to display

predictable reactivity with Brønsted acids,[10] Lewis acids,[11,12] and organic electrophiles.[13] We hypothesized that the typically high activation barrier to nitride-alkyne metathesis could be overcome by precomplexation with an Lewis acid (Scheme 4.1), weakening the Mo≡N bond and making it more susceptible to metathesis. The borane $B(C_6F_5)_3$ was particularly attractive due to its strong Lewis acidity and relative inertness compared to other boranes.[14,15]

4.2   Results

4.2.1 Formation and Characterization of Molybdenum Nitride-Borane

Our initial studies focused on pyridine complex **1**, developed by Fürstner as a stable, convenient alkyne metathesis precatalyst and is now commercially available.[7] However, upon reaction of **1** with 1 equiv $B(C_6F_5)_3$, we observed the formation of $B(C_6F_5)_3 \cdot$pyridine only;[16] **1-B** was generated with 2 equiv $B(C_6F_5)_3$. Catalytic amounts of **1-B** reacted with 1-phenyl-1-butyne in toluene at 90 °C overnight to generate diphenylacetylene and 3-hexyne.

Encouraged by these results, we then turned our focus to Mo-nitride **2**, the precursor to **1**, which Fürstner reported to be active in alkyne metathesis upon *in-situ* substitution with appropriate silanol ligands.[7] Reaction of **2** with $B(C_6F_5)_3$ in DCM solvent generated **2-B** in quantitative yield as a white solid. Crystals suitable for X-ray analysis were formed from slow diffusion of pentane into a DCM solution of **2-B** at -30°C under Ar. Analysis of the structure of **2-B** dispalyed some unusual attributes (Figure 4.1a). First, the Mo≡N bond length of 1.696(3) Å[17] is elongated compared to

terminal nitrido complexes of Mo.[18] Furthermore, the Mo-N-B bond angle is 159.3°, significantly distorted from the expected linearity. Neither **2** nor **2-B** were metathesis-active with 3-hexyne or 1-phenyl-1-butyne.

To directly compare the structural effects of Lewis acid addition to Mo-nitrides, the well-studied Mo-nitride **3**[19] was prepared and complexed with $B(C_6F_5)_3$ to generate **3-B**. Crystals suitable for X-ray analysis were grown from slow diffusion of pentane into a DCM solution of **3** and $B(C_6F_5)_3$ (Figure 4.1b). The Mo≡N bond length in **3-B** (1.692(5) Å) is significantly longer (>3σ) than in **3** (1.661(4) Å).[19] Furthermore, a weakening of the Mo≡N bond is observed by IR (Figure 4.2). This is in contrast to the Mo≡N bond length in MoN[N(*t*-Bu)Ar]$_3$·BF$_3$, which does not deviate significantly from the free nitride.[11] As with **2**, neither **3** nor **3-B** were metathesis-active with 3-hexyne or 1-phenyl-1-butyne.

4.2.2 Lewis Acid Effects on Alkyne Metathesis of Small Molecules

From these data, it became clear that a different strategy for nitride/alkyne metathesis was necessary, and the choice of ligand may be critical. We previously reported that the Mo-alkylidyne Mo(CEt)[N(*t*-Bu)Ar]$_3$ in conjunction with an electron-poor phenol was extremely active toward alkyne metathesis.[2] With this in mind, we envisaged that Lewis acid complexation of Mo-nitrides, followed by ligand displacement with electron-poor phenols, may lead to enchanced rates of Mo-alkylidyne formation. Due to its ease of preparation, we decided on **2** as the Mo-nitride precursor of choice for use in catalytic reactions.

Reaction of **2** or **2-B** in toluene with 3 equiv 4-nitrophenol led to the precipitation of a red solid which was insoluble in non-coordinating solvents such as CCl_4 and toluene but very soluble in THF and MeCN. Attempts to metathesize this complex in any solvent were unsuccessful, possibly due to its insolubility in non-coordinating solvents and the known unreactivity of Mo-nitrides toward alkyne metathesis in coordinating solvents.[5] The insoluble solid, as well as the adducts with coordinating solvents, resisted attempts at crystallization, both from solution and *via* sublimation. However, reaction of **2** and **2-B** with 3 equiv 2-trifluoromethylphenol generated a complex souble in non-coordinating solvents. Attempts to crystallize these complexes were unsuccessful.

The metathesis activity of **2** versus **2-B** with 2-trifluoromethylphenol was tested for the effect of borane addition. The results are summarized in Table 4.1. It is clear that the presence of borane accelerates metathesis with alkynes. Notably, metathesis of the diarylalkyne 4(4-methoxyphenyl)phenylacetylene (Entries 5-6), which has not previously been reported to occur with Mo-nitrides, is rapid in the presence of $B(C_6F_5)_3$, establishing equilibrium at 90 °C *in 20 minutes*. By contrast, metathesis in the absence of borane led to less than 10% conversion after 12 h at 90 °C. Lewis acid activation of the nitride thus appears to be necessary to efficiently metathesize diarylalkynes.

Cross-metathesis of diphenylacetylene and 3-hexyne to generate 1-phenyl-1-butyne is also accelerated by the addition of borane (Table 4.1, Entries 3-4). The reaction of 10 equiv 3-hexyne with **2** or **2-B** and 2-trifluoromethylphenol at 90°C led

exclusively to alkyne polymerization and no alkylidyne was observed by ^{13}C NMR.

4.2.3 Lewis Acid Effects on Alkyne Metathesis Depolymerization-Macrocyclization

Our efforts in depolymerization of linear poly(arylene ethynylene)s led us to explore the effects of Lewis acid addition in alkyne metathesis depolymerization/macrocyclization (DPMAC). Polymer **4** (Scheme 4.3) was chosen as a case study due to the good solubility of **4** in most solvents and the typically excellent yields of macrocyclization from monomeric constituents.[20] Preactivation of the nitride with a small alkyne was necessary due to the relatively low concentration of the depolymerization reaction conditions; this was to assure that at least some alkylidyne was formed prior to depolymerization. The GPC results are shown in Figure 4.3. After 24 h, preactivation of the nitride with 2 equiv B(C$_6$F$_5$)$_3$ led to a lower PDI of the resultant polymer with more macrocycle formation, indicating higher initial alkylidyne formation.

4.3   Mechanistic Studies

4.3.1 Verification of Alkylidyne Formation

Proof of the overall transformation shown in Scheme 4.1 requires the verification of product formation. The best evidence would be the presence of an alkylidyne peak at ca. 300 ppm in the ^{13}C NMR; however, due to rotational equilibria of many alkylidynes and the low intensity of quaternary carbons, it can sometimes be

difficult to observe this peak. This peak was not observed in our studies. However, indirect evidence for alkylidyne formation *via* the formation of nitriles is also suitable. Reaction of **2-B**/Ph$_3$SiOH with 2 equiv 5-decyne (Scheme 4.4) demonstrates that alkyldyne is formed by monitoring the formation of valeronitrile by ^{1}H NMR (Figure 4.4). After 48 h at 90 °C, the conversion of 5-decyne to valeronitrile was 38%, significantly more than the "trace" amount found by Fürstner after 6 d at 110 °C in the absence of borane.[3] However, full conversion to alkylidyne was not observed.

4.3.2 Role of Lewis Acid

The rate-promoting nature of B(C$_6$F$_5$)$_3$ toward nitride-alkyne metathesis has been established. However, the mechanistic role of the Lewis acid in this reaction is unclear. Our attempts to understand this mechanism have been hindered by our inability to synthesize a metathesis-active, Lewis base-free Mo nitride, even though a few examples exist.[21]

Competition for the Lewis acidic borane by free Lewis bases may be a key mechanistic step (Scheme 4.5). When pendant ligands on precursor **2** are displaced by a phenol or silanol, the resulting amine and silanols are Lewis bases. Thus, a competition between these free Lewis bases and the Mo-nitride for the borane may exist. If this is the case, then the Lewis acid's main role is to inhibit free Lewis bases from coordinating to the molybdenum, thereby inhibiting nitride-alkyne metathesis.

A competition experiment was undertaken to explore the ultimate fate of the Lewis acid. When ^{15}N-labeled **1-B** was treated with 2 equiv pyridine in CD$_2$Cl$_2$ two

distinct peaks in the ^{15}N NMR with a 1.7 : 1 ratio formed (Fig. 4.5). The major peak at 427 ppm was free Mo-nitride **1**•pyridine, while the minor peak at 186 ppm was **1-B**•pyridine. Thus, Lewis base competition for borane can be envisaged.

However, in the absence of strong Lewis bases like pyridine, competition may not be an issue. A mixture of **1-B**, trifluoro-*o*-cresol (3 equiv), and diphenylacetylene (5 equiv) in toluene-d_8 was heated to 70 °C for 30 min. The ^{11}B peak shifted from -3.7 ppm before heating to -10.3 ppm after heating. This may indicate the formation of $B(C_6F_5)_3$•NCPh, but the linewidth of this peak (165 Hz) is far too narrow for a nitrile complexed with $B(C_6F_5)_3$ (~300-500 Hz).[14] However, it does not appear to be $HN(SiMe_3)_2$•$B(C_6F_5)_3$, which has a ^{11}B shift of 2.78 ppm ($LW_{1/2}$ = 321.17 Hz) in toluene-d_8. It is most likely that the peak at -10.3 ppm is $(ArO)_3MoN$•$B(C_6F_5)_3$, meaning that complete displacement with phenol requires heating. The mechanistic role of the Lewis acid is still unclear; future work will require the formation, characterization, and mechanistic analysis of a Lewis base-free, metathesis-active Mo nitride.

4.3.3 Attempts to Synthesize a Lewis Base-Free Molybdenum Nitride

Attempts to synthesize and characterize $MoN(OC(CF_3)_2Me)_3$,[5,21] to date the only fully-characterized metathesis-active Mo nitride lacking a Lewis base, were unsuccessful. We then turned to the Fürstner system $MoN(OSiPh_3)_3$ to see if it could be isolated. Reaction of **2** with 3 equiv Ph_3SiOH in ether led to the immediate precipitation of a white solid (Scheme 4.6). After filtration of this material, the filtrate

formed very large crystals suitable for X-ray crystallographic analysis. The crystals were shown to be $MoN(OSiPh_3)_3(H_2O)$ (**5**) (Figure 4.6), consistent with ^1H NMR analysis that indicated a broad singlet at 1.48 ppm with an integration of 2. Despite the dried starting materials, it is apparent that $MoN(OSiPh_3)_3$ is hygroscopic. However, also likely is the possibility that dehydration of the free Me_3SiOH molecules to form hexamethyldisiloxane and water leads to the formation of the aqua-complex. Addition of drying agents such as molecular sieves do not remove the bound water.

4.4　Conclusion

In summary, we have shown that the addition of the Lewis acid $B(C_6F_5)_3$ to Mo nitrides leads to enhanced rates of formation of Mo alkylidynes. The exact role of the borane is unclear; it is likely a combination of factors. Activation of the nitride towards metathesis and the prevention of free Lewis bases from Mo coordination are the two most likely possibilities. Future work will be devoted to studying the mechanistic role of the borane in this reaction.

4.5　Experimental Section

Materials. Unless otherwise stated, all starting materials and reagents were purchased from commercial sources and used without further purification. $MoN(OTMS)_2[N(TMS)_2]$ (**2**)[7], $MoN(Ot\text{-}Bu)_3$[19] (**3**) and polymer **4**[22] were prepared according to literature procedures. $B(C_6F_5)_3$ was purified by sublimation. All solvents were purified by degassing with Ar gas followed by passage through columns of

activated alumina and molecular sieves.

General Methods. All reactions were prepared in an argon-filled glove box and run under an inert atmosphere. The reaction vessels used, unless otherwise specified, were 5 mL vials fitted with PTFE/silicone septa. All glassware was oven-dried before use. Reactions were monitored by gas chromatography using dodecane as an internal standard.

Physical Characterization. ^{1}H NMR spectra were referenced to residual solvent peaks or TMS (δ = 0 ppm). ^{19}F NMR was calibrated using $CFCl_3$ (δ = 0 ppm) as an external standard. ^{11}B NMR was calibrated using $BF_3 \cdot Et_2O$ (δ = 0 ppm) as an external standard. Chemical shifts (δ) are expressed in parts per million (ppm). Splitting constants (J) are expressed in Hz. Splitting patterns are designated as s, singlet; d, doublet; t, triplet; dd, doublet of doublets; td, triplet of doublets; m, multiplet. ATR-IR was performed on isolated substrates without solvent. Gas chromatography samples were injected onto a capillary column. The injector temperature was 250 °C and the detector temperature was 280 °C with a H_2 carrier gas flow of 16 mL/min. The column temperature program was as follows: 100 °C for 3 min, ramp to 300 °C at 40 °C/min, then hold for 3 min for a total run time of 11.00 min.

Synthetic Procedures

$MoN(OTMS)_2[N(TMS)_2] \cdot B(C_6F_5)_3$ (2-B). In a glove box, **2** (50 mg, 0.111 mmol) was dissolved in dichloromethane (1 mL). $B(C_6F_5)$ (57 mg, 0.111 mmol) was added,

causing the pale yellow solution to darken slightly. Colorless crystals suitable for X-ray analysis were grown by slow diffusion of pentane into the solution at -30 °C under argon.

NMR (CD$_2$Cl$_2$, 400 MHz): ^{1}H: δ 0.317 (s, 18H); 0.141 (s, 18H). ^{19}F: δ -131.4 (d, J = 18.8 Hz, 6F); -159.8 (t, J = 18.8 Hz, 3F); -165.58 (td, J = 18.8 Hz, 7 Hz, 6F). ^{11}B: -3.43 (LW$_{1/2}$ = 135 Hz).

MoN(Ot-Bu)$_3$· B(C$_6$F$_5$)$_3$ (3-B). In a glove box, **3** (30 mg, 0.091 mmol) was dissolved in dichloromethane (1 mL). B(C$_6$F$_5$) (45 mg, 0.091 mmol) was added, causing the colorless solution to turn yellow. Colorless crystals suitable for X-ray analysis were grown by slow diffusion of pentane into the solution at -30 °C under argon; these crystals decomposed quickly when taken out of solution. Crystallographic analysis indicated that crystals of **3-B** contained one highly disordered pentane per asymmetric unit which could not be suitably refined; prior to final refinement, the pentane was removed using PLATON/SQUEEZE.[23]

NMR (CD$_2$Cl$_2$, 400 MHz): ^{1}H: δ 1.313 (s). ^{19}F: -132.0 (dd, J = 24 Hz, 8 Hz); -159.3 (t, J = 24 Hz); -165.6 (td, J = 24 Hz, 8 Hz). δ. ^{11}B: -4.28 (LW$_{1/2}$ = 114 Hz). IR (ATR, cm^{-1}): 2986, 1644, 1516, 1457, 1394, 1367, 1282, 1244, 1155, 1058, 974, 935, 914, 858, 790, 770, 738, 678. Anal. Calc'd for C$_{30}$H$_{27}$BF$_{15}$MoNO$_3$: C 42.83, H 3.23; N 1.66; Found: C 42.54, H 3.26, N 1.70.

Typical procedure for alkyne metathesis screens in Table 1, Entries 1, 3, and 5.

In a glove box, **2** (10 mg, 0.022 mmol) was dissolved in toluene (1 mL). $B(C_6F_5)_3$ (22 mg, 0.044 mmol) was added and the solution stirred until the $B(C_6F_5)_3$ dissolved. 2-trifluoromethylphenol (11 mg, 0.066 mmol) was added, resulting in a distinct color change from yellow to deep red. Dodecane (20 μL) and alkyne(s) (0.22 mmol) were added, the vial sealed, and heated to 90 °C. For Entry 3, 0.22 mmol each of diphenylacetylene and 3-hexyne were added. 20 μL aliquots of the reaction mixture were diluted to 1 mL with EtOAc and analyzed by gas chromatography.

Typical procedure for alkyne metathesis screens in Table 1, Entries 2, 4, and 6. Same as above, but with no $B(C_6F_5)_3$ added.

Depolymerization of 4. To a 20 mL vial with septum-topped cap, **1** (26 mg, 0.026 mmol) was dissolved in 1 mL toluene, followed by the addition of $B(C_6F_5)_3$ (26 mg, 0.052 mmol) and diphenylacetylene (10 mg, 0.056 mmol). The vial was sealed and heated to 90 °C for 20 minutes. The solution was cooled, diluted with 4 mL of toluene, and **4** (100 mg, 10 equiv) was added under Ar gas. The solution was stirred for 48 h at 60 °C. 0.5 mL aliquots were removed periodically and their solvent was removed prior to GPC analysis.

Preparation of 5. **1** (0.5 g, 1.11 mmol) was dissolved in 10 mL ether. Ph_3SiOH (0.921 g, 3.33 mmol) was then added and the solution was stirred for 48 h at room temperature. The resulting white precipitate was filtered and washed with ether.

NMR (CD_2Cl_2, 500 MHz, -20 °C): ^{1}H: δ 7.57. (m, 18H), 7.36 (t, J = 8 Hz, 7H), 7.28 (t, J = 9 Hz, 4H), 7.19 (t, J = 8 Hz, 11H), 7.06 (t, J = 8 Hz, 5H). ^{13}C: δ 136.4, 136.0, 135.4, 135.2, 134.9, 130.2, 130.0, 129.6, 128.0, 127.7, 109.8.

The filtrate was allowed to sit for a week, upon which time crystals of $MoN(OSiPh_3)_3(H_2O)$•Et_2O appeared. The ether was highly disordered and electron densitiy in the solvent region was subsequently removed using SQUEEZE.[23]

Crystal Data

Crystal data for **2-B**: $C_{30}H_{36}BF_{15}MoN_2O_2Si_4$, M = 960.70, monoclinic, space group $P2_1/n$, a = 14.367(5) Å, b = 17.170(6) Å, c = 16.896(6) Å , $β$ = 92.256(9)°, V = 4165(2) Å^3, Z = 4, D_c = 1.532 g cm^{-3}, $μ$(Mo-K) = 0.527 mm^{-1}, F(000) = 1936, T = 193 K. R1 (I > 2σ) = 0.0541, wR2 (all data) = 0.1559 for 7582 independent reflections with a goodness-of-fit of 1.032.

Crystal data for **3-B**: $C_{30}H_{27}BF_{15}MoNO_3$, M = 841.27, orthorhombic, space group Fdd2, a = 21.3488(18) Å, b = 66.889(5) Å, c = 10.0299(10) Å , V = 14323(2) Å^3, Z = 16, D_c = 1.561 g cm^{-3}, $μ$(Mo-K) = 0.476 mm^{-1}, F(000) = 6720, T = 193 K. R1 (I > 2σ) = 0.0472, wR2 (all data) = 0.0866 for 6055 independent reflections with a goodness-of-fit of 0.962.

Crystal Data for 5: $C_{54}H_{47}MoNO_4Si_3$•Et_2O, M = 1028.26, monoclinic, space group

*P*2$_1$/*c*, *a* = 10.2077(6) Å, *b* = 26.9638(13) Å, *c* = 19.8601(9) Å , *β* = 102.642(2)° *V* = 5333.7(5) Å^3, *Z* = 4, *D*$_c$ = 1.28 g cm^{-3}, *μ*(Mo-K) = 0.361 mm^{-1}, *F*(000) = 2144, *T* = 193 K. R1 (*I* > 2σ) = 0.0380, wR2 (all data) = 0.0937 for 11765 independent reflections with a goodness-of-fit of 1.047.

4.6   Figures and Schemes
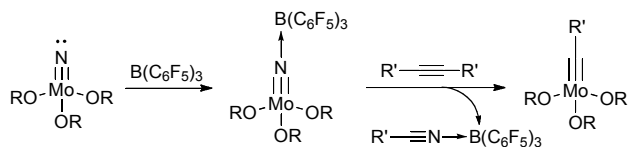
Scheme 4.1. Promotion of molybdenum nitride-alkyne metathesis by precomplexation with borane.
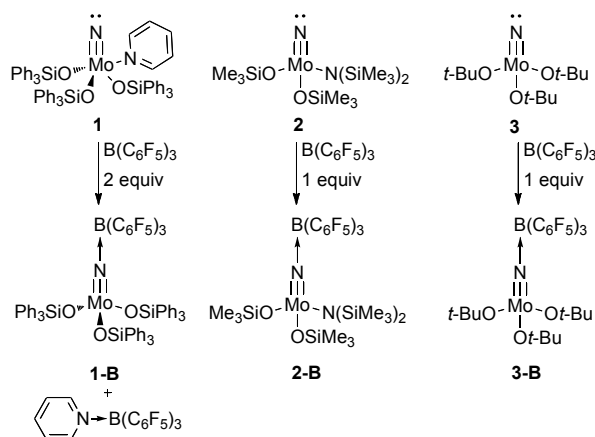
Scheme 4.2. Reactions of various Mo-nitrides with $B(C_6F_5)_3$.
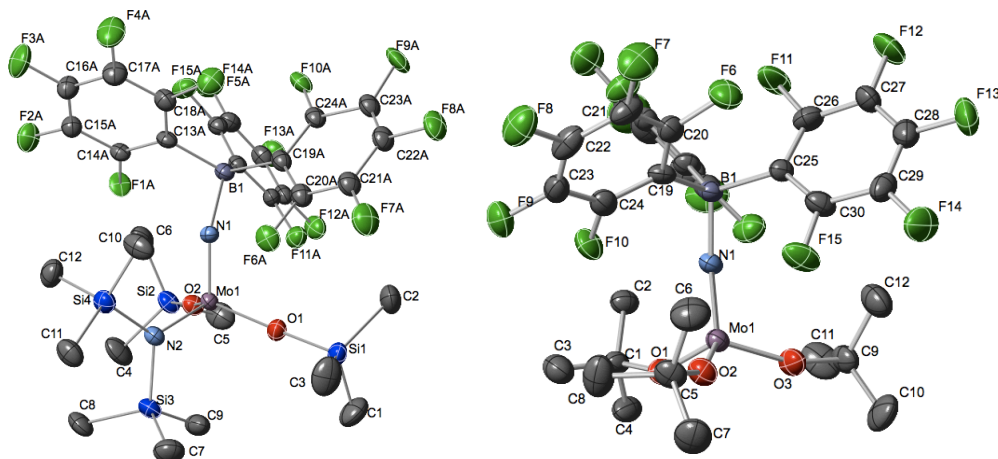
Figure 4.1. Thermal ellipsoid plots (35% probability) of (a) **2-B** (left) and (b) **3-B** (right).

%T

1150 1100 1050 1000 950 900 850

Wavenumber cm-1

1019

936

3
3-B
B(C₆F₅)₃
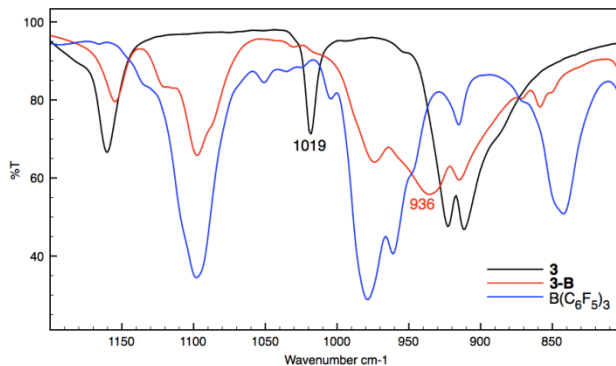
Figure 4.2. ATR-IR spectra of **3**, **3-B**, and (C₆F₅)₃. The reported (for **3**)[19] and proposed (for **3-B**) Mo≡N stretches are labelled.

Table 4.1. Effect of borane addition on alkyne metathesis

$$R_1 \!\!-\!\!\!\equiv\!\!\!-\!\! R_2 + R_3 \!\!-\!\!\!\equiv\!\!\!-\!\! R_4 \xrightleftharpoons[\text{toluene, 90 °C}]{\substack{\textbf{2}\,(10\text{ mol \%}) \\ 2\text{-(CF}_3)\text{C}_6\text{H}_4\text{OH (30 mol \%)} \\ \text{B(C}_6\text{F}_5)_3\ (0\text{-}20\text{ mol \%})}} R_1 \!\!-\!\!\!\equiv\!\!\!-\!\! R_3 + R_2 \!\!-\!\!\!\equiv\!\!\!-\!\! R_4$$

Entry	R₁	R₂	R₃	R₄	Borane[a]	convn (%) 1 h[b]
1	Ph	Et	Ph	Ph	**2-B**	64
2	Ph	Et	Ph	Ph	**2**	29
3	Ph	Ph	Et	Et	**2-B**	55
4	Ph	Ph	Et	Et	**2**	3
5	Ph	4-OMePh	Ph	4-OMeC₆H₄	**2-B**	51
6	Ph	4-OMePh	Ph	4-OMeC₆H₄	**2**	8

[a] **2-B** was made *in-situ* from 10 mol% of **2** and 20 mol% B(C₆F₅)₃. [b] percent conversion of starting material (R₁–≡–R₂) by GC after 1 h.
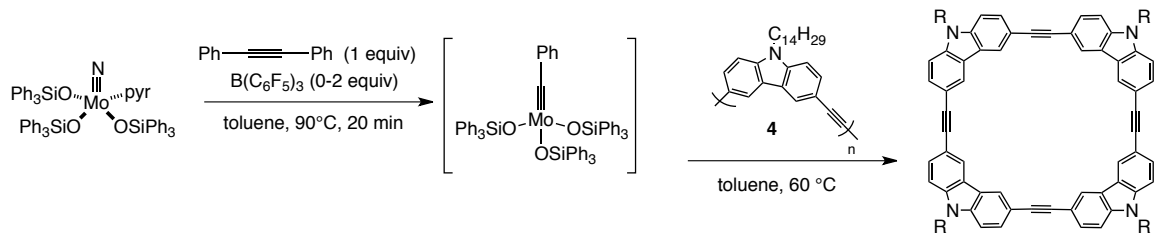
Scheme 4.3. Alkyne metathesis depolmyerization with a Lewis acid-activated molybdenum nitride.

GPC of AM Depolymerization of C14-Carbazoleethynylene

Legend:
- SM
- Macrocycle
- After 24 h at 60°C
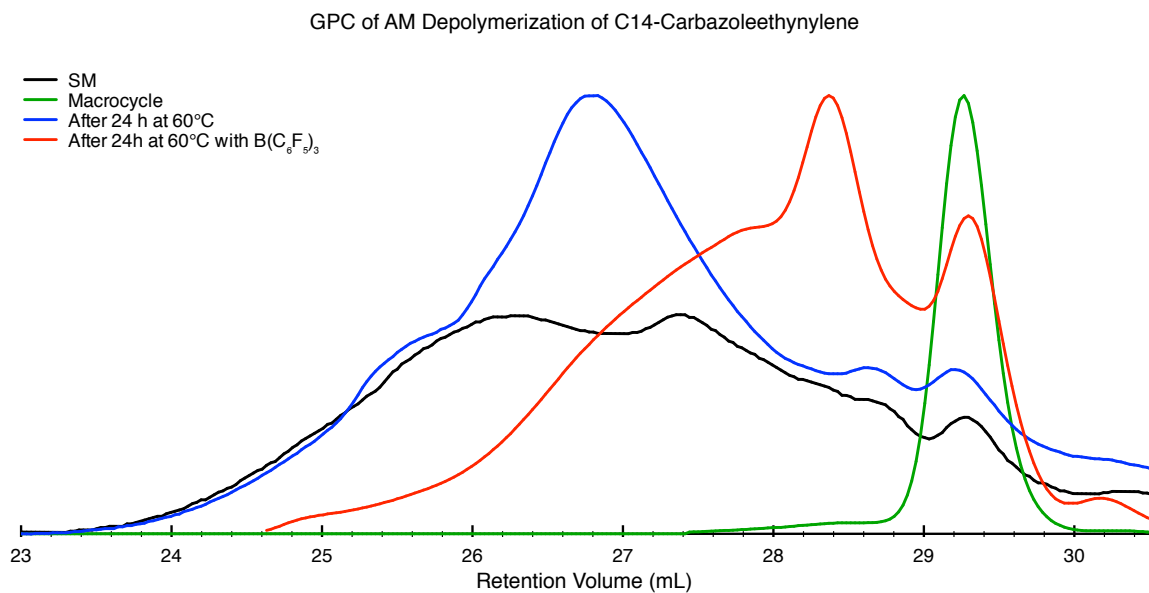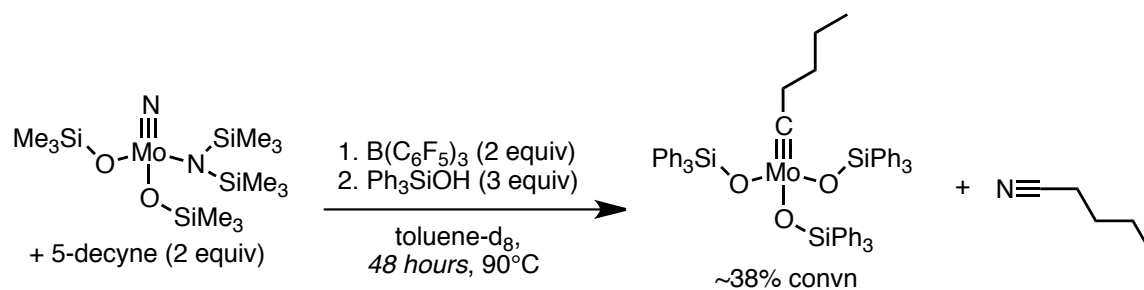- After 24h at 60°C with B(C$_6$F$_5$)$_3$

Retention Volume (mL)

Figure 4.3. Comparison of GPC traces of alkyne metathesis depolymerization of **4** with and without the addition of borane.

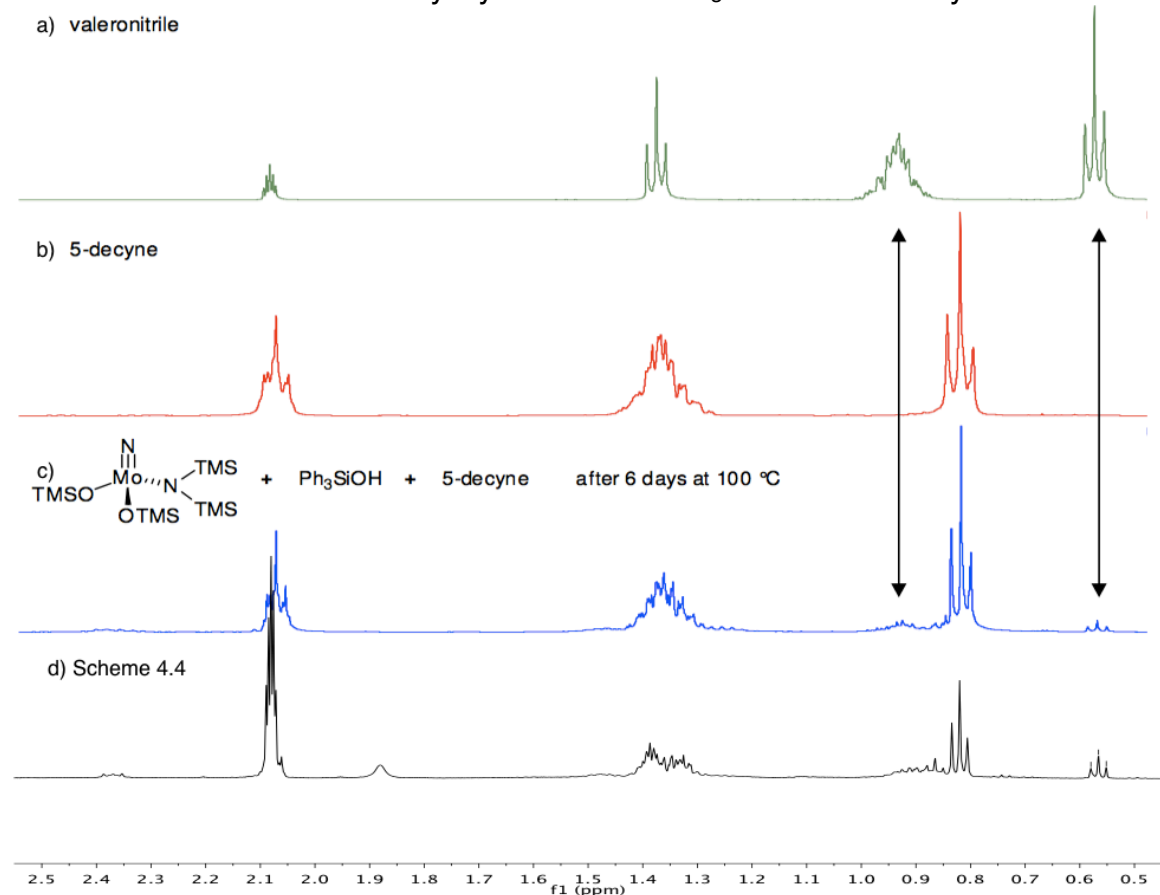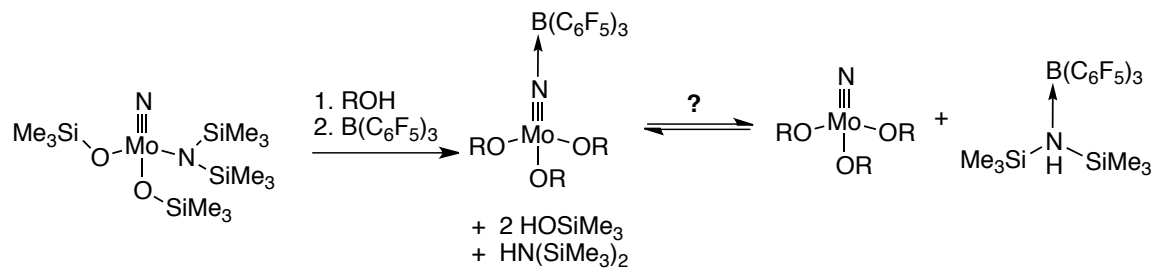**Scheme 4.4.** Formation of alkylidyne from **2-B**/Ph₃SiOH and 5-decyne.

Figure 4.4. Comparison of the ¹H NMR spectra of the reaction of **2**/Ph₃SiOH in the absence and presence of borane. (Parts a), b), c) from Ref. 3, Used with permission. Copyright 2010, American Chemical Society.)

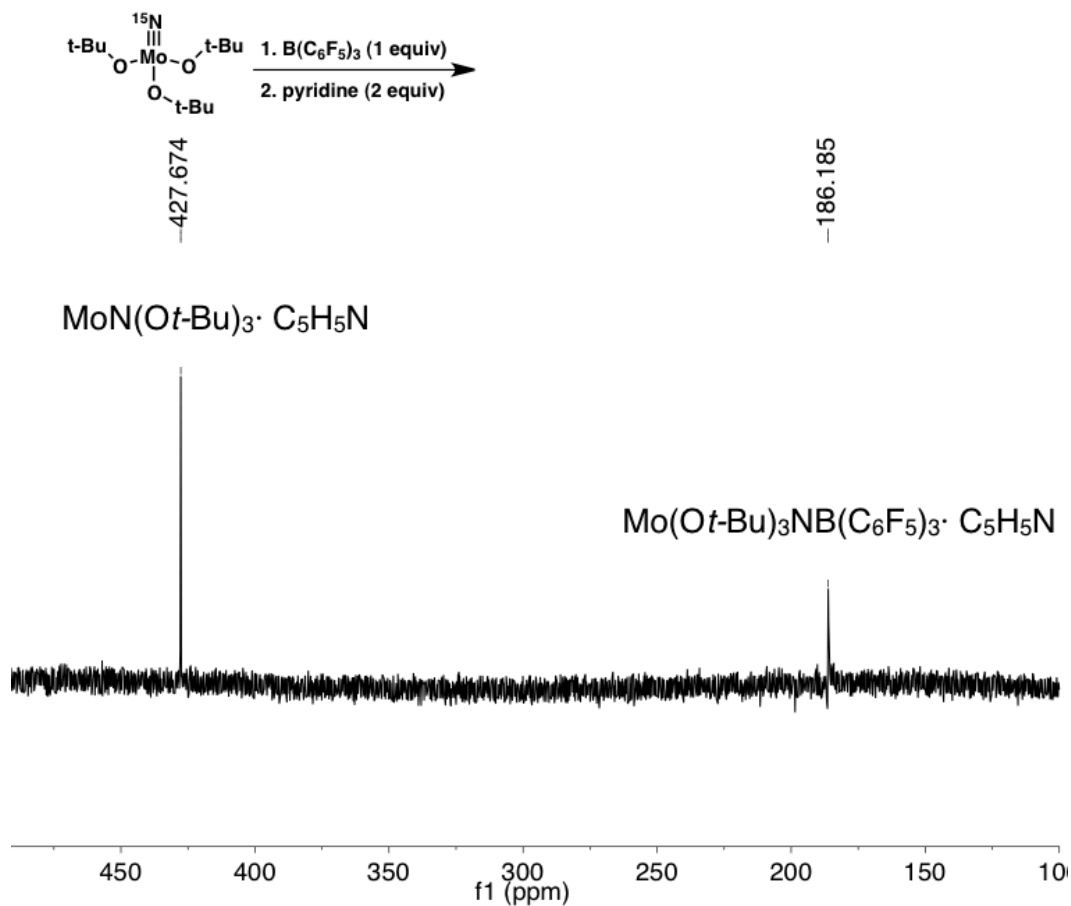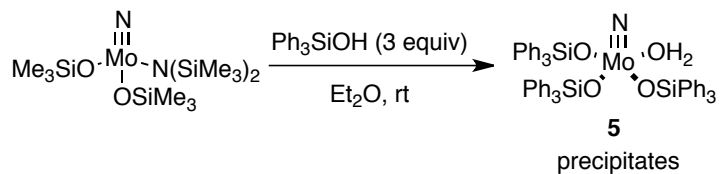**Scheme 4.5**. Competition for Lewis acid from free amine in solution.

MoN(O*t*-Bu)₃· C₅H₅N

Mo(O*t*-Bu)₃NB(C₆F₅)₃· C₅H₅N

Figure 4.5. ^{15}N NMR of the reaction of **1-B** with pyridine.

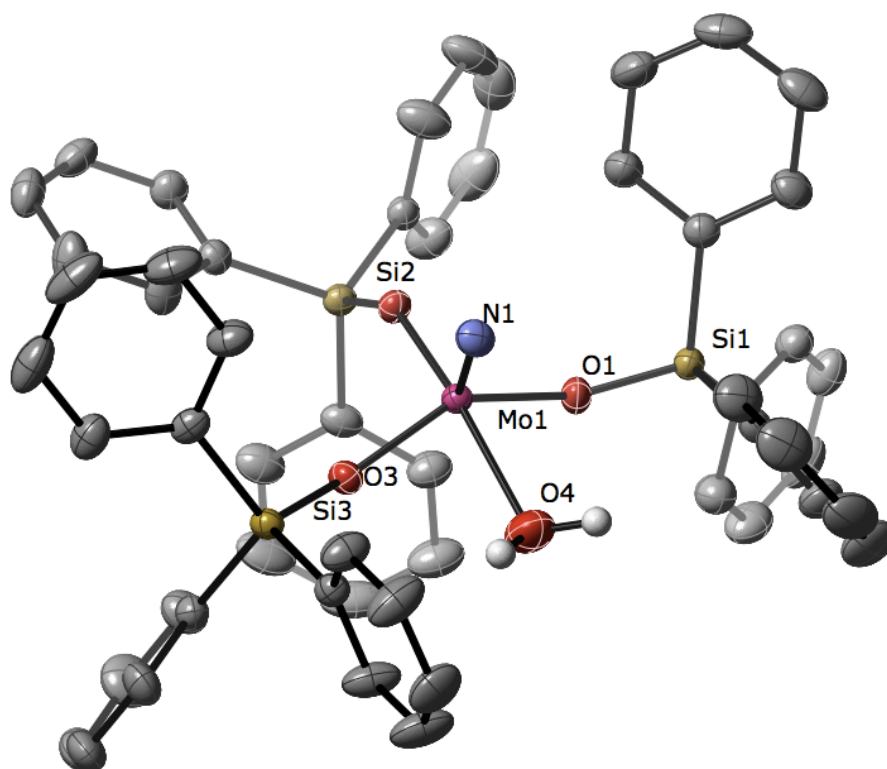**Scheme 4.6.** Formation of **5**.

Figure 4.6. Ellipsoid plot (50% probability) of **5**. Phenyl hydrogens omitted for clarity.

4.7   References

[1]   Fürstner, A. In *Handbook of Metathesis*; Grubbs, R. H., Ed.; Wiley-VCH: Weinheim, 2003; Vol. 2, p 432-462.

[2]   Zhang, W.; Kraft, S.; Moore, J. S. *J. Am. Chem. Soc.* **2004**, *126*, 329-335.

[3]   Heppekausen, J.; Stade, R.; Goddard, R.; Fürstner, A. *J. Am. Chem. Soc.* **2010**, *132*, 11045-11057.

[4]   Dehnicke, K.; Strähle, J. *Angew. Chem., Int. Ed. Engl.* **1992**, *31*, 955-978.

[5]   Gdula, R. L.; Johnson, M. J. A. *J. Am. Chem. Soc.* **2006**, *128*, 9614-9615.

[6]   Freudenberger, J. H.; Schrock, R. R. *Organometallics* **1986**, *5*, 398-400.

[7]   Bindl, M.; Stade, R.; Heilmann, E. K.; Picot, A.; Goddard, R.; Fürstner, A. *J. Am. Chem. Soc.* **2009**, *131*, 9468-9470.

[8]   Benchelck, A.; Petit, M.; Mortreux, A.; Petit, F. *J. Mol. Catal.* **1982**, *15*, 93-101.

[9]   Bly, R. K.; Dyke, K. M.; Bunz, U. H. F. *J. Organomet. Chem.* **2005**, *690*, 825-829.

[10]   Yoshida, T.; Adachi, T.; Yabunouchi, N.; Ueda, T.; Okamoto, S. *J. Chem. Soc., Chem. Commun.* **1994**, 151-152.

[11]   Sceats, E. L.; Figueroa, J. S.; Cummins, C. C.; Loening, N. M.; Wel, P. V. d.; Griffin, R. G. *Polyhedron* **2004**, *23*, 2751-2768.

[12]   Doerrer, L. H.; Graham, A. J.; Green, M. L. H. *J. Chem. Soc., Dalton Trans.* **1998**, 3941-3946.

[13]   Sarkar, S.; Abboud, K. A.; Veige, A. S. *J. Am. Chem. Soc.* **2008**, *130*, 16128-16129.

[14]   Jacobsen, H.; Berke, H.; Döring, S.; Kehr, G.; Erker, G.; Fröhlich, R.; Meyer, O. *Organometallics* **1999**, *18*, 1724-1735.

[15]   Erker, G. *Dalton Trans.* **2005**, 1883-1890.
[16]   Vela, J.; Lief, G. R.; Shen, Z.; Jordan, R. F. *Organometallics* **2007**, *26,* 6624–6635.
[17]   Chiu, H.-T.; Chuang, S.-H.; Lee, G. H.; Peng, S. M. *Adv. Mater.* **1998**, *10,* 1475-1479.
[18]   Allen, F. A. *Acta Crystallogr., Sect. B: Struct. Sci.* **2002**, *58,* 380-388.
[19]   Chan, D. M.-T.; Chisholm, M. H.; Felting, K.; Huffman, J. C.; Marchant, N. S. *Inorg. Chem.* **1986**, *25,* 4170–4174.
[20]   Zhang, W.; Moore, J. S. *J. Am. Chem. Soc.* **2004***, 126,* 12796-12796.
[21]   Gdula, R. L.; Johnson, M. J. A.; Ockwig, N. W. *Inorg. Chem.* **2005**, *44,* 9140–9142.
[22]   Brizius, G.; Kroth, S.; Bunz, U. H. F. *Macromolecules* **2002**, *35,* 5317-5319.
[23]   Spek, A. L. *J. Appl. Cryst.* **2003**, *36,* 7-13.

Chapter 5

Crystallographic Analysis of Carbazole-Ethynylene Macrocycles

5.1.   Introduction

Shape-persistent macrocycles (SPMs) constitute a distinct class of small molecule architectures whose properties can emulate analogous architectures of higher order such as polymers, but with better control of covalency.[1-5] The use of SPMs as functional materials has benefited from recent advancements in their preparative methods. Traditionally, widespread utilization of SPMs was hindered by tedious preparation, often requiring dilute conditions, small scales, and difficult separations. The recent implementation of methodologies wherein the bond-formation event is under thermodynamic control, otherwise known as dynamic covalent chemistry,[6] has enabled a diverse array of macrocycles to be generated from simple precursors in a less synthetically rigorous manner. Our laboratory has developed an alkyne metathesis-based approach to the dynamic covalent formation of arylene ethynylene macrocycles (AEMs). This method has also proven useful and efficient for large-scale preparation.[7-10]

The functional applications of many conjugated systems are directly tied to their solid-state packing; thus, rigorous characterization of functional small molecules in the solid state is critical to optimization of bulk properties.[11] Despite major efforts, structure-property analysis to relate chemical identity with a particular solid-state interaction remains difficult. The identity of all components of the molecule contribute to overall solid-state packing. For example, the attachment of alkyl chains to large aromatic

moieties is typically utilized to enhance solubility and ease of processing. However, such derivation can lead to a dramatic change in solid-state properties. One dramatic example reported by Anthony is the functionalization of pentacene with silylalkynes, which changes the solid-state packing from the orthogonal "herringbone" motif to one in which cofacial interactions are dominant, leading to increases in charge-carrier mobility in the solid state.[12,13]

One major advantage of functional small molecules over less well-defined materials is the ability to explore intermolecular interactions in a highly accurate way using X-ray crystallography. The first AEM characterized by X-ray crystallography, a *m*-phenylene ethynylene [6]cycle bearing phenol groups, assembles to form porous cavities generated by hydrogen bond interactions.[14] Subsequent crystallographic investigations of SPMs have demonstrated a significant diversity in the solid-state packing of this class of materials.[14-22]

In this chapter, we present an extensive crystallographic investigation of AEMs containing a carbazole-ethynylene backbone (**1**) (Fig. 5.1). We recently reported that AEMs of this type readily form fluorescent nanofibril aggregates that rapidly quench in the presence of explosive vapors such as DNMB. It is thought that the quenching event is due to electron transfer through aggregation of the pi-system brought about by pi-pi stacking interactions through the macrocycle backbone. However, the nature of these interactions is unclear. Herein, we demonstrate, using X-ray crystallographic analysis, that packing of **1** in the solid state is highly dependent on the choice of side chain. Co-crystals of **1**-containing macrocycles with strong organic acceptors, which act as a

model system for the interaction of electron-poor guests with these host materials, have also been characterized and investigated. Furthermore, for the first time, we demonstrate the polymorphism of an AEM, in this case of macrocycle **2**, as a caveat of the limitations of crystallographic analysis of small molecules.

Crystallographic investigations of SPMs are highly sought-after, due not only to the insights such investigations give, but also because of the relative paucity of crystallographic data of such materials. The preparation and analysis of SPM-containing crystals can be quite challenging. Some systems do not crystallize at all; attempts to grow macrocycles containing **1** with pendant tetradecyl or ACTC ($CO_2C(CH_3)_2C_{11}H_{23}$) chains, both of which are of great interest due to their application as fluorescent sensors, have been unsuccessful. SPMs containing alkyl chains which lack order can lead to difficulty in their refinement. Furthermore, the shape-persistence and large size of SPMs generally leads to the formation of cavities in which volatile, disordered solvent can reside. Such "solvated" crystals, if not treated properly, can decompose in seconds when taken out of solution.[19]

5.2 Synthesis and Crystal Preparation

Macrocycles **1** were prepared *via* precipitation-driven alkyne metathesis of precursors bearing functionalities that precipitate from solution upon cross-metathesis, a process developed in our laboratory (Scheme 5.1).[8] The synthetic protocol is modular and allows for a library of monomer units with differing alkyl chains to be prepared in a straightforward manner. Following Fürstner's reports,[23,24] we have found that Mo

alkylidynes bearing triphenylsilyloxy ligands make superior alkyne metathesis catalysts, with greater efficiency and tolerance compared to previously-used phenoxy ligands. Yields of macrocyclization were generally good.

The solubilities of the macrocycles were highly dependent on the identity of the alkyl chain. Macrocycle **4** exhibited excellent solubility in a range of solvents; however, the solubilities of **2** and **3** were limited to halogenated solvents.

Crystals suitable for X-ray diffraction were obtained by slow diffusion of ether into a solution of **2-4** in a halogenated solvent, typically dichloromethane, at room temperature over several days. The crystals were uniform in quality, without apparent polymorphism (except for **2**). The lack of *ordered* heavy atoms in **1** precluded the use of Mo radiation for all but large and high-quality crystals; the use of Cu sources were required for the others. (It should be noted that in **3**, the DCM solvent was quite ordered and the quality of the data using Mo radiation reflects this.) The shape-persistent cavity in **1** led us to explore the effects of small molecule incorporation into crystals of **1**. Thus, crystals of **2** with azobenzene guest and **4** with the strong acceptors *p*-chloranil and TCNQ were also prepared, in a similar manner to **2-4**. A summary of crystallographic data is presented in Table 5.1.

5.3   Crystal Structures of Carbazole-Containing Macrocycles

5.3.1 Crystals of the C$_{10}$[4]cycle

Crystals of **2** gave two polymorphs: long, thin rods (**2a**), which contained one long crystal axis; and hexagonal plates (**2b**), which contained two. **2a** was indefinitely stable

after removal from solution; by contrast, **2b** rapidly decomposed upon removal from solution, becoming striated within a few minutes and opaque within an hour. However, crystals of **2b** were stable when rapidly cooled to -100 °C and immersed in inert oil.

2a crystallizes in the monoclinic space group $P2_1$ (Fig. 5.2). The macrocycle is mostly planar with a macrocycle plane deviation of 0.10 Å (the macrocycle plane is defined as the least-squares plane of the non-hydrogen atoms of the macrocycle, not including the pendant alkyl chains; the deviation from this plane is the standard deviation of all atoms that define the plane). The molecule adopts a chair-like orientation, with the alkyl chains propagating nearly perpendicularly to the macrocycle plane. The two macrocycles in the unit cell are related by a twofold screw axis. The packing consists of two stacks of parallel macrocycles whose macrocycle planes intersect at 75.5° (Fig. 3a). The macrocycle rows propagate along the *a*-axis. Along the *b*-axis, there are alternating stacks of macrocycles and alkyl chains; the alkyl chains are also arranged in parallel rows propagating down the *a*-axis. The ends of two of the alkyl chains on one side are slightly disordered. Rows of macrocycles are not parallel down the *c*-axis, leading to a "staggered" arrangement; this leads to an arrangement where an alkyl chain lies above and below the middle of the macrocycle (Fig. 3b). This arrangement turns out to be critical to understanding solvent effects in the crystal.

The interior cavity of each macrocycle contains one disordered dichloromethane. The solvent positions in **2a** were unable to be accurately determined and thus the electron density present in the disordered solvent regions was removed using the solvent bypass ("SQUEEZE") procedure in PLATON.[25] Despite the fact that **2a** contains

free, disordered solvent, the crystals appear to not decompose even after several weeks of sitting under oil and ambient conditions. This could be due to several factors not yet explored: the solvent may be "trapped" in the macrocycle cavity and unable to escape; or, if the solvent were to escape, the overall crystallinity would not be affected and the resulting void space would be filled by something else.

The following experiment illustrates that both of the above factors may be in play. Crystals of **2a** were immersed in methanol for several weeks; the resulting crystals **2a·MeOH** were then characterized by X-ray diffraction (Fig. 5.4). The DCM was replaced by disordered MeOH as evidenced by the electron count given by SQUEEZE;[25] as in **2a**, the solvent positions in **2a·MeOH** were unable to be accurately determined and thus the electron density present in the disordered solvent regions was removed. **2a·MeOH** crystallized in the space group $P2_1$, the same as **2a·DCM**, with similar unit cell parameters; the unit cell volume of **2a·MeOH** (V = 4110.6 Å^3) is smaller than **2a** (V = 4094.8 Å^3) by only 15.8 Å^3.

Most notable in the structure of **2a·MeOH** is the extreme disorder of the alkyl chain C(67)–C(76), where it is much more disordered than in **2a**. A model wherein the full alkyl chain was disordered about two positions with isotropic displacement restraints gave the best refinement statistics. The disorder can be rationalized as follows. In the crystal, the disordered alkyl chains lie above and below the macrocycle cavity (Fig. 5.5). The unit cell volume change of 15.8 Å^3 is less than the difference in volume between two dichloromethanes (V_{DCM} = 76.8 Å^3) and two methanols (V_{MeOH} = 51.2 Å^3), where

$$2\ V_{diff} = 2(76.8\ \text{Å}^3 - 51.2\ \text{Å}^3) = 51.2\ \text{Å}^3$$

Thus, the alkyl chains are likely disordered to accommodate for the volume change. This may indicate that crystals of **2a** are indefinitely stable due to alkyl chain disorder preventing destruction in crystallinity. A visualization of the solvent volumes in **2a**·DCM and **2a**·MeOH (Fig. 5.6) is illustrative. Note that in **2a**·MeOH, the disordered alkyl chain appears to be responsible for the diminished void volume.

The morphology of **2b**, a polymorph of **2a**, is fascinating. **2b** crystallizes in the higher-symmetry space group *C*2/c; half the macrocycle is related by inversion symmetry (Fig. 5.7). As with **2a**, the macrocycle is mostly planar with a macrocycle plane deviation of 0.07 Å. The molecule again adopts a chair-like orientation, and the overall packing motif is similar along the *a*- and *b*-axes. However, the packing along the *c*-axis is not staggered as in **2a**, but aligned; this means that alkyl chains no longer lie near the macrocycle cavity, but rather along an edge of the macrocycle. This leads to expansive solvent "channels" in the crystal, which propagate indefinitely along the *b*-axis (Fig. 5.8). The solvent channels are created by alternating rows of macrocycle and alkyl chains; there appear to be significant interactions between alkyl chain and macrocycles (Fig. 5.9). DCM solvent prevents collapse of the alkyl chains into the cavity; thus, when crystals of **2b** are removed from solvent, crystallinity is quickly lost. It is likely that collapse of **2b** leads to **2a**; however, we have not yet been able to verify that such a crystal-to-crystal transformation can occur.

It should be stressed that the crystals of **2a** and **2b** were grown from the *same solution* under the *same conditions*. The remarkably large solvent channels present in

2b are absent in **2a**; this should serve as a caveat that a single crystal study may not tell the entire story of the solid-state chemistry of a novel material.

5.3.2 Crystals of the C$_6$[4]cycle

Slow diffusion of ether into a solution of **3** in DCM gave large prisms **3**·DCM that diffracted Mo X-rays very well- much better than the other macrocycles studied in this report. Refinement statistics for crystals of **3** were superior to the other samples as a result. These crystals were not stable when removed from solution and lost crystallinity within hours, indicative of a solvated complex.

3·DCM crystallizes in the triclinic space group *P*-1 (Fig. 5.10). Half the macrocycle is related by inversion symmetry. **3**·DCM forms ordered slip-stacks of macrocycles. In stark contrast to **2**, cofacial interactions between macrocycles dominate the packing motif, indicated by the short distance between macrocycle planes (3.296 Å) (Fig. 5.11). By contrast, the distance between two macrocycles in **2b** is much longer, 7.23 Å, due to alternating alkyl chain-macrocycle packing; thus, in **2b**, alkyl chain-macrocycle interactions dominate (2.9 Å). Also unique in **3** is the lack of disordered solvent; as in the other crystals, DCM was located within the cavity of the macrocycle. However, **3**·DCM was the only case in this study where positions for a solvent molecule guest were able to be refined acceptably. Hirschfeld surface analysis indicates that close contacts from hydrogens in the DCM guest to the macrocycle host may be responsible for the ordered solvent.

Crystals of **3·DCE** were grown from diffusion of ether into a solution of 1,2-dichloroethane (**3·DCE**). The solvent guest was much more disordered in this case compared to **3·DCM**. **3·DCE** is unique in that one of the carbazoles in the macrocycle is disordered away from the macrocycle plane (Fig. 5.12). This led to the pendant alkyl chain being disordered as well. This may be due to a solvent effect, as the disordered carbazole is adjacent to the solvent-containing cavity of the macrocycle and there appears to be close contact between the carbazole and the solvent.

That cofacial aromatic-aromatic interactions would increase as alkyl chain length decreases is a sensible explanation for the changes in crystal morphology from **2** to **3**. These results indicate that the length of the C_{10} chain may give rise to novel morphologies such as **2b** due to the similar lengths of the ordered C_{10} chain (11.435 Å) and the macrocycle (lateral N-N distance 12.298 Å). One may presume that as these alkyl chains get shorter, aromatic interactions will completely dominate the packing motif; upon complete removal of the alkyl chain, one may expect columnar architectures like those found in phenol-containing *m*-phenylene ethynylene [6]cycles. A systematic series of macrocycles containing **1** with varying alkyl chain lengths is forthcoming. Attempts to crystallize a macrocycle containing C_9 alkyl chains has as of yet been unsuccessful.

5.3.3 Crystals of the Tg[4]cycle

As shown above, alkyl chain length affects the morphology of crystals containing **1**. However, the identity of the atoms within the chain can also have a major impact on

the packing. We have demonstrated the utility of the Tg (triethylene glycol monomethyl ether) group as a useful solubilizing group for extended *m*-phenylene-ethynylene oligomers, in particular for foldamers.[26] The polyether Tg group allows for high solubility of oligomers in a variety of solvents of moderate polarity, including acetone, THF, and acetonitrile. As a result, **4** displayed the highest solubility of any **1**-containing macrocycle synthesized thus far. Crystals of **4** were grown from DCM/ether; long needles were obtained. Crystals of **4**·DCM were indefinitely stable when taken out of solution and immersed in inert oil.

4·DCM crystallizes in the monoclinic space group $P2_1/c$ (Fig. 5.13). The macrocycle lies on an inversion center. The most notable aspect of **4** is the lack of order in the Tg chain- both chains of the asymmetric unit are highly disordered. This disorder hints at one reason the Tg group is an excellent solubilizing group for aromatic compounds; Tg-aromatic interactions are far less pronounced than Tg-Tg interactions. The alkyl-aromatic interactions present in **2** are not as present as in **4**, nor are the aromatic cofacial interactions seen in **3**. The severe disorder and random orientation makes it appear that the Tg group is acting merely as a "space-filler" for the crystal; the Tg groups appear to be in different "domains" than the macrocycle, akin to phase separation (Fig. 5.14). This makes sense due to the large difference in polarity between the polar Tg group and the nonpolar macrocycle.

5.4   Host-Guest Macrocycle Co-Crystals

5.4.1 C_{10}[4]cycle : Azobenzene

To gain insight into the nature of the interactions of macrocycle hosts and guest molecules, a number of host-guest co-crystals were prepared. The possibility of **2** acting as a molecular host where guests reside in the cavity of the crystals was explored using a relatively nonpolar chromophore, azobenzene. **2**•azobenzene was prepared by dissolving a small amount of **2** in a saturated solution of azobenzene in DCM. Orange plates formed of a single morphology. **2**•azobenzene crystallizes as a 1:1 **2**:azobenzene co-crystal in the monoclinic space group $P2_1/n$ (Fig. 5.15). There was no solvent present in the crystals. The packing motif is similar to **2a**, with alternating macrocycle-alkyl chain packing. However, these stacks do not run parallel down a crystallographic axis like in **2a-b**; they are distorted a bit due to the presence of the azobenzene (Fig. 5.16). Interestingly, the azobenzene does not reside in or near the cavity of the macrocycle, but rather in between the macrocycles! This leads to the distorted, nonparallel alignment. Alkyl chains reside within the macrocycle cavity, leading to no void spaces for solvent to reside. These cavity-filling alkyl chains are disordered as a result.

5.4.2 Tg[4]Cycle : *p*-Chloranil

To investigate the effects of electronics on co-crystal formation, co-crystals of **1** with electron-poor aromatics were investigated. Slow diffusion of ether into a solution containing **4** in DCM saturated with *p*-chloranil gave mostly crystals of **4**. One deep blue crystal **4**•chloranil also formed, which was mechanically separated and analyzed by X-

ray diffraction. **4**•chloranil was a 1:1 **4**:chloranil co-crystal that crystallized in the space group $P2_1/n$ (Fig. 5.17). The blue color is indicative of the formation of a charge-transfer complex. As with **4**, the Tg groups in **4**•chloranil were disordered and displayed little regularity. The chloranil lies in between two macrocycle planes with a distance of 3.41 Å (Fig. 5.18), directly above and below the carbazole. This indicates that the carbazole part is the most electron-rich part of the macrocycle. Geometrically, the macrocycle itself is distorted; it adopts a saddle shape with a macrocycle plane deviation of 0.21 Å, much larger than seen in **4** (0.048 Å). We first assumed that this was due to electronic effects due to the charge-transfer complex, but the planarity of **4**•TCNQ (see below) suggests otherwise. It actually appears to be a steric effect from an adjacent Tg group pointing up near the end of one of the non-interacting carbazoles.

5.4.3 Tg[4]cycle:TCNQ

The organic acceptor tetracyanoquinodimethane (TCNQ) has long been utilized as the electron-accepting material *par excellence* for studying organic and inorganic donor-acceptor complexes. Slow diffusion of ether into a solution containing **4** and TCNQ gave black plates **4**•TCNQ exclusively; no free **4** was found. This black crystalline material was found to be stacks of thinner plates; as a result, only very thin plates gave acceptable diffraction data.

4•TCNQ crystallizes in the triclinic space group *P*-1 (Fig. 5.19). As a result, the orthogonal stacks present in **4**•chloranil are absent here; interactions between aromatic moieties are exclusively cofacial and edge-to-edge. In contrast to **4**•chloranil, the

macrocycle is planar with a low macrocycle plane deviation of 0.05 Å. The macrocycle-TCNQ face-to-face interactions in **4**•TCNQ (3.301 Å) are closer than in **4**•chloranil (3.408 Å) (Fig 5.20). By comparison, the face-to-face interactions in TTF•chloranil are slightly shorter (3.302 Å).[27]

5.5   Conclusion

An extensive crystallographic analysis of macrocycles **1** with varying pendant alkyl chains and their co-crystals with various organic guests has been carried out. Varying alkyl chain lengths and atom identities within the chains lead to different packing motifs; van der Waals interactions between alkyl chains and aromatic parts of the macrocycles become more prevalent with longer chain lengths. As evidenced by **2a-b**, polymorphism of large aromatic systems may belie the full story of the solid-state chemistry of a novel material. The Tg group appears to be an excellent solubilizing group due to its inability to form extended van der Waals interactions with aromatic moieties, thus leading to "phase separation." Strong electron acceptors form charge-transfer complexes with cofacial interactions, whereas more electron-rich guests such as azobenzene simply insert themselves in between macrocycles. Additional crystallographic studies on various AEMs should give a more complete picture as to the nature of these interesting materials, and shed light on their functional properties.

5.6   Experimental Section

Low-temperature diffraction data for **2b**, **3**•DCM, **4**, and **4**•chloranil were collected on a Bruker-AXS ApexII CCD detector with graphite-monochromated Mo Kα radiation (λ = 0.71073 Å), performing phi and omega scans. Low-temperature diffraction data for **2a**•DCM, **2a**•MeOH, **2**•azobenzene, **3**•DCE, and **4**•TCNQ were collected on a Bruker-AXS ApexII CCD detector with graphite-monochromated Cu Kα radiation (λ = 1.54178 Å), performing phi and omega scans. All structures were solved by direct methods and refined against F^2 on all data by full-matrix least squares with SHELXL-97.[28] All non-hydrogen atoms were refined anisotropically. All hydrogen atoms were included in the model at geometrically calculated positions and refined using a riding model. The isotropic displacement parameters of the hydrogen atoms were fixed to 1.2 times the U value of the atoms they are linked to (1.5 U for methyl groups). In all cases except **3**•DCM, **3**•DCE, and **2**•azobenzene, disordered solvent was present. Since positions for the solvent molecules were poorly determined a second structural model was refined with contributions from the solvent molecules removed from the diffraction data using the solvent bypass ("SQUEEZE") procedure in PLATON.[25] No positions for the host network differed by more than two su's between these two refined models. The electron count from the "squeeze" model converged in satisfactory agreement with the number of solvate molecules predicted by the complete refinement. The "squeeze" data are reported here. **2a**•DCM and **2a**•MeOH crystallized in the non-centrosymmetric space group $P2_1$, but due to the lack of refined atoms heavier than O, absolute structure could not be determined due to the ambiguity of the Flack parameters. The Hooft parameters

from Bayesian statistical analysis were inconclusive as well.{Hooft, 2008 #1112 Thus, Friedel pairs were merged for **2a**·DCM and **2a**·MeOH after refinement was complete.

Crystal Preparation

The following general protocol was used for the growth of crystals suitable for X-ray diffraction for **2a**·DCM, **2b**, **3**·DCM, and **4**. A small amount (~1-5 mg) of macrocycle was added to a 20 mL vial and dissolved in dichloromethane (3-5 mL). The vial was placed uncovered in a large jar containing ether and the jar was sealed. Vapor diffusion of ether into the DCM solution over several days led to the formation of crystals suitable for X-ray analysis. **2a**·DCM (long needles) and **2b** (hexagonal plates) were mechanically separated under a microscope under inert oil.

2a·MeOH: Crystals of **2a** were submerged in MeOH for several weeks. No loss in crystallinity was observed.

3·DCE: The general protocol was used, but 1,2-dichloroethane was used in lieu of dichloromethane.

Co-crystal formation for **2**·azobenzene, **4**·chloranil and **4**·TCNQ: Macrocycle (1-5 mg) was dissolved in a saturated solution of guest in dichloromethane. Slow diffusion of ether into the DCM solution gave crystals suitable for X-ray diffraction. For **2**·azobenzene and **4**·TCNQ, co-crystals were formed exclusively; for **4**·chloranil, blue crystals were mechanically separated from crystals of **4** under inert oil.

5.7 Figures and Schemes

1

$$-C_{10}H_{21} \ (\mathbf{2})$$
$$R = -C_6H_{13} \quad (\mathbf{3})$$
$$-(CH_2CH_2O)_3CH_3 \ (\mathbf{4})$$
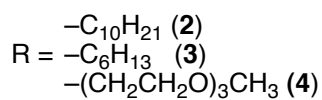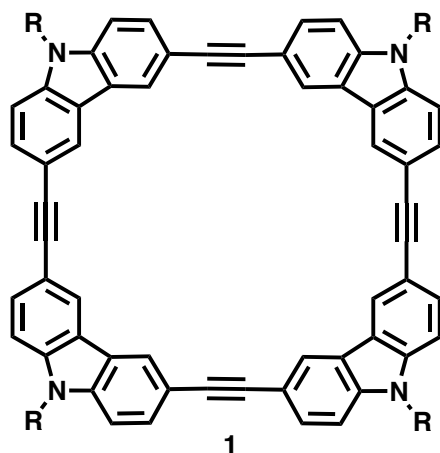
Figure 5.1. The carbazole-ethynylene macrocycle **1** with various alkyl chains **2-4**.
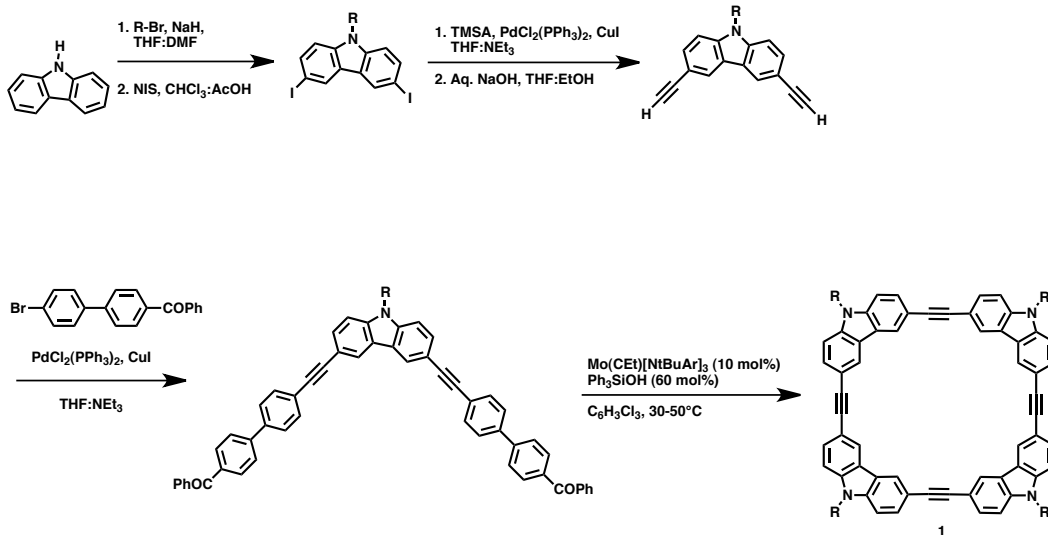
Scheme 5.1. General synthetic scheme for the preparation of macrocycles **1**.

Table 5.1. Crystallographic Data

	2a·DCM	**2a**·MeOH	**2a**·azobenzene	**2b**	**3**·DCM
Lab number	n0796	n0791	n0771	ba00m	ba12m
Moiety formula	$C_{96}H_{108}N_4$ ·(CH_2Cl_2)	$C_{96}H_{108}N_4$ ·(CH_3OH)	$C_{96}H_{108}N_4$ ·$C_{12}H_{10}N_2$	$C_{96}H_{108}N_4$ ·$2(CH_2Cl_2)$	$C_{80}H_{76}N_4$ ·$2(CH_2Cl_2)$
space group	$P2_1$	$P2_1$	$P2_1/n$	$C2/c$	P-1
a (Å)	19.3461(6)	19.4024(7)	8.5568(4)	42.960(17)	9.0398(9)
b (Å)	8.9264(3)	8.9759(3)	25.6445(12)	9.082(4)	14.0715(13)
c (Å)	24.7549(8)	24.5083(7)	19.7548(9)	24.092(10)	14.9754(14)
α (deg)	90	90	90	90	68.419(3)
β (deg)	105.939(2)	106.389(3)	95.635(3)	105.579(11)	77.031(3)
γ (deg)	90	90	90	90	73.791(4)
V (Å^3)	4110.6(2)	4094.8(2)	4313.9(3)	9055(7)	1685.1(3)
Z	2	2	2	4	1
D_x (g cm^{-3})	1.065	1.070	1.155	1.091	1.245
T (K)	100	100	100	193	120
Total Reflections	30444	23349	38665	68724	33246
Ind. Reflections	7630	7383	7668	8238	7441
$R(F)^a$ ($I > 2\sigma$)	0.0877	0.0892	0.0532	0.0567	0.0531
$R_w(F^2)^b$ (all data)	0.2442	0.2529	0.1589	0.1564	0.1552
GooF S	1.063	1.038	1.041	0.903	1.045
MC Plane Deviation^c (Å)	0.1001	0.1126	0.1078	0.0770	0.0548
Disordered Solvent Volume^d (Å^3)	332	266	n/a	1347	n/a

^{a} $R(F) = \sum ||F_o| - F_c||/\sum |F_o|$ for $F_o^2 > 2\sigma(F_o)^2$.
^{b} $R_w(F_o^2) = [\sum w(F_o^2 - F_c^2)^2/\sum wF_o^4]^{1/2}$, $w^{-1} = \sigma^2(F_o)^2 + [M(F_o^2)]^2 + [N(F_o^2 + 2F_c^2)/3]$ for $F_o^2 \geq 0$; $w^{-1} = \sigma^2(F_o^2)$ for $F_o^2 < 0$. M and N are weighting variables.
^{c} Macrocycle plane is the least-squares plane of the macrocycle atoms, not including hydrogens or pendant alkyl chains. MC plane deviation is the standard deviation from the plane of all atoms defining the MC plane.
^{d} The total disordered solvent-containing volume per unit cell as calculated by SQUEEZE/PLATON.

Table 5.1 (cont.)

	3·DCE	**4**	**4·chloranil**	**4·TCNQ**
Lab number	n0801	ba97L	ba06m	n0784a
Moiety formula	$C_{80}H_{76}N_4$ $\cdot C_2H_4Cl_2$	$C_{84}H_{84}N_4O_{12}$ $\cdot CH_2Cl_2$	$C_{84}H_{84}N_4O_{12}$ $\cdot C_6O_2Cl_4$ $\cdot 0.5(CH_2Cl_2)$	$C_{84}H_{84}N_4O_{12}$ $\cdot C_{12}H_4N_4$ $\cdot 2(CH_2Cl_2)$
space group	P-1	$P2_1/c$	$P2_1/n$	P-1
a (Å)	9.2308(4)	11.904(3)	15.950(6)	12.0366(3)
b (Å)	13.2487(6)	17.824(4)	22.533(8)	13.6441(4)
c (Å)	15.2331(7)	17.998(4)	24.699(9)	15.0439(4)
α (deg)	68.242(2)	90	90	87.972(2)
$β$ (deg)	74.840(2)	90.102(7)	108.284(5)	87.789(2)
$γ$ (deg)	75.250(2)	90	90	64.530(2)
V (Å^3)	1643.98(13)	3818.8(14)	8429(5)	2228.37(10)
Z	1	2	4	1
D_x (g cm^{-3})	1.204	1.241	1.251	1.152
T (K)	100	193	193	100
Total Reflections	18509	60761	83161	13677
Ind. Reflections	5777	7049	15429	6803
$R(F)$ ($I > 2σ$)	0.0484	0.0766	0.0735	0.0793
$R_w(F^2)$ (all data)	0.1383	0.2150	0.1962	0.2503
GooF S	1.043	1.027	0.921	1.068
MC Plane Deviation (Å)	0.1134; 0.2154[e]	0.0483	0.2107	0.0536
Disordered Solvent Volume (Å^3)	n/a	272	548	186

---

[e] Each value corresponds to a disorder in one carbazole of the macrocycle.
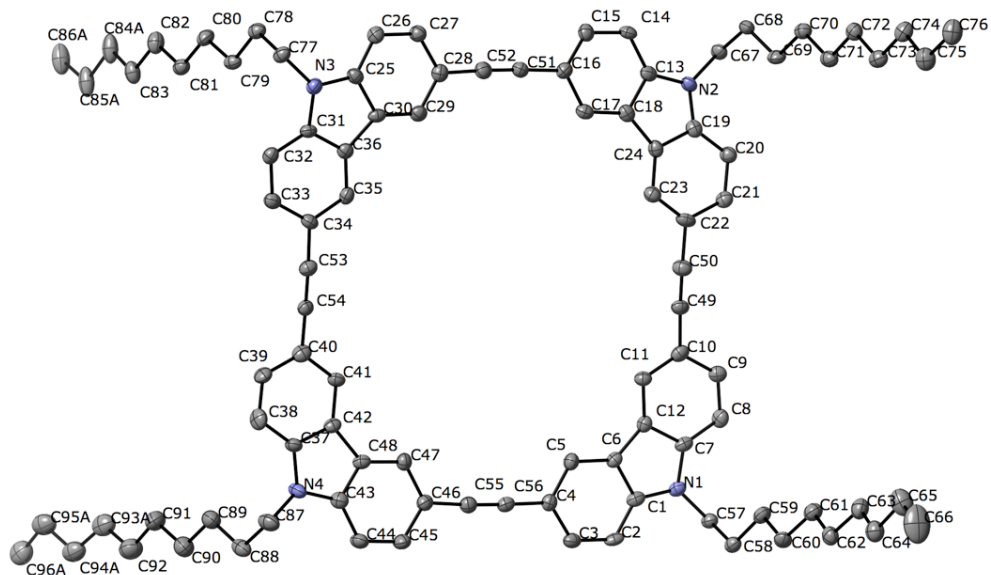
Figure 5.2. Structure of **2a**·DCM. Ellipsoids at 35% probability. Hydrogens removed for clarity.
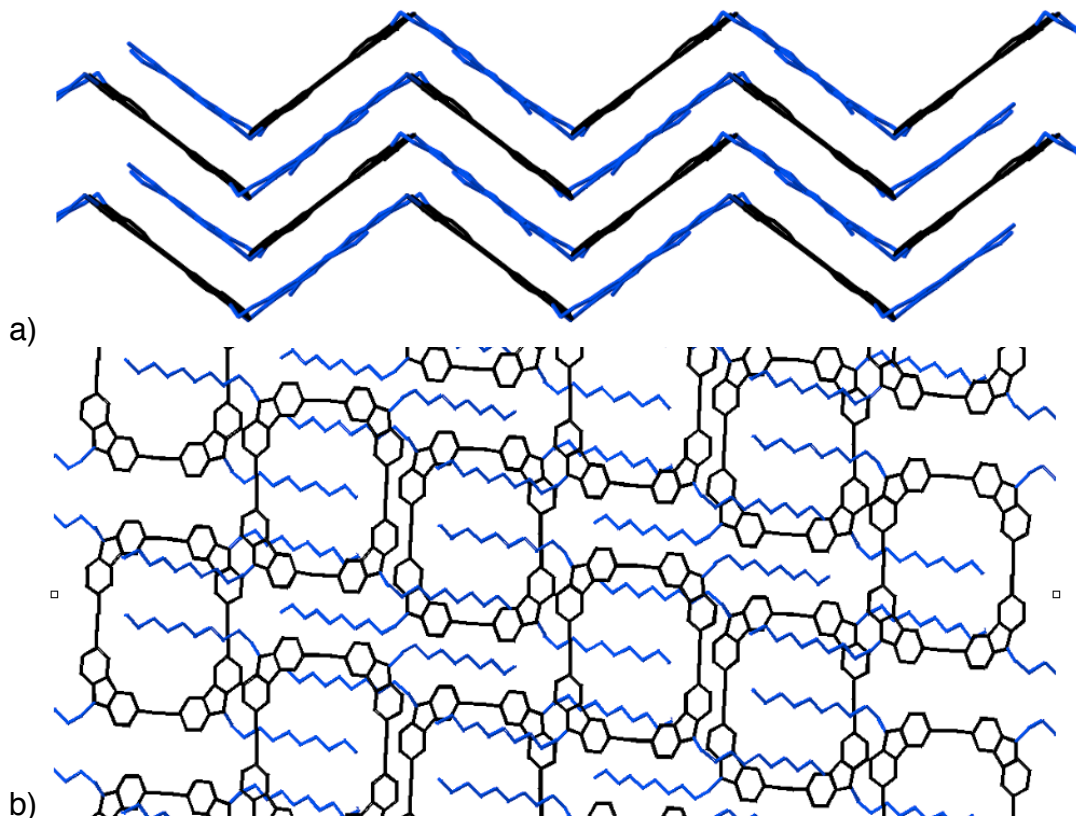
Figure 5.3. Packing of **2a**·DCM looking down the (a) crystallographic *a*-axis and (b) crystallographic *b*-axis. Hydrogens omitted for clarity. Alkyl chains in blue, macrocycles in black..
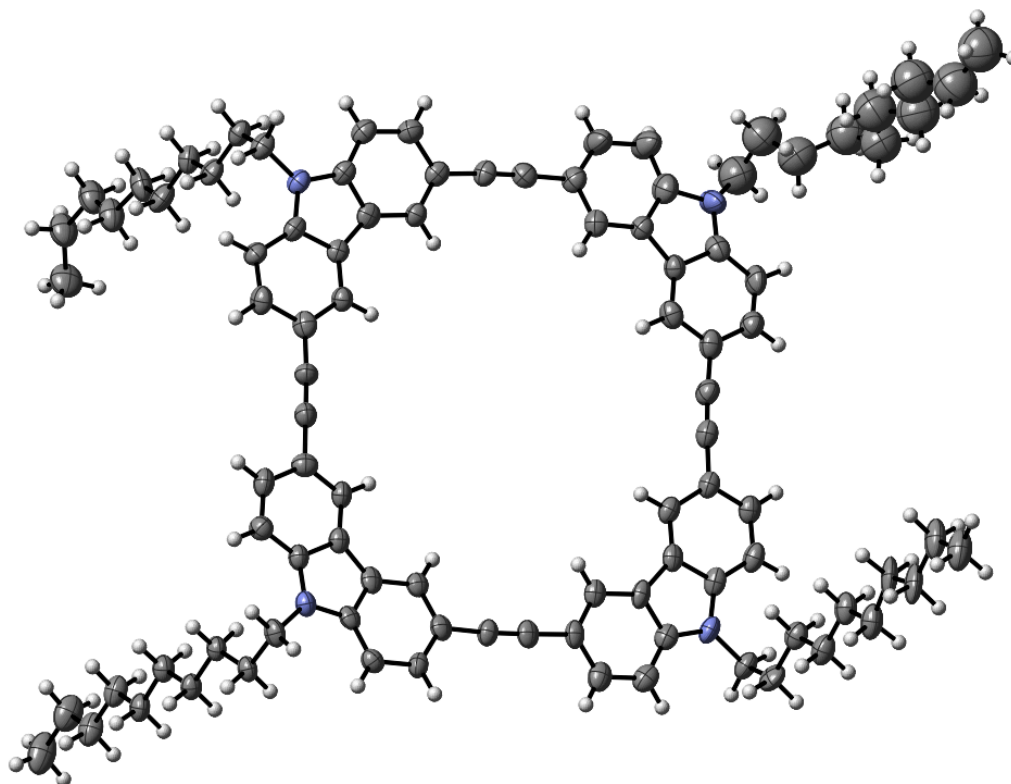
Figure 5.4. Structure of **2a·**MeOH. Ellipsoids at 35% probability.
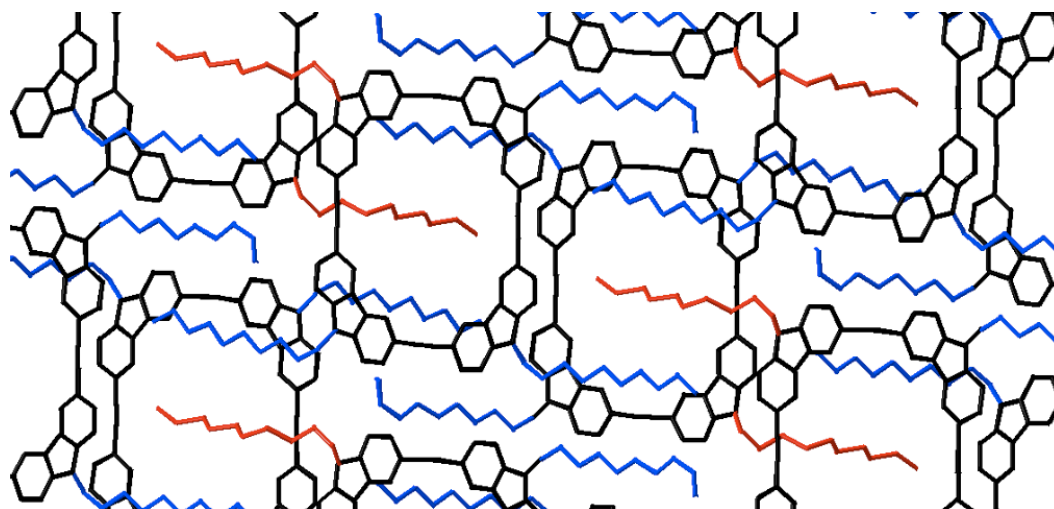
Figure 5.5. Packing of **2a·**MeOH down the crystallographic *b*-axis. Highly disordered alkyl chain in red, other alkyl chains blue, macrocycles black. Hydrogens omitted for clarity.
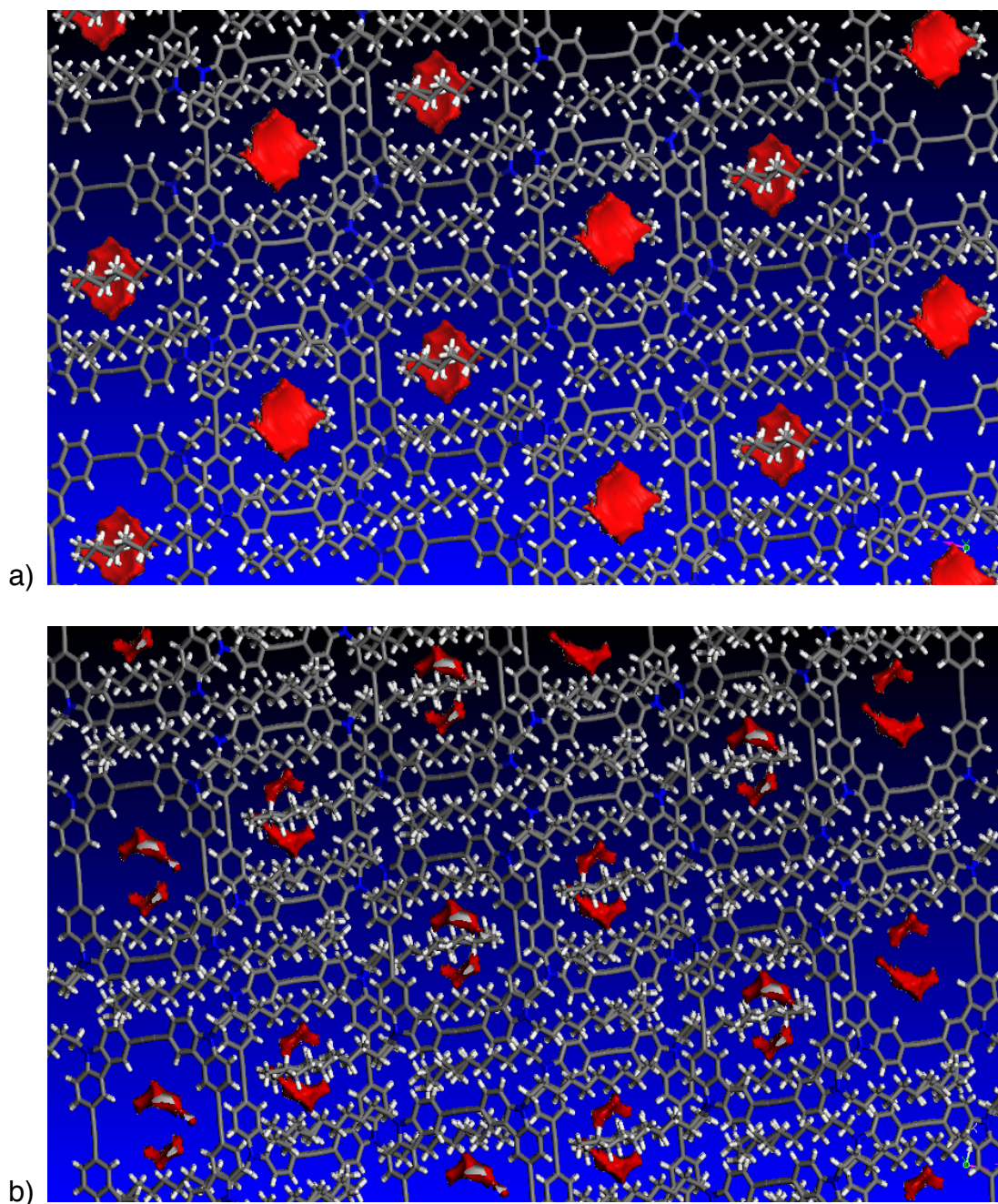
Figure 5.6. Visualization of the solvent volumes in (a) **2a·**DCM and (b) **2a·**MeOH. Solvent volumes in red. Note that the solvent void area in **2a·**MeOH is significantly smaller than in **2a·**DCM due to alkyl chain disorder.
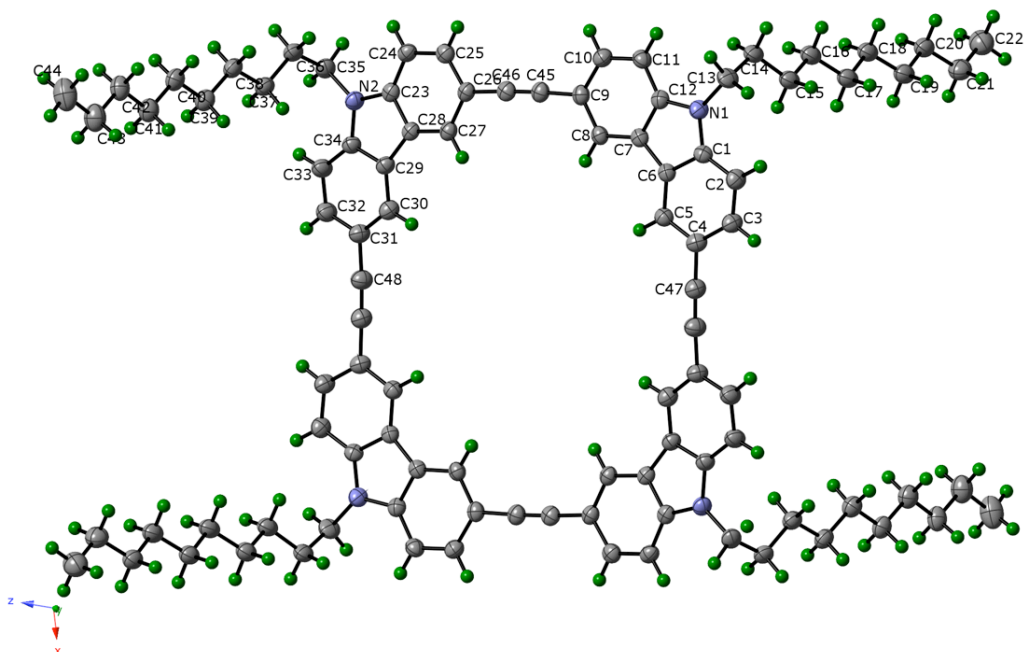
Figure 5.7. Structure of **2b**. Ellipsoids at 35% probability. The unlabeled half of the macrocycle is related by the symmetry operation (0.5 − x, -0.5 + y, -z).
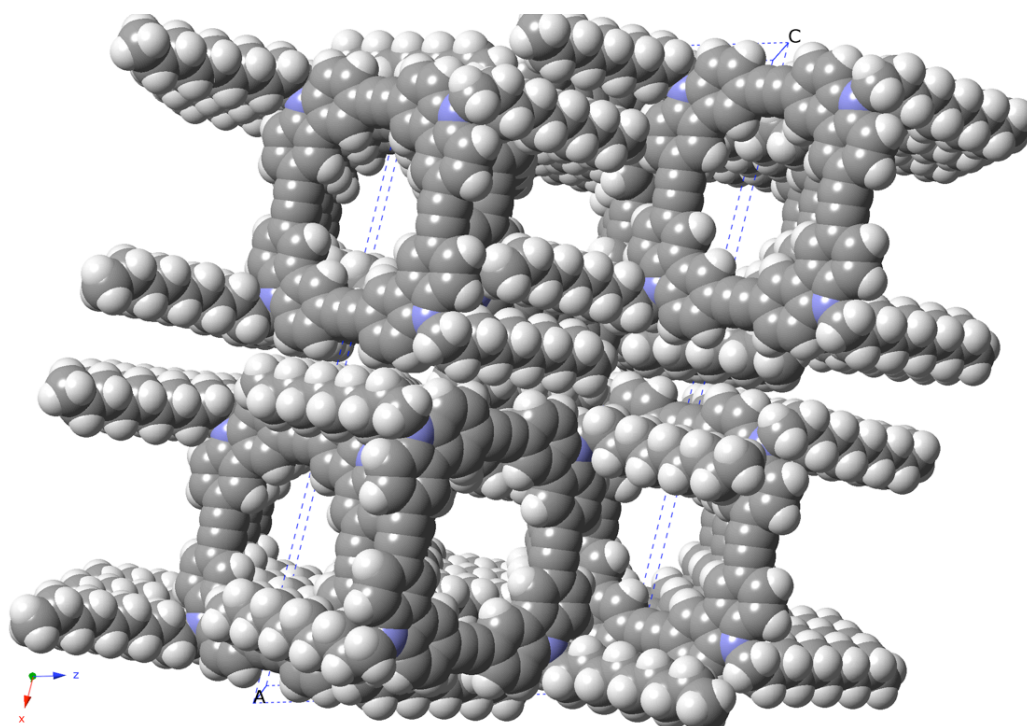
Figure 5.8. Space-filling representation of the packing of **2b** down the *b*-axis.
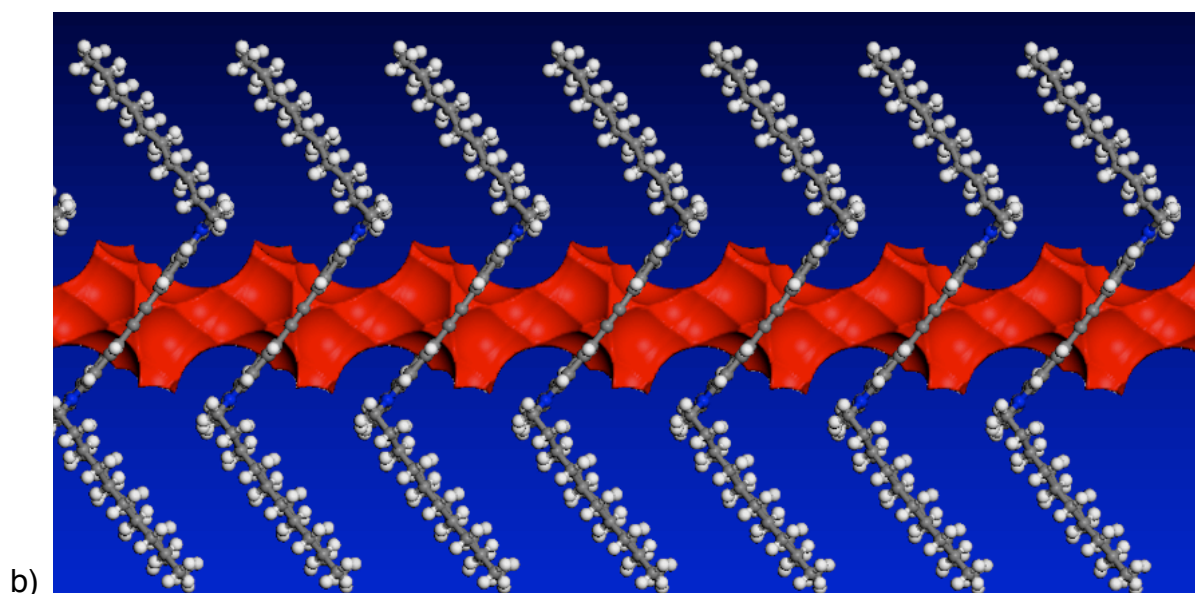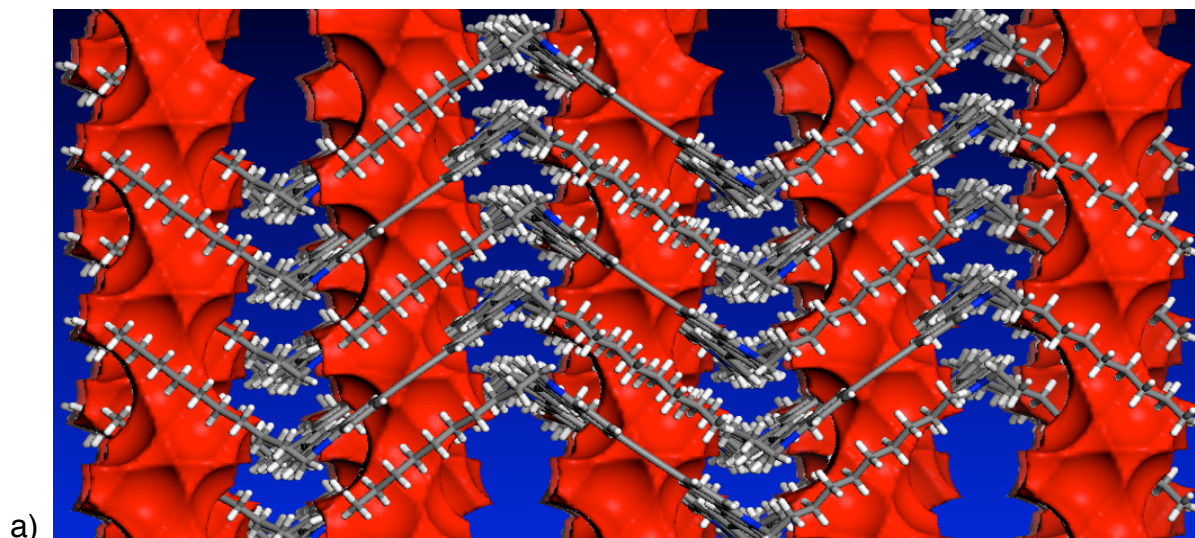
Figure 5.9. Visualization of the solvent channels in **2b·**DCM looking down the (a) *a*-axis and the (b) *c*-axis. Solvent channels are in red.
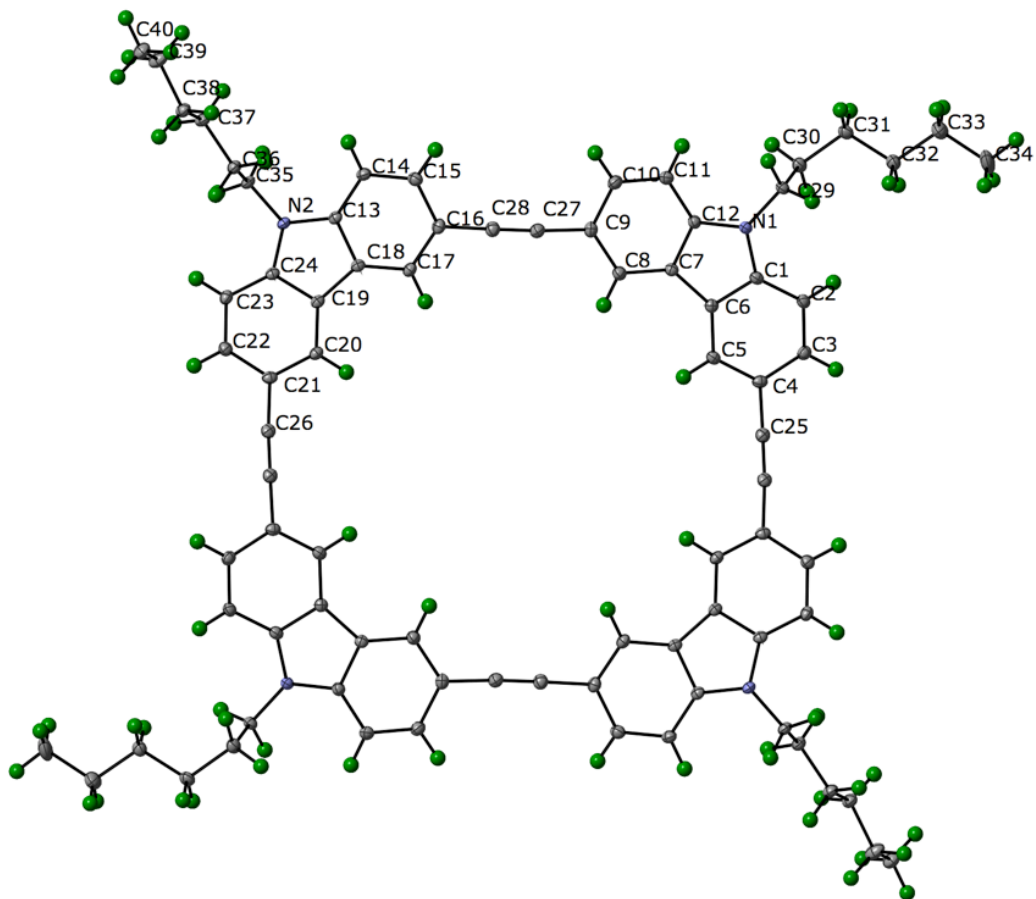
Figure 5.10. Structure of **3**•DCM, ellipsoids at 35% probability. The unlabeled atoms are related by the symmetry operation (-x, -y, -z).
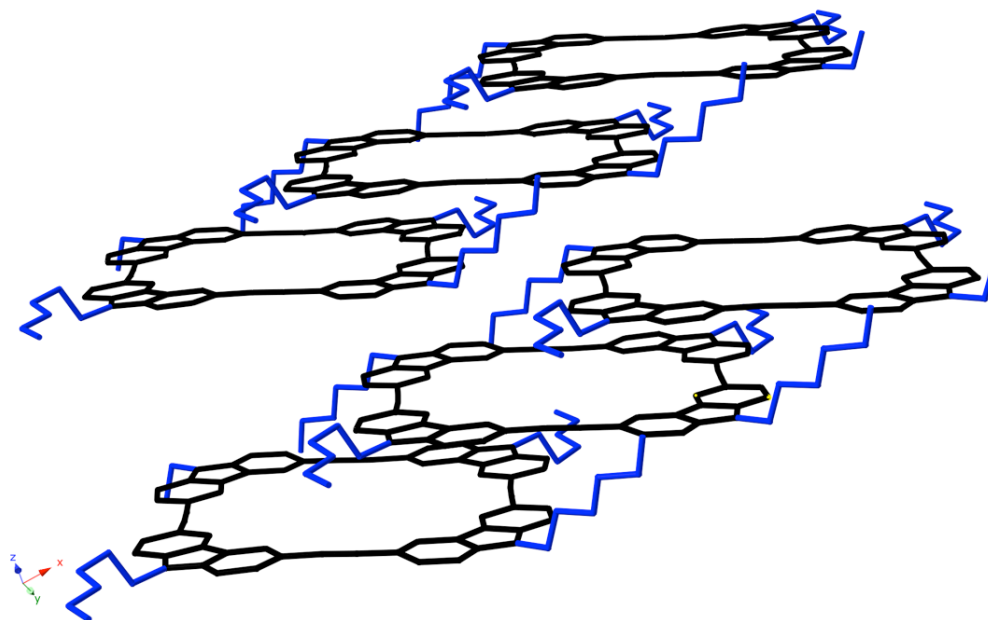

Figure 5.11. Packing of **3**•DCM. Alkyl chains in blue, macrocycles in black.
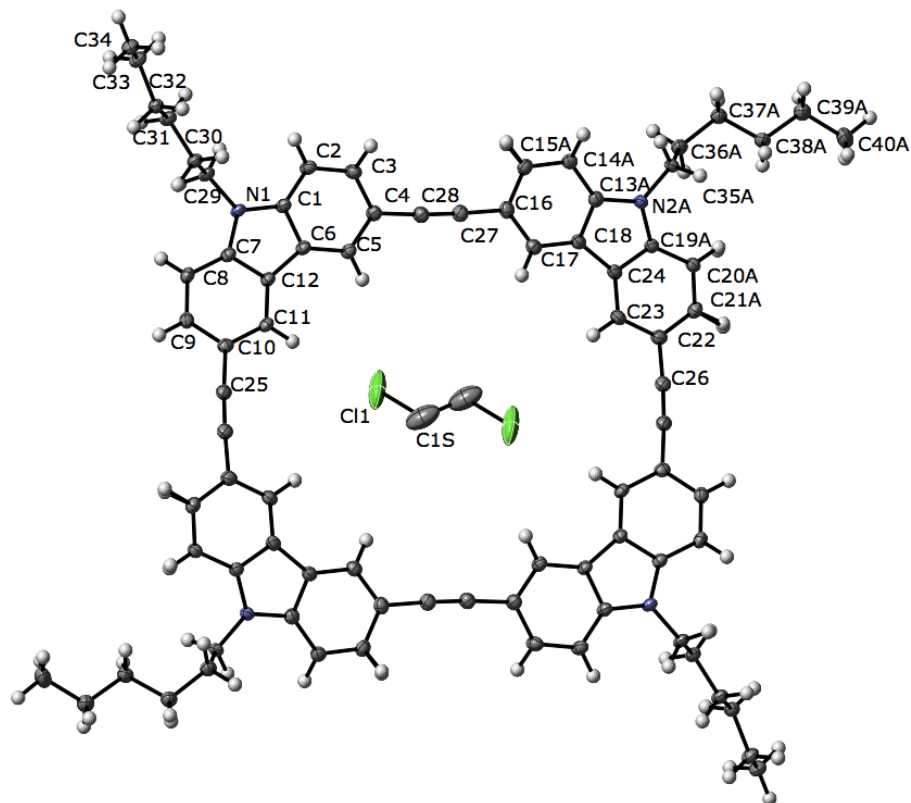
Figure 5.12. Structure of **3**·DCE. Ellipsoids at 35% probability.
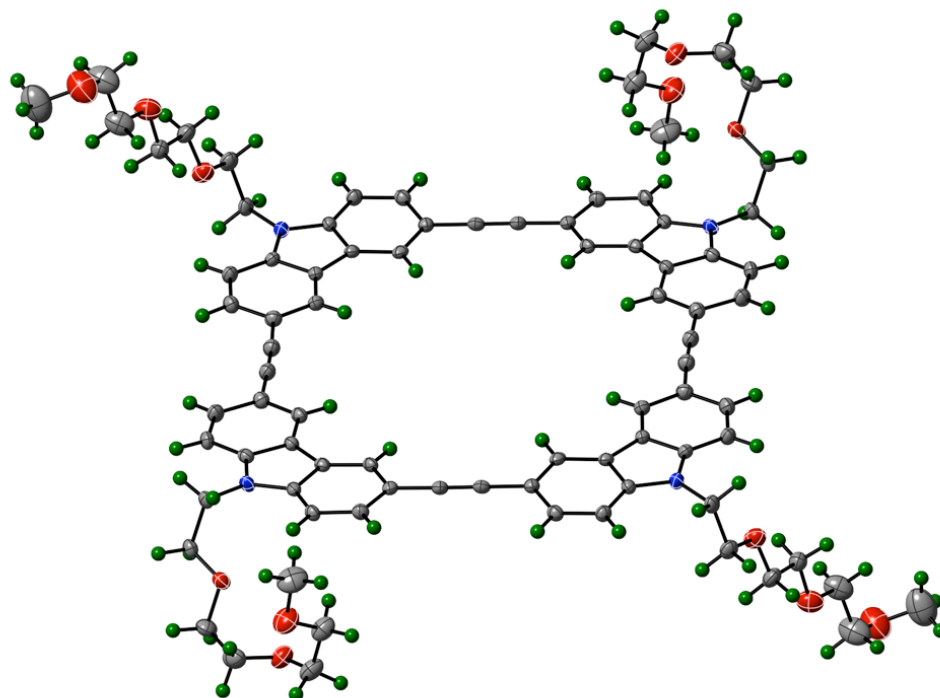
Figure 5.13. Structure of **4**. Thermal ellipsoids at 35% probability.
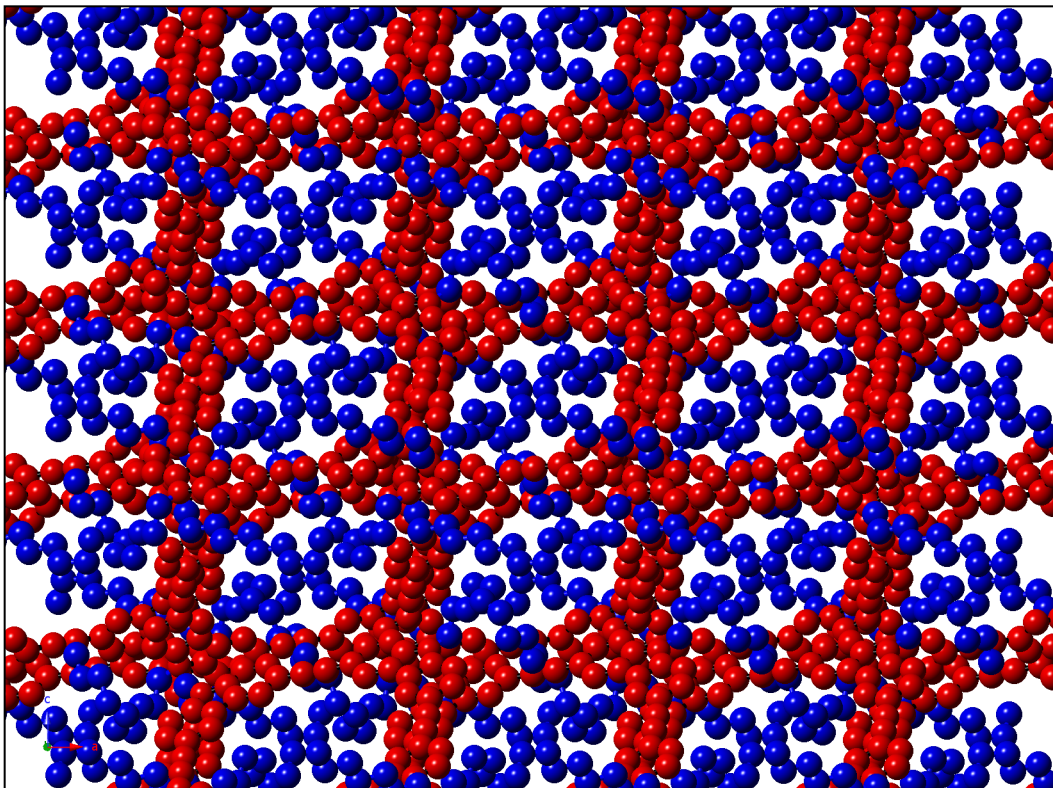
Figure 5.14. Ball-and-stick representation of the packing of **4**•DCE, looking down the *b*-axis. Tg chains in blue, macrocycles in red. Hydrogens omitted for clarity.
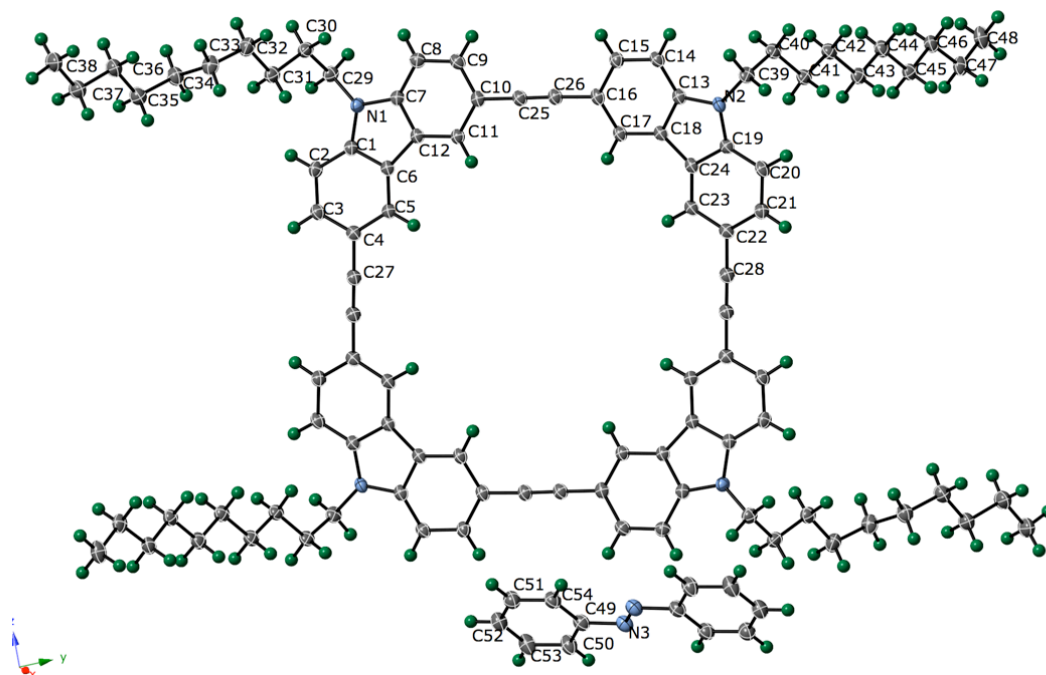
Figure 5.15. Structure of **2**•azobenzene, thermal ellipsoids at 35% probability. The unlabeled atoms are related by the symmetry operation (-x,-y,-z).
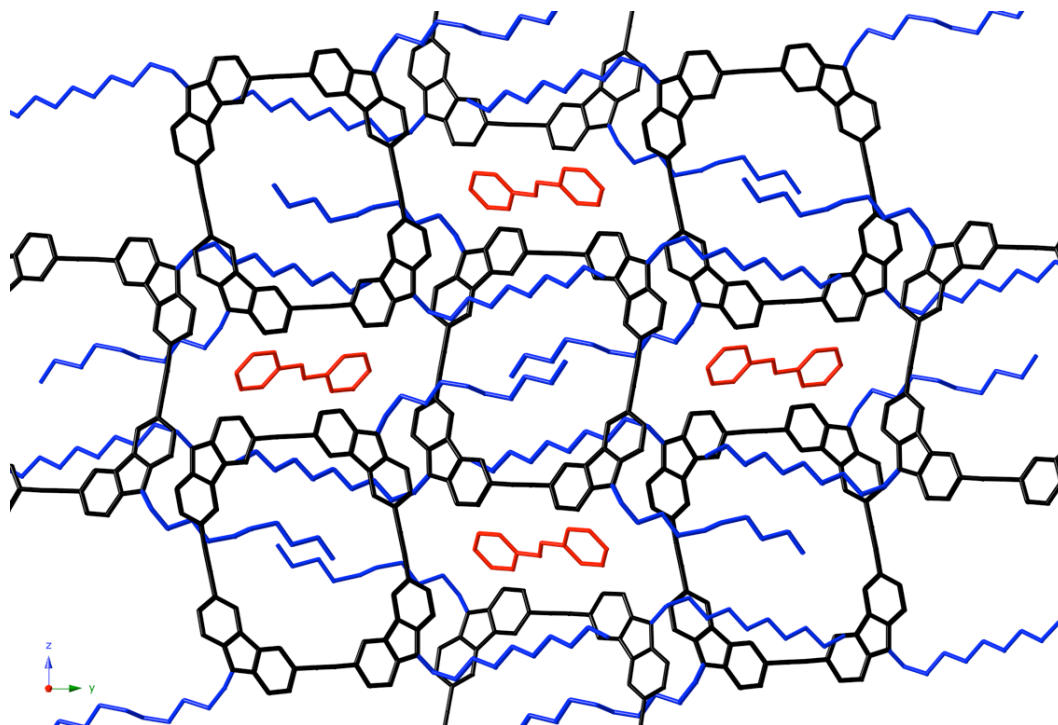
Figure 5.16. Packing of **2**•azobenzene, looking down the *a*-axis. C_{10} chains in blue, azobenzenes in red. Hydrogens omitted for clarity.
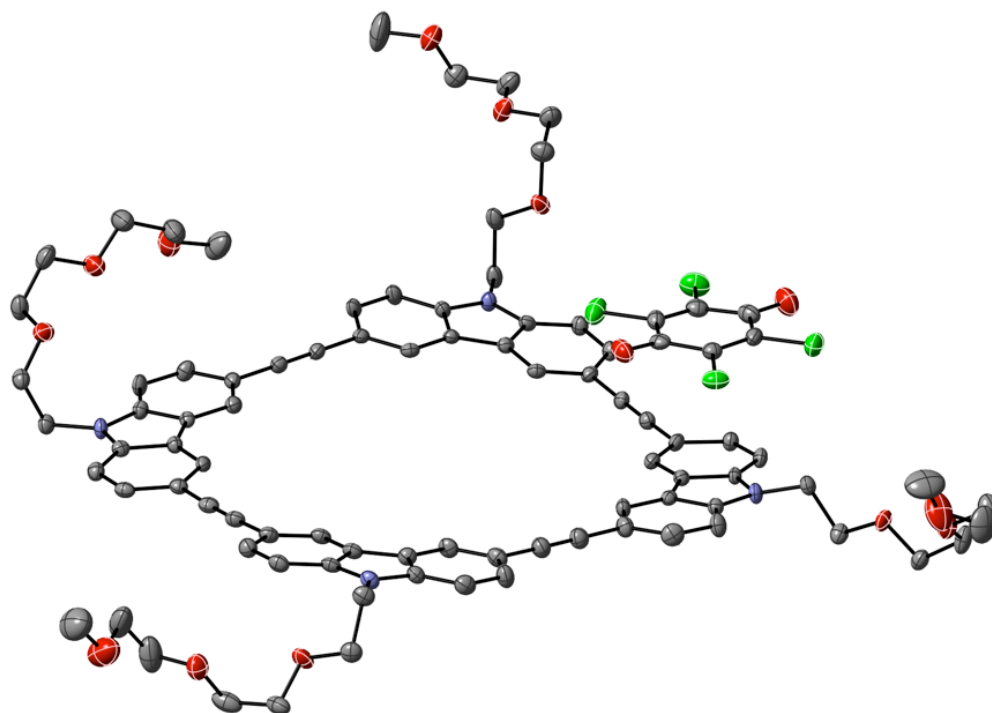
Figure 5.17. Structure of **4**•chloranil. Ellipsoids at 35% probability. Hydrogens omitted for clarity.
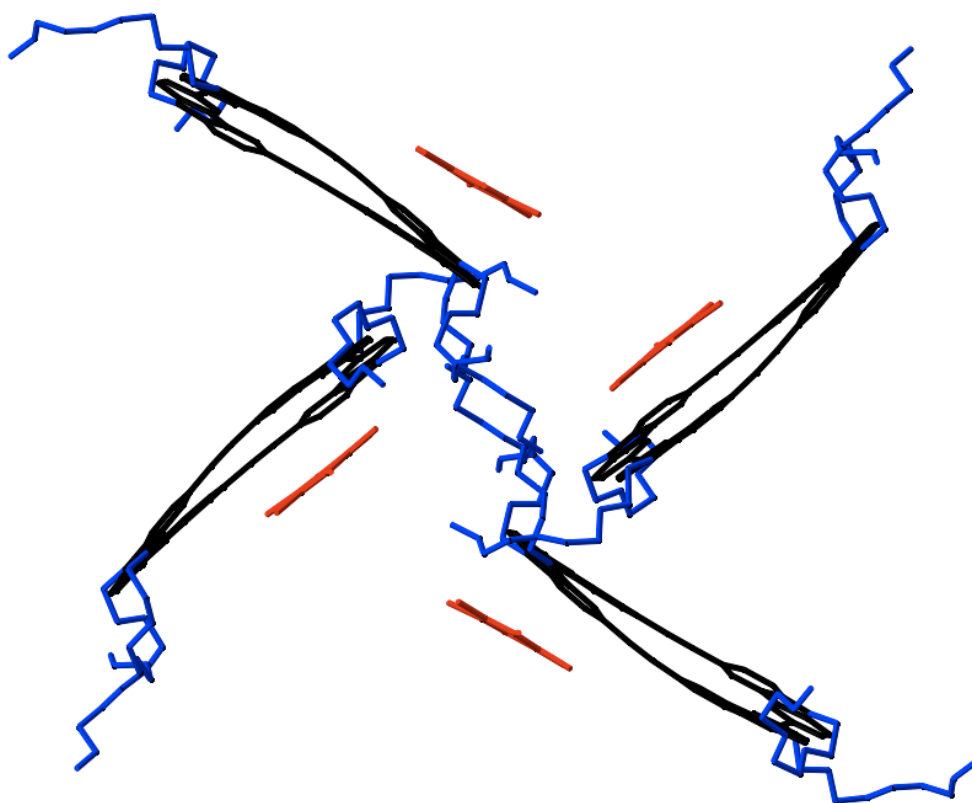
Figure 5.18. Packing of **2**•chloranil. Chloranil in red, Tg chains in blue. Hydrogens omitted.
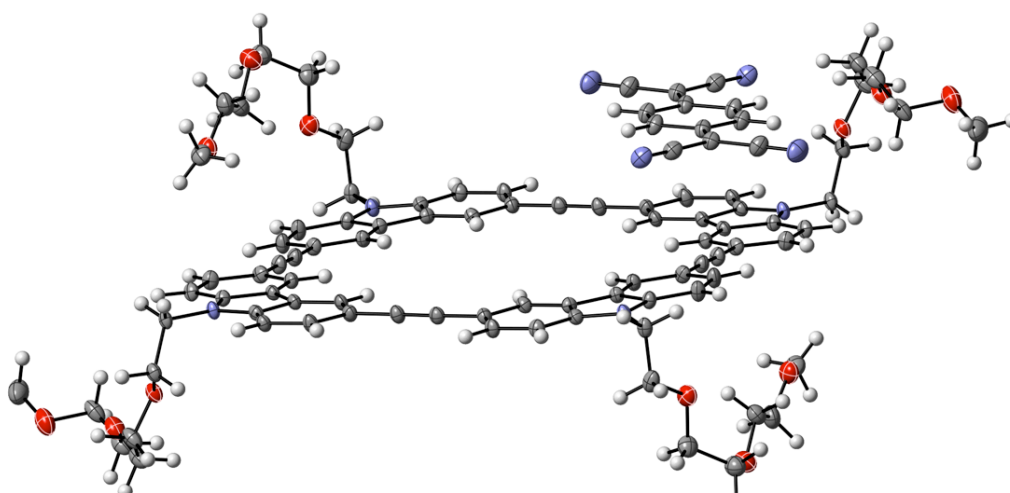

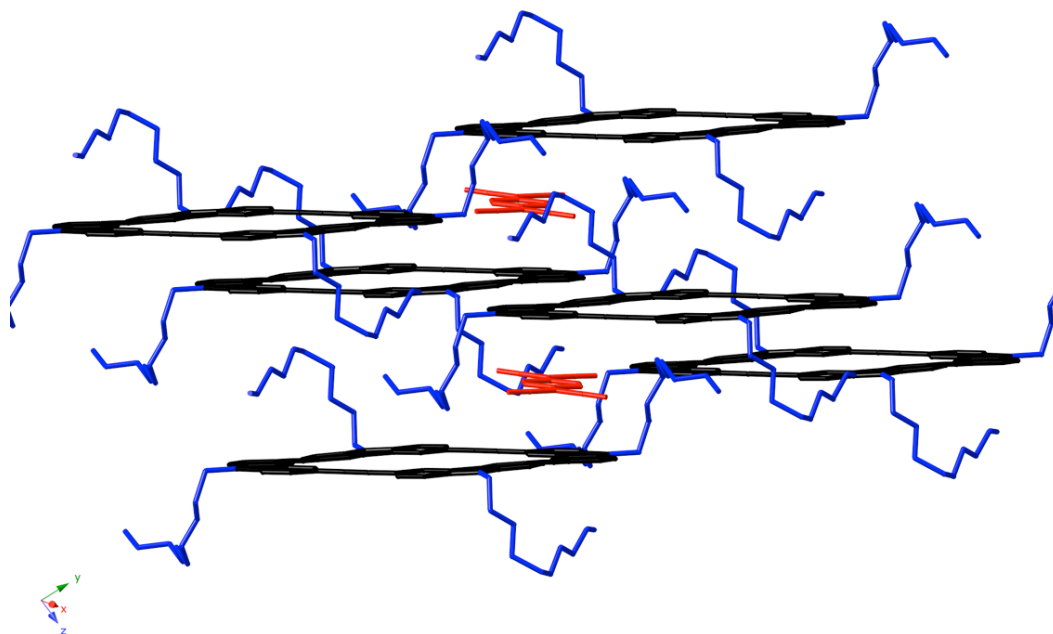**Figure 5.19.** Structure of **2**•TCNQ. Ellipsoids at 50% probability.

Figure 5.20. Packing of **2·**TCNQ. Tg chains in blue, TCNQ molecules in red. Hydrogens omitted for clarity.

5.8   References

[1]   Moore, J. S. *Acc. Chem. Res.* **1997**, *30*, 402-413.

[2]   Watson, M. D.; Fechtenkotter, A.; Mullen, K. *Chem. Rev.* **2001**, *101*, 1267-1300.

[3]   Pasini, D.; Ricci, M. *Curr. Org. Synth.* **2007**, *4*, 59-80.

[4]   Grave, C.; Schlüter, A. D. *Eur. J. Org. Chem.* **2002**, 3075-3098.

[5]   Tahara, K.; Tobe, Y. *Chem. Rev.* **2006**, *106*, 5274-5290.

[6]   Rowan, S. J.; Cantrill, S. J.; Cousins, G. R. L.; Sanders, J. K. M.; Stoddart, J. F. *Angew. Chem. Int. Ed.* **2002**, *41*, 898-952.

[7]   Zhang, W.; Brombosz, S. M.; Mendoza, J. L.; Moore, J. S. *J. Org. Chem.* **2005**, *70*, 10198-10201.

[8]   Zhang, W.; Moore, J. S. *J. Am. Chem. Soc.* **2004**, *126*, 12796-12796.

[9]   Zhang, W.; Moore, J. S. *J. Am. Chem. Soc.* **2005**, *127*, 11863-11870.

[10]   Zhang, W.; Moore, J. S. *Angew. Chem., Int. Ed.* **2006**, *45*, 4416-4439.

[11]   Hoeben, F. J. M.; Jonkheijm, P.; Meijer, E. W.; Schenning, A. P. H. J. *Chem. Rev.* **2005**, *105*, 1491-1546.

[12]   Anthony, J. E.; Brooks, J. S.; Eaton, D. L.; Parkin, S. R. *J. Am. Chem. Soc.* **2001**, *123*, 9482-9483.

[13]   Anthony, J. E.; Eaton, D. L.; Parkin, S. R. *Org. Lett.* **2002**, *4*, 15-18.

[14]   Venkararaman, D.; Lee, S.; Zhang, J.; Moore, J. S. *Nature* **1994**, *371*, 591-593.

[15]   Kawase, T.; Noriko Ueda; Darabi, H. R.; Oda, M. *Angew. Chem., Int. Ed.* **1996**, *35*, 1556-1558.

[16]   Ge, P.-H.; Fu, W.; Herrmann, W. A.; Herdtweck, E.; Campana, C.; Adams, R. D.; Bunz, U. H. F. *Angew. Chem. Int. Ed.* **2000**, *39*, 3607-3610.

[17]   Höger, S.; Enkelmann, V.; Bonrad, K.; Tschierske, C. *Angew. Chem., Int. Ed.* **2000**, *39*, 2267–2270.

[18]   Hosokawa, Y.; Kawase, T.; Oda, M. *Chem. Commun.* **2001**, 1948-1949.

[19]   Müller, P.; Uson, I.; Hensel, V.; Schlüter, A.-D.; Scheldrick, G. M. *Helv. Chim. Acta* **2001**, *84*, 778-785.

[20]   Höger, S.; Morrison, D. L.; Enkelmann, V. *J. Am. Chem. Soc.* **2002**, *124*, 6734-6736.

[21]   Grave, C.; Lentz, D.; Schäfer, A.; Samori, P.; Rabe, J. P.; Franke, P.; Schlüter, A.-D. *J. Am. Chem. Soc.* **2003**, *125*, 6907–6918.

[22]   Traber, B.; Oeser, T.; Gleiter, R. *Eur. J. Org. Chem.* **2005**, 1283-1292.

[23]   Bindl, M.; Stade, R.; Heilmann, E. K.; Picot, A.; Goddard, R.; Fürstner, A. *J. Am. Chem. Soc.* **2009**, *131*, 9468-9470.

[24]   Heppekausen, J.; Stade, R.; Goddard, R.; Fürstner, A. *J. Am. Chem. Soc.* **2010**, *132*, 11045-11057.

[25]   Spek, A. L. *J. Appl. Cryst.* **2003**, *36*, 7-13.

[26]   Nelson, J. C.; Saven, J. G.; Moore, J. S.; Wolynes, P. G. *Science* **1997**, *277*, 1793-1796.

[27]   García, P.; Dahaoui, S.; Katan, C.; Souhassou, M.; Lecomte, C. *Faraday Discuss* **2007**, *135*, 217-235.

[28]   Sheldrick, G. M.; Universität Göttingen: Göttingen, Germany, 1997.

Chapter 6

Hirshfeld Surface Analysis of Non-Centrosymmetric *N*-alkylDABCOnium Trihalozincates

6.1   Introduction

Non-centrosymmetric (NCS) solids are an important class of materials due to their unique bulk properties, such as nonlinear optical susceptibility, piezoelectricity and pyroelectricity (Fig. 6.1).[1,2] The absence of inversion symmetry in a crystalline lattice is commonly known to be a requirement for the incorporation of chiral, non-racemic molecules; however, in crystallography, there is a distinction between "handedness" in a molecule (absolute configuration) and "handedness" in a solid (absolute structure). Chiral, non-racemic molecules such as proteins crystallize in the so-called "chiral" class of space groups which contain only rotational symmetry elements (proper rotations and improper screw rotations); that is, any symmetry element that would invert the configuration of the crystalline species is forbidden. By contrast, achiral molecules that may contain mirror planes but not inversion centers may crystallize in either centrosymmetric or non-centrosymmetric space groups; if they do crystallize in NCS space groups, they may display one or more of several novel bulk properties as outlined in Fig. 6.1.

The rational design of NCS solids is not straightforward, especially when the asymmetric unit lacks chirality. This stems from a tendency for molecules to preferentially crystallize in centrosymmetric space groups; the centrosymmetric space

group $P2_1/c$ is by and far the most common space group for small achiral molecules. Thus, some overriding packing factor must predominate in NCS solids.

6.2   The Hirshfeld Surface

The challenge of a systematic and thorough bulk analysis of factors influencing packing geometry of solids was raised by Desiraju over a decade ago.[3] Typically, packing influences are described through looking at strong, classic intermolecular interactions such as hydrogen bonding. Such analyses do not give a *complete* picture, however; subtler effects, such as weaker H-bonding or van der Waals interactions, may be present and overlooked. A more holistic method for the visualization of interactions was developed by Spackman et al. in the Hirshfeld surface.[4-6] The Hirshfeld surface is described as the 0.5 isosurface of the weight function $w(r)$:[7,8]

$$w(\mathbf{r}) = \rho_{promolecule}(\mathbf{r}) / \rho_{procrystal}(\mathbf{r})$$

where the spherical electron densities of the molecule of interest (the promolecule) divided by the spherical electron densities of the crystal (the procrystal). At $w(\mathbf{r}) = 0.5$, the electron density of the promolecule is larger than that of the remaining molecules. This is in contrast to, for example, a van der Waals surface where neighboring molecules are not accounted for. The Hirshfeld surface is thus a unique contour to explore the effects of close interactions, as intermolecular distances are very easily mapped onto the Hirshfeld surface. The visualization of Hirshfeld surfaces and mapping of intermolecular distances are easily done using the program CrystalExplorer.[9] The d_{norm} value is conveniently mapped on the Hirshfeld surface:

$$d_{norm} = \frac{d_i - r_i^{vdW}}{r_i^{vdW}} + \frac{d_e - r_e^{vdW}}{r_e^{vdW}}$$

where d_i is the distance from a point on the surface to the nearest nucleus inside the surface, d_e is the distance from a point on the surface to the nearest nucleus outside the surface, and r^{vdW} are the van der Waals radii of the nucleus. The d_{norm} value allows for a convenient visualization of close contacts that "normalizes" large vs. small atom contacts. Fingerprint plots, on which the distances of the nearest atoms to the molecule of interest can be mapped, provide a useful summary of the kinds and magnitudes of intermolecular interactions.

Probing the origins of non-centrosymmetry using Hirshfeld surfaces has been undertaken in once instance before, looking at the polymorphism of a highly-active nonlinear optical organic material.[10] Here, we present an investigation of the Hirshfeld surfaces for a unique class of small molecules **1** (Scheme 6.1) that appear to preferentially crystallize in non-centrosymmetric space groups.

6.3   Results and Discussion

The *N*-alkylDABCOnium trihalozincate zwitterions **1** are easily prepared from an alkyl halide, DABCO, and a zinc halide. Crystals of **1** tend to be highly stable and easily prepared either from slow cooling of hot aqueous solutions or layering of solutions. A summary of crystallographic data is presented in Table 6.1. Protonated analogue **7** was prepared from DABCO and $ZnBr_2$ in an aqueous HBr solution. All crystals contained only **1** with no solvent nor apparent disorder. Bromomethyl analogue **3** gave polymorphs depending on the crystallization method: **3a** was grown *via* hydrothermal synthesis; and

3b was grown from layering a solution of $ZnBr_2$ in MeOH onto a solution of DABCO in CH_2Br_2.

Compounds **2, 3a, 3b, 4,** and **7** crystallized in polar, noncentrosymmetric space groups; compounds **5**, **6** and **8** crystallized in centrosymmetric space groups. Notably, the polymorphs **3a** and **3b** both crystallize in NCS space groups. Hirshfeld surfaces were computed using the program CrystalExplorer. Fingerprint plots of the close contacts can be found in Section 6.6.

To probe the origins of non-centrosymmetry on the effects seen on the Hirshfeld surface, it may be best to first compare compounds **4** and **5**, which differ by an electrophilic iodine on the alkyl chain. Hirshfeld countour plots with plotted d_{norm} values indicate that H-I close contracts are predominant for both (Fig. 6.2). As seen in both, antiparallel arrangements leads to close contacts between electron-rich iodine and electron-poor hydrogens near the cationic nitrogen atom. However, the magnitude and direction of the H-I contacts differ somewhat. This appears to be due to the presence of I-I contacts in **4** that are not present in **5**. The electron-poor iodine on the alkyl chain interacts with the electron-rich iodine attached to zinc. This ultimately leads to an antiparallel arrangement which is not governed by mirror symmetry, thus leading to the crystallization of **4** in the non-centrosymmetric space group. This interaction also appears to disallow antiparallel arrangement of molecules as seen in **5**, which leads to centrosymmetry. This is also true in **3b**, which is isomorphous with **4**.

The fingerprint plots of close contacts placed on Hirshfeld surfaces can show distinct similarities in compounds that are not readily seen in molecular visualizations.

Compounds **2** and **3a** both crystallize in the NCS space group Cc but are not isomorphous. **2** has two molecules in the asymmetric unit while **3a** has one. However, an analysis of the fingerprint plots of **2** and **3a** reveal striking similarities. First, in both, the d_i and d_e values for H-X and H-H are of similar magnitude. Secondly, the relative amounts of H-H, H-X, and X-X contacts are relatively similar, differing only by a few percent. Despite the differences seen in the packing, **2** and **3a** actually have similar intermolecular interactions which ultimately lead to crystallization in the same NCS space group. Similarly, the distribution of close contacts as shown in the fingerprint plots of isomorphous **3b** and **4** display very striking similarities.

By contrast, phenyl analogue **6** crystallizes in the centrosymmetric space group Pbca. The fingerprint plot for **6** is slightly different from **2-5**, in that d_{norm} H-H contact distances are much closer (~1.1 Å) than they are in **2-5** (1.3-1.4 Å). The presence of inversion symmetry is due to H-Br contacts between the tribromozincate and protons adjacent to the DABCOnium cation (Fig. 6.3). The magnitude and directionality of H-X contacts thus appear to define these molecule's propensities to crystallize in a CS or NCS space group.

The presence of other functionalities may also influence a molecule's preference for centrosymmetry. Analysis of **8** shows that H-H contacts between inversion-related benzyl and methoxy protons appear to be the predominant source of inversion symmetry (Fig. 6.4). The fingerprint plot does also show slight pi-pi stacking as evidenced by C-C close contacts between the phenyl rings which may also give rise the to the inversion symmetry.

Protonated analogue **7** crystallizes in the NCS space group Cc. The lack of inversion symmetry is easily visualized in the Hirshfeld surface. The strong H-bond donor proton on the cationic DABCOnium center leads to strong interactions with adjacent bromines (Fig. 6.5). Due to the rigidity of the scaffold, this leads to unidirectional rows of molecules without inversion symmetry. Clearly, the predominating H-bonding interactions from the DABCOnium proton are responsible for it crystallizing in a NCS space group.

The directionality of H-bonding motifs ultimately leads to crystallization in an NCS space group. It is worth comparing NCS **7** with centrosymmetric **5**. Both compounds are fully-rigid scaffolds but they differ by inversion symmetry. In the case of **5**, H-I interactions between the methyl group and iodine lead to bidirectional rows of molecules and inversion symmetry. In the case of **7**, the directionality of the DABCOnium proton does not allow it to interact with another molecule going in the opposite direction; thus, the long "rows" present in the packing of **7** are unidirectional.

6.4 Conclusion

The Hirshfeld surface provides a convenient visualization of intermolecular interactions in crystals. In the case of compounds **1**, Hirshfeld surface analysis provided a useful tool for probing the origins of centrosymmetry and non-centrosymmetry. H-X interactions appear to be the critical factor to all compounds **1**, with subtle differences leading to the presence, or absence of, centrosymmetry in the crystal. The directionality of close contacts dictates centrosymmetry in the crystal; if contacts are bidirectional, then inversion symmetry is present. If they are not, then inversion symmetry is absent.

6.5   Experimental Section

Synthesis. Crystals of compounds **3a**, **4**, **5**, **6**, **7** and **8** were prepared accordingly. DABCO (5 mmol) and alkyl halide (5 mmol) were dissolved in acetone (10 mL). After a few minutes to a few hours, crystals of the alkylation product formed. The acetone was decanted and the crystals dissolved in water (10 mL). Zinc halide (5 mmol) was added to the solution, resulting in the immediate precipitation of **1**. The solutions were heated and water added until the solids dissolved. In the case of **5** and **6**, a small amount of ethanol was added to aid in crystallization. Crystals formed after slow cooling of the solutions overnight.

Crystals by layering. Compounds **2** and **3b** were prepared in the following manner. A solution of DABCO in CH_2X_2 was layered with a solution of ZnX_2 in methanol. Crystals of **1** formed at the interface over several days.

X-Ray Diffraction Studies. Low-temperature diffraction data for **2-8** were collected on a Bruker-AXS ApexII CCD detector with graphite-monochromated Mo Kα radiation (λ = 0.71073 Å), performing phi and omega scans. All structures were solved by direct methods and refined against F^2 on all data by full-matrix least squares with SHELXL-97.[11] All non-hydrogen atoms were refined anisotropically. All hydrogen atoms were included in the model at geometrically calculated positions and refined using a riding model. The isotropic displacement parameters of the hydrogen atoms were fixed to 1.2 times the U value of the atoms they are linked to (1.5 U for methyl groups). In the case of **7**, a racemic twin prevented an accurate calculation of the Flack parameter; however,

7 was reliably solved in Cc as opposed to C2/c; pseudoinversion symmetry in the crystal was checked and not found.[12] Attempts to solve and refine **7** in C2/c were unsuccessful.
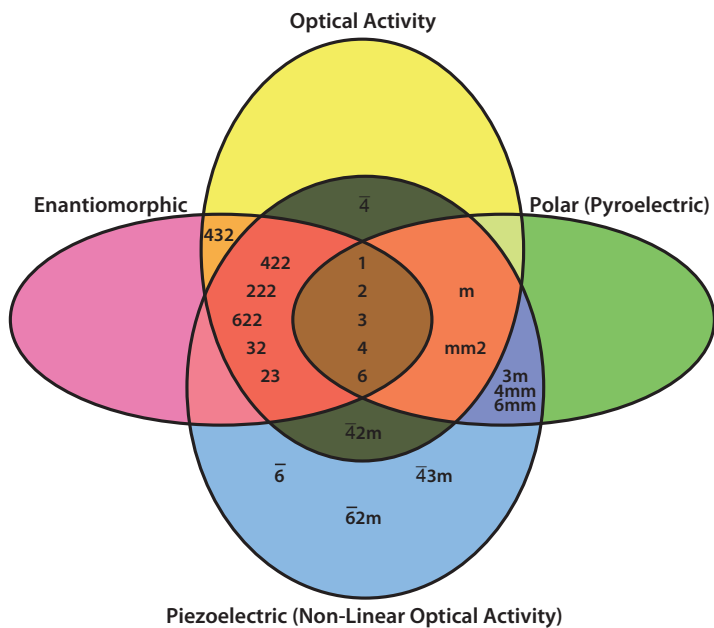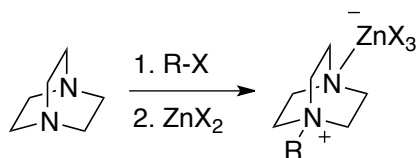
6.6   Figures and Schemes

Figure 6.1. Non-centrosymmetric point groups and their respective bulk properties. Adapted from Ref. 1.

1

Entry	R =	X =
2	CH_2Cl	Cl
3	CH_2Br	Br
4	CH_2I	I
5	CH_3	I
6	Ph	Br
7	H	Br
8	4-OMePh	Cl

Scheme 6.1. Overview of the compounds presented in this chapter.

Table 6.1. Summary of Crystallographic Information for Chapter 6

Chapter number	2	3a	3b	4
Lab number	ba39h	ba07i	ba23h	ba55i
Moiety formula	$C_7H_{14}Cl_4N_2Zn$	$C_7H_{14}Br_4N_2Zn$	$C_7H_{14}Br_4N_2Zn$	$C_7H_{14}I_4N_2Zn$
space group	Cc	Cc	Pca2_1	Pca2_1
a (Å)	14.5063(6)	7.131(5)	15.3151(8)	15.6757(8)
b (Å)	18.7955(7)	14.416(10)	7.2029(4)	7.5787(4)
c (Å)	11.4966(4)	13.699(9)	12.6774(7)	13.4451(6)
β (deg)	127.4960(18)	103.145(8)	90	90
V (Å^3)	2486.97(18)	1369.2(16)	1398.48(13)	1597.30(14)
Z	8	4	4	4
D_x (g cm^{-3})	1.781	2.480	2.428	2.907
T (K)	193	193	193	193
Total Reflections	17493	7154	20330	24630
Ind. Reflections	4381	2527	2572	2904
$R(F)$ [1] $(I > 2\sigma)$	0.0324	0.0179	0.0362	0.0229
$R_w(F^2)$ [2] (all data)	0.0806	0.0394	0.0924	0.0470
GooF S	1.048	0.954	1.039	1.057
Flack Parameter	0.085(11)	0.023(10)	0.04(2)	0.02(3)

Chapter number	5	6	7	8
Lab number	ba46i	b01j	ba89j	ba33i
Moiety formula	$C_7H_{15}I_3N_2Zn$	$C_{13}H_{19}Br_3N_2Zn$	$C_6H_{13}Br_3N_2Zn$	$C_{14}H_{21}Cl_3N_2OZn$
space group	P2$_1$/n	Pbca	Cc	P2$_1$/c
a (Å)	11.2071(7)	12.212(3)	9.6037(8)	9.081(3)
b (Å)	9.8035(6)	14.018(3)	9.4556(7)	15.447(5)
c (Å)	13.1021(8)	19.021(4)	12.5529(9)	11.989(4)
β (deg)	97.936(3)	90	97.285	99.626(6)
V (Å^3)	1425.73(15)	3256.0(12)	1130.71(15)	1658.2(10)
Z	4	8	4	4
D_x (g cm^{-3})	2.671	2.074	2.457	1.623
T (K)	193	193	193	193
Total Reflections	4070	28667	10311	16467
Ind. Reflections	3848	2991	2344	3044
$R(F)$ $(I > 2\sigma)$	0.0343	0.0221	0.0374	0.0249
$R_w(F^2)$ (all data)	0.0745	0.0486	0.0872	0.0631
GooF S	1.038	1.130	1.058	1.068
Flack Parameter	n/a	n/a	0.5	n/a

---

[1] $R(F) = \sum ||F_o| - |F_c||/\sum |F_o|$ for $F_o^2 > 2\sigma(F_o)^2$.

[2] $R_w(F_o^2) = [\sum w(F_o^2 - F_c^2)^2/\sum wF_o^4]^{1/2}$, $w^{-1} = \sigma^2(F_o)^2 + [M(F_o^2)]^2 + [N(F_o^2 + 2F_c^2)/3]$ for $F_o^2 \geq 0$; $w^{-1} = \sigma^2(F_o^2)$ for $F_o^2 < 0$. M and N are weighting variables.
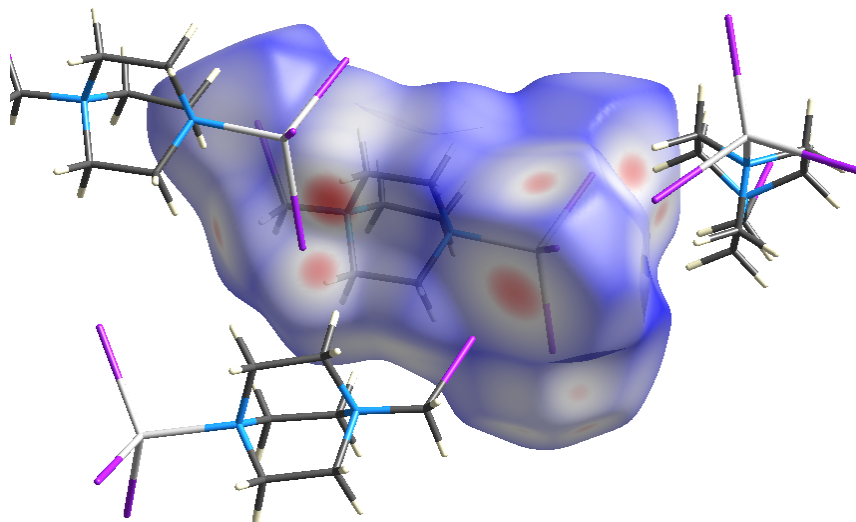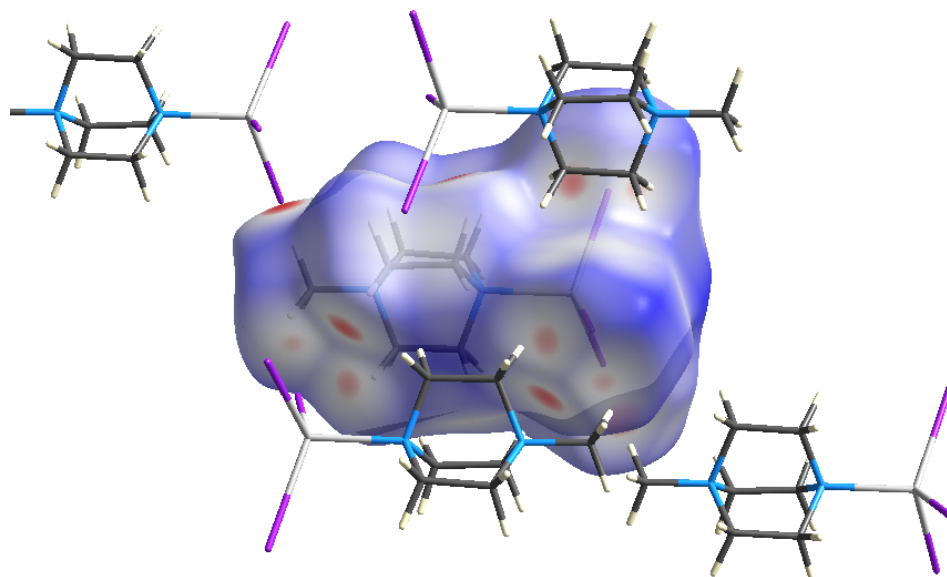
Figure 6.2. Hirshfeld surfaces (d$_{norm}$ plotted) for a) **4** and b) **5**. Red indicates closer contacts, blue indicates more distant contacts. Note in **5** the H-I contacts between inversion-related units.
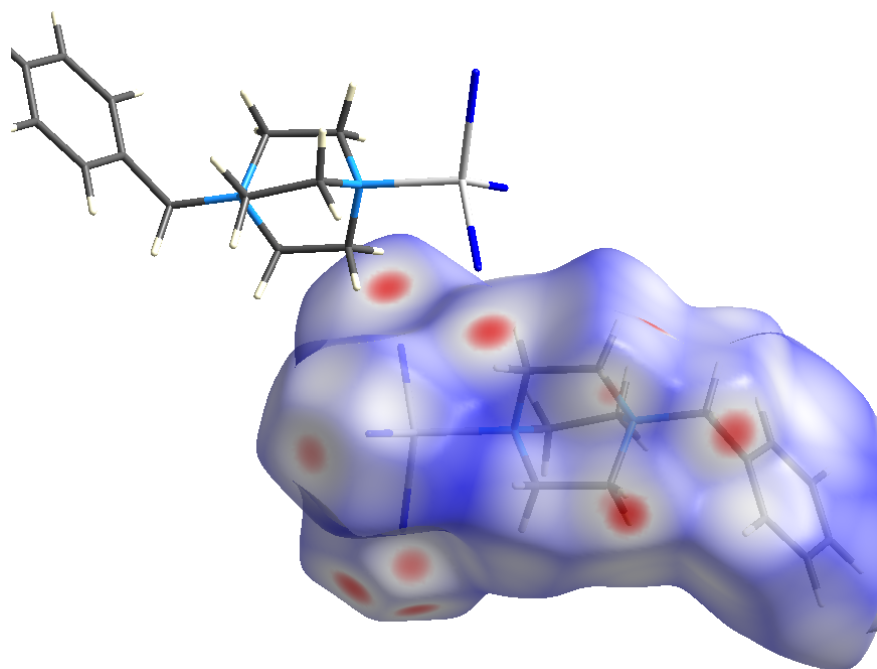
Figure 6.3. Hirshfeld surfaces (d_{norm} plotted) for H-Br contacts between inversion-related units in **6**.
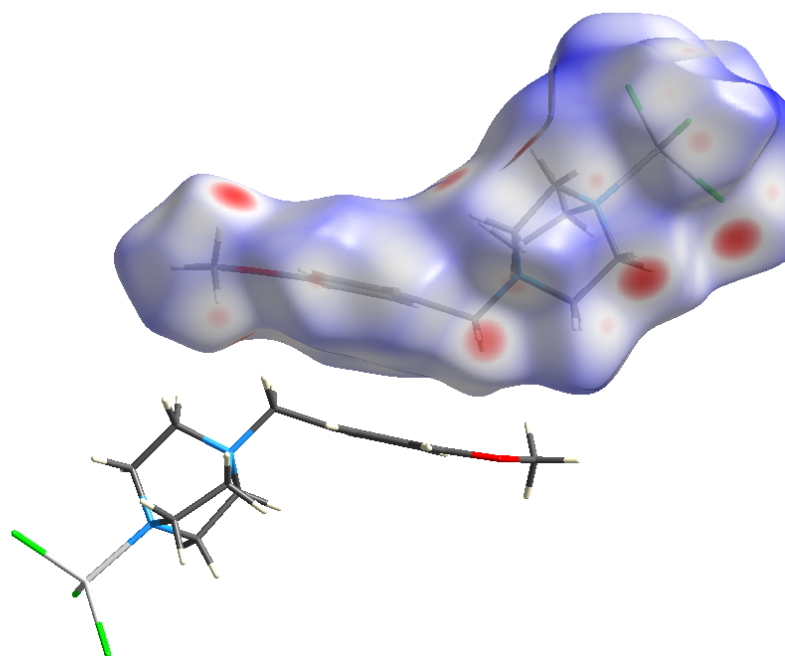

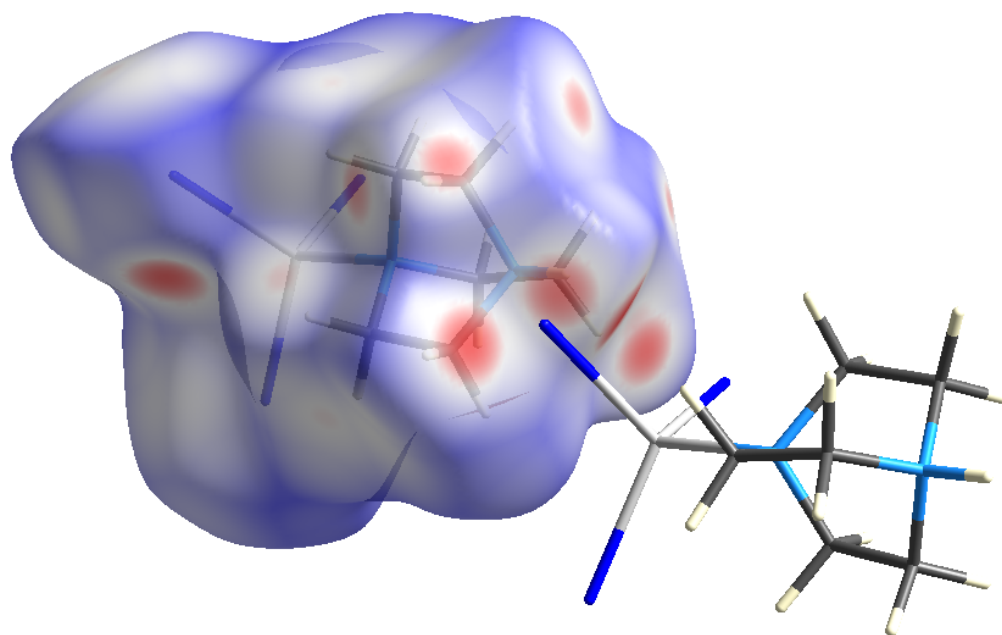**Figure 6.4.** Hirshfeld surfaces (d_{norm} plotted) for close contacts between inversion-related units in **8**.

Figure 6.5. Hirshfeld surfaces (d_{norm} plotted) showing H-bonding interactions in **7**.

Figure 6.6   Fingerprint Plots for 2-8

Compound **2**
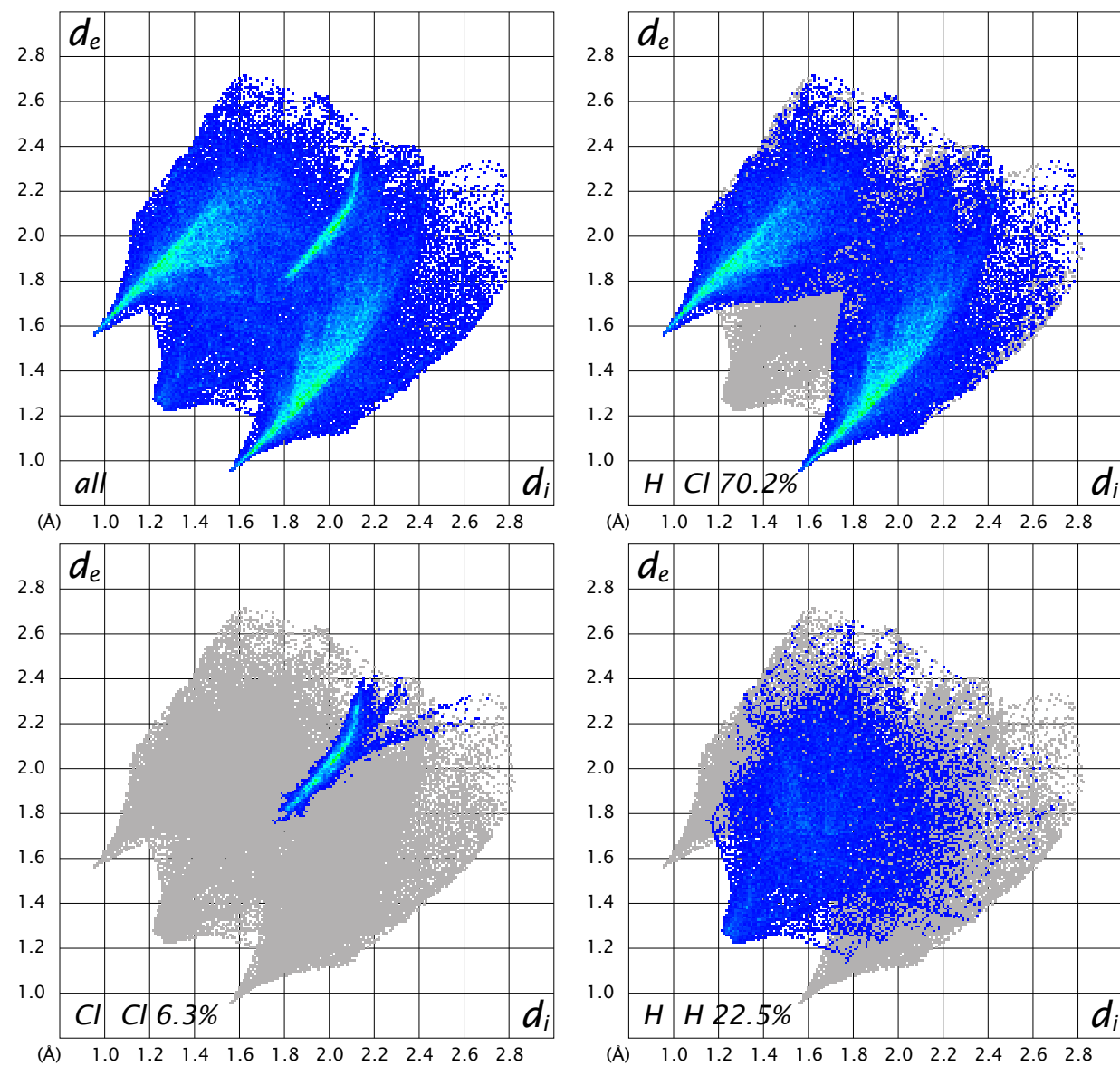
Figure 6.6 (cont.)
Compound **3a**
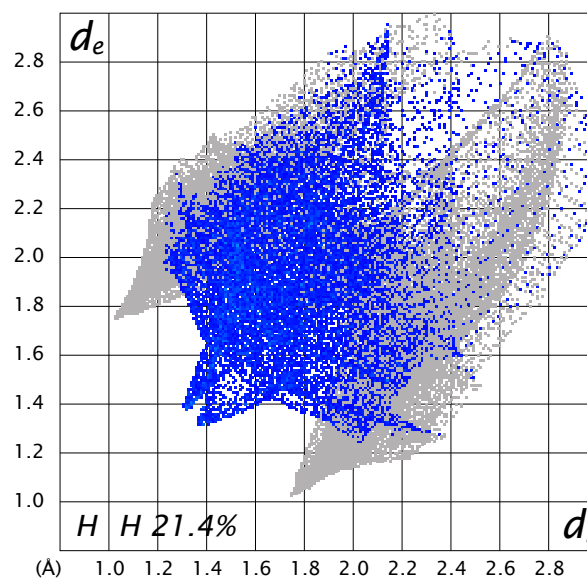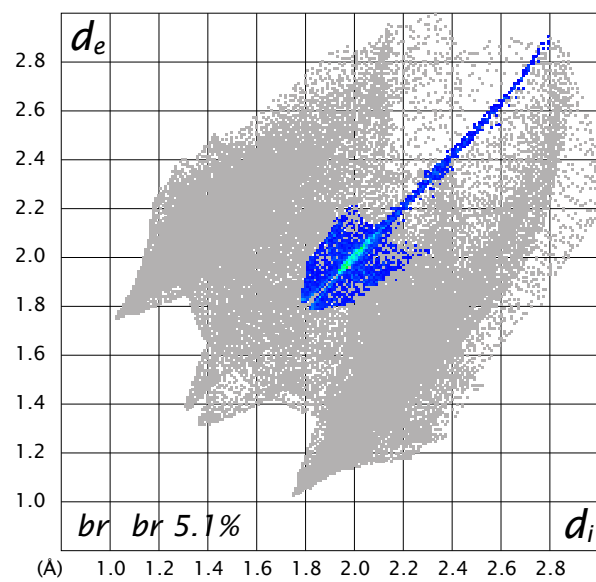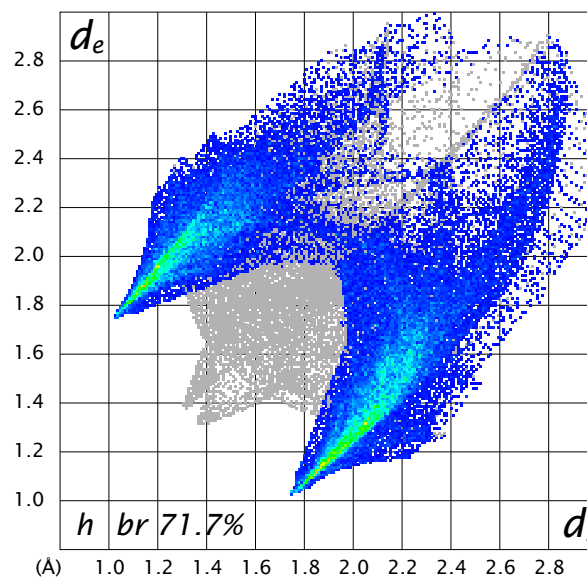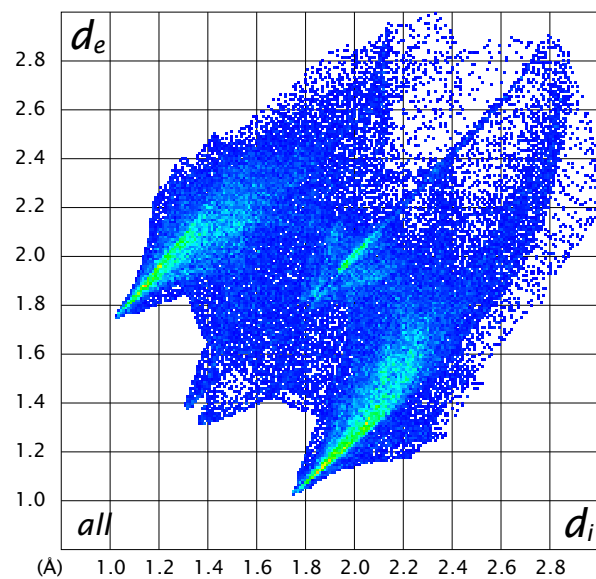
Figure 6.6 (cont.)
Compound **3b**
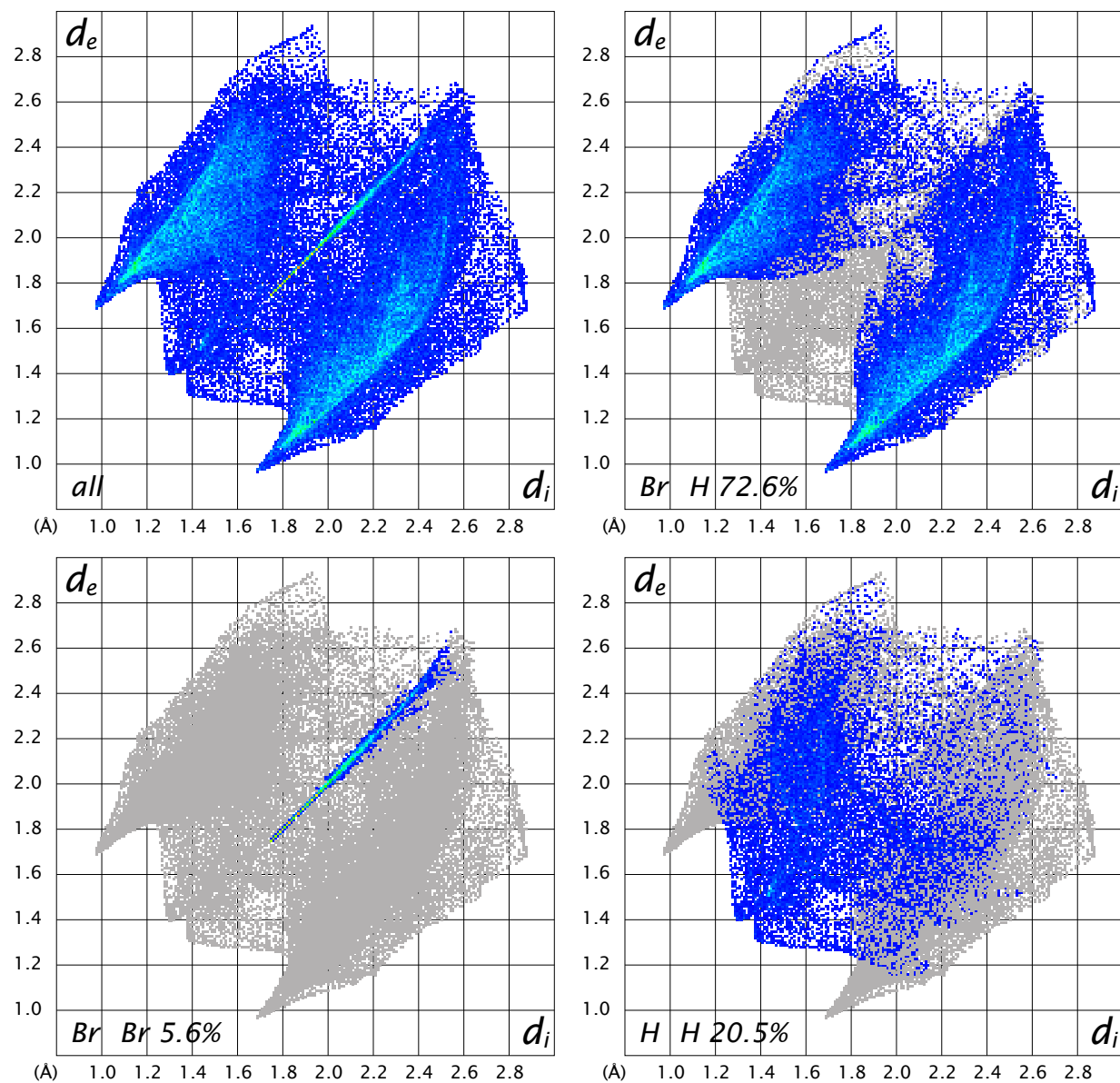
Figure 6.6 (cont.)
Compound **4**
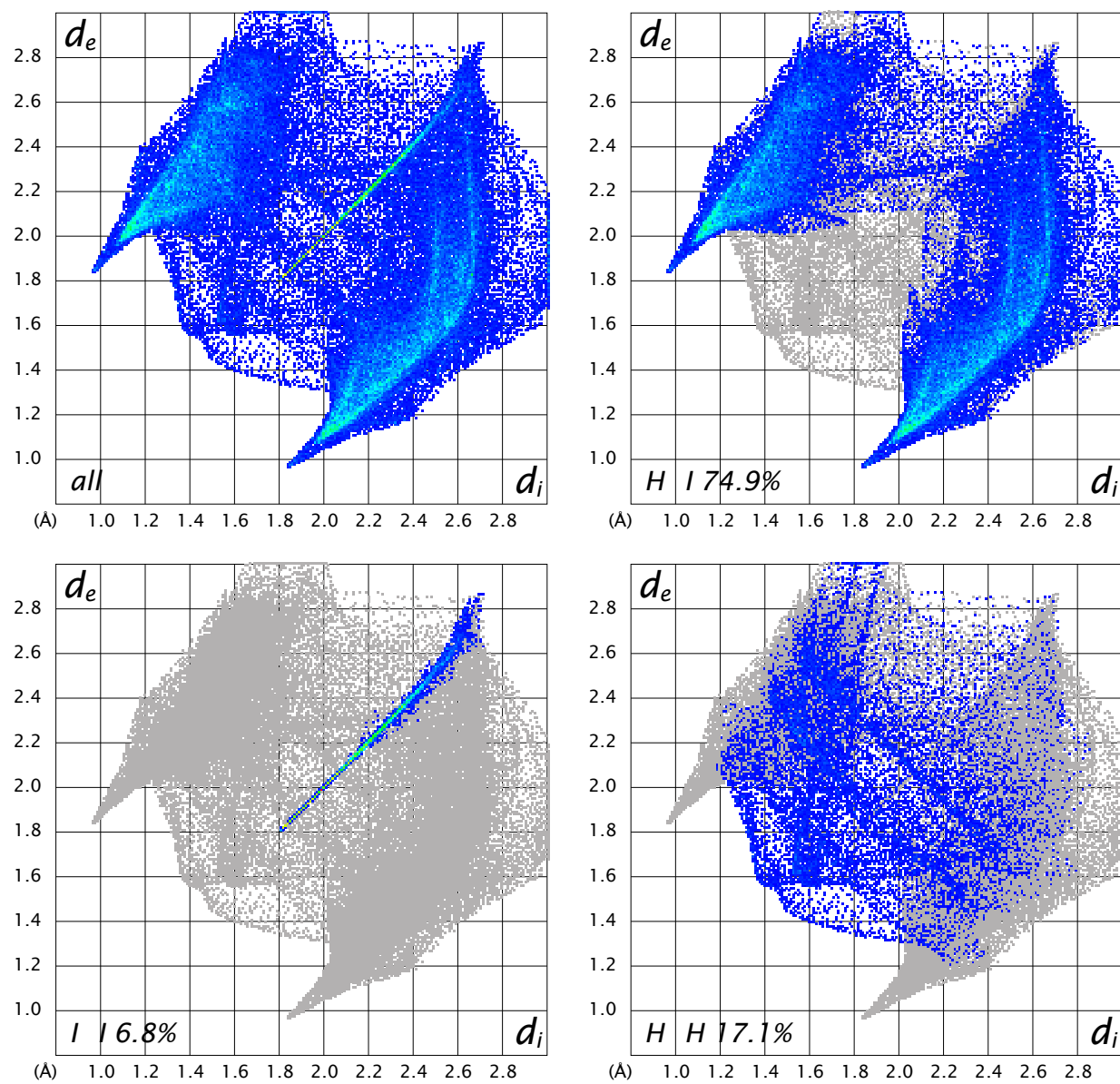
Figure 6.6 (cont.)
Compound **5**
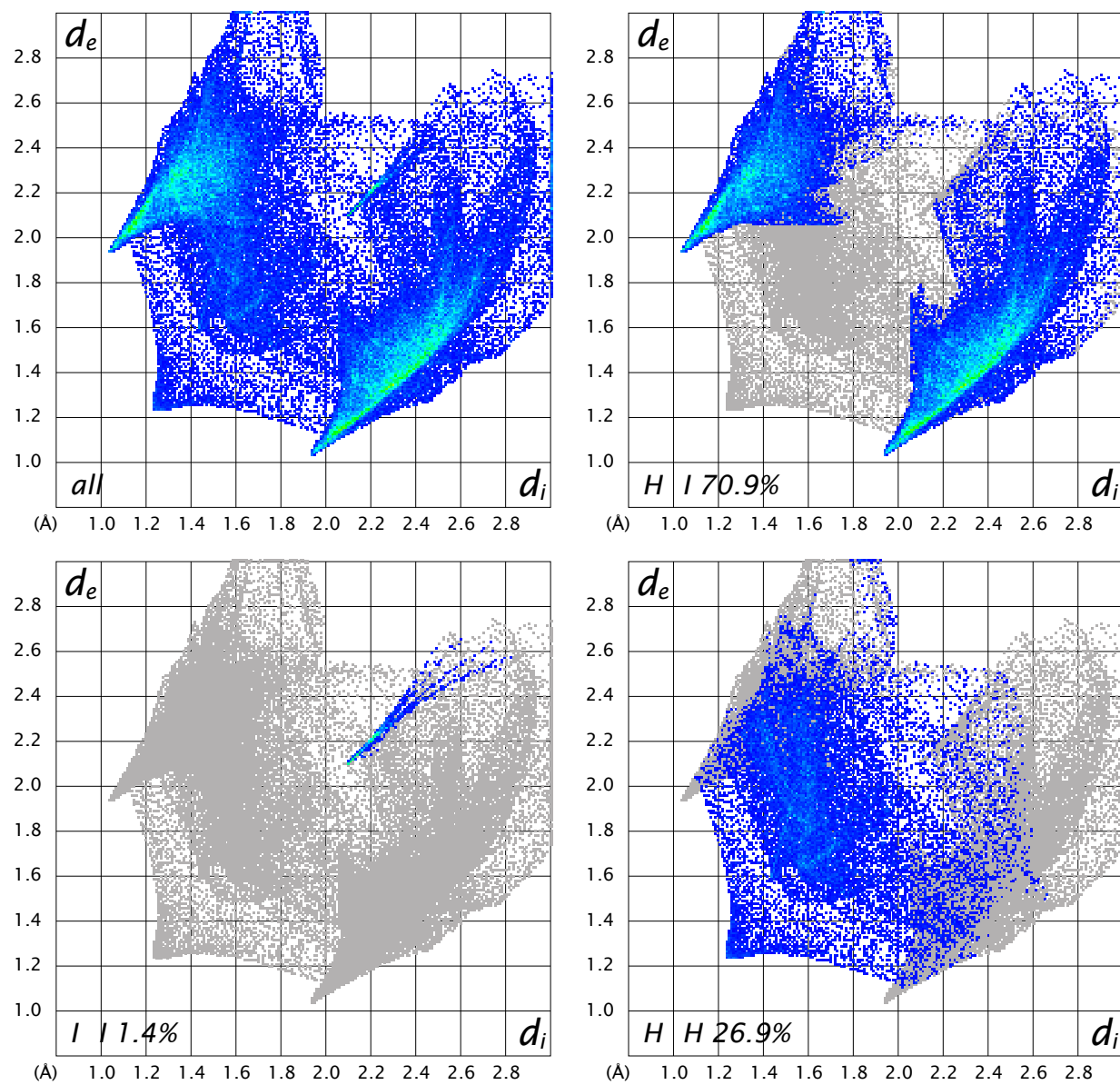
Figure 6.6 (cont.)
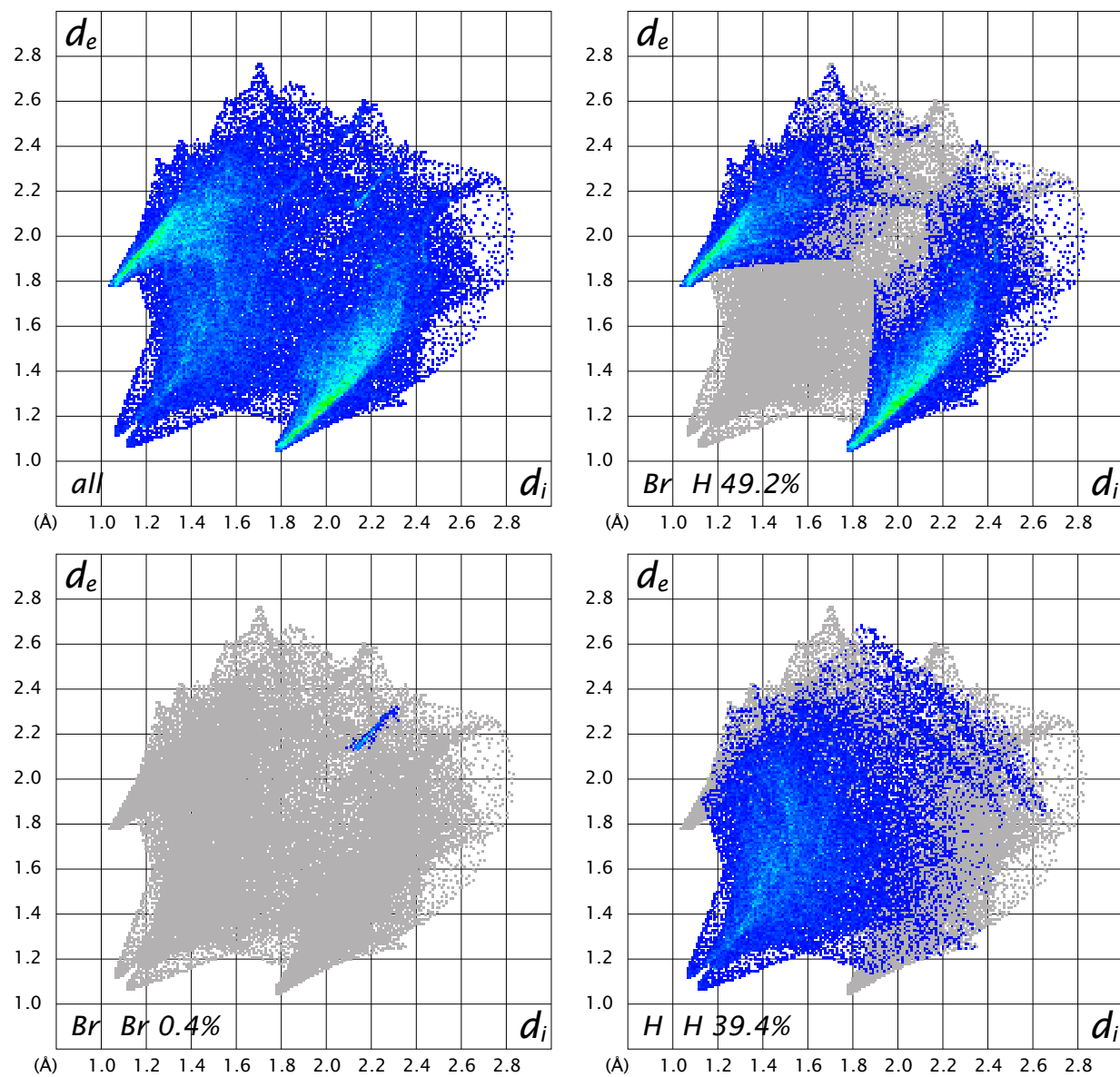Compound **6**

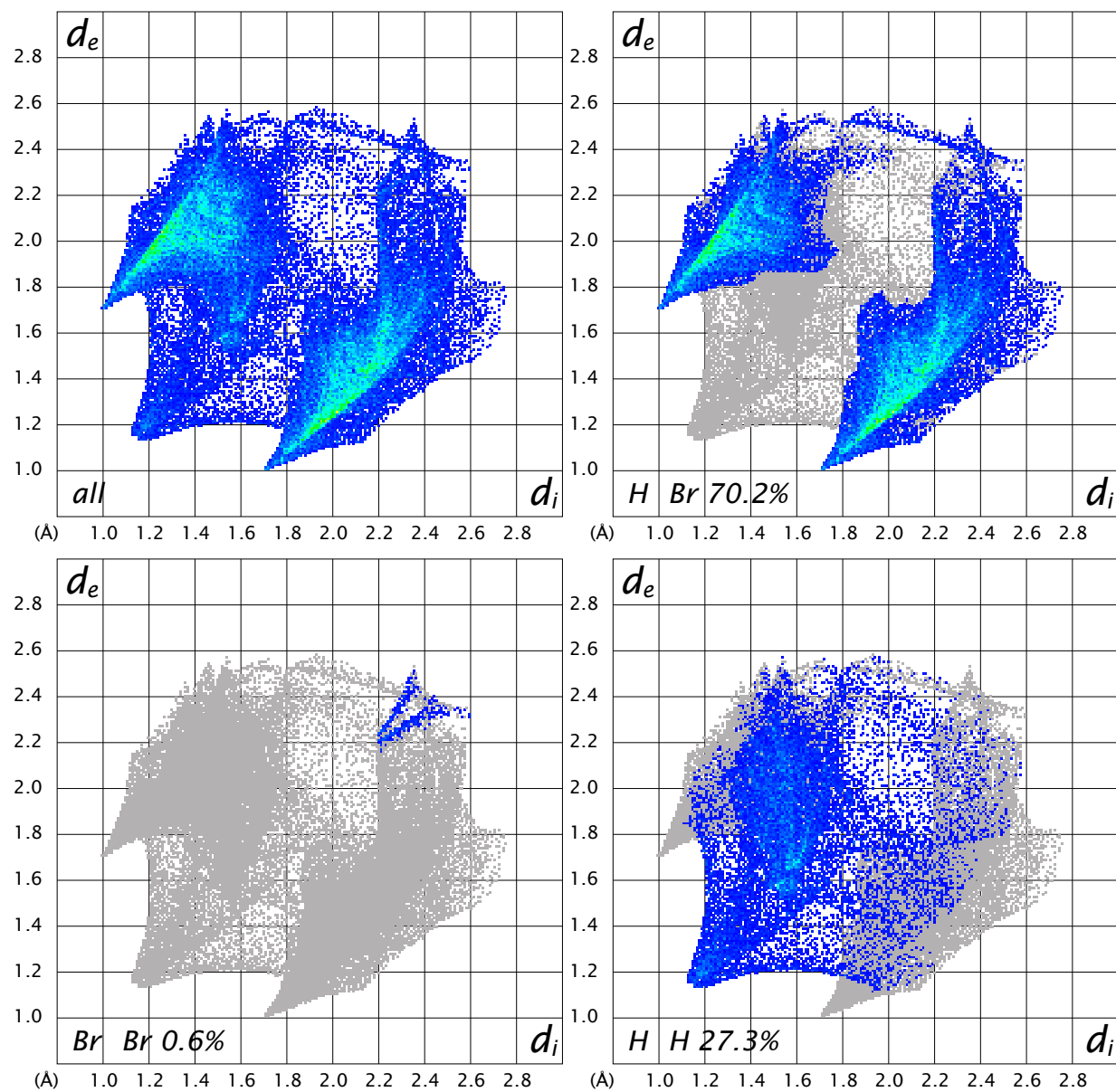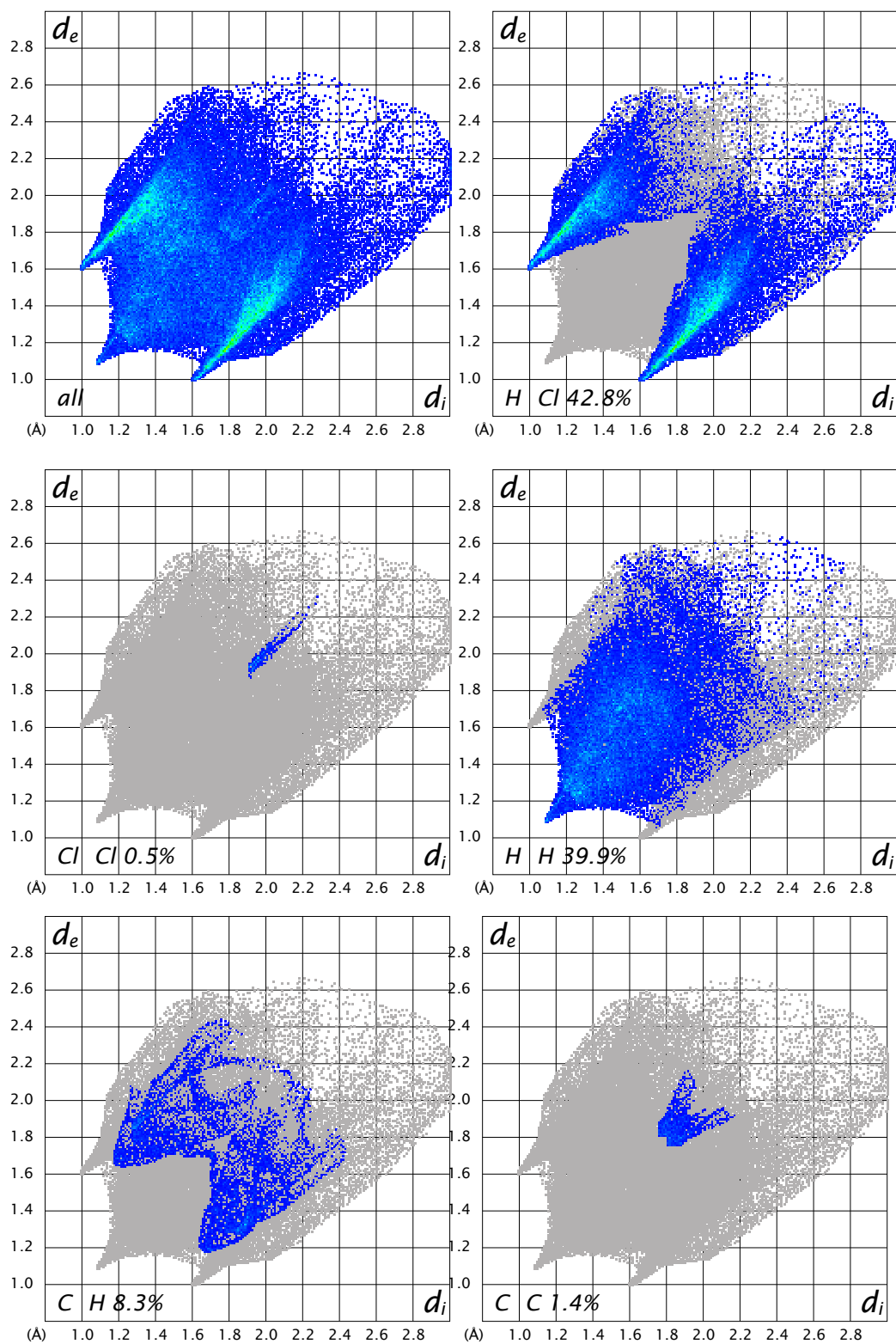**Figure 6.6 (cont.)**
Compound **7**

Figure 6.6 (cont.)
Compound **8**

6.7 References

[1]   Halasyamani, P. S.; Poeppelmeier, K. R. *Chem. Mater.* **1998**, *10*, 2753-2769.
[2]   Ok, K. M.; Chi, E. O.; Halasyamani, P. S. *Chem. Soc. Rev.* **2006**, *35*, 710-717.
[3]   Desiraju, G. R. *Chem. Commun.* **1997**, 1475-1482.
[4]   McKinnon, J. J.; Jayatilaka, D.; Spackman, M. A. *Chem. Commun.* **2007**, 3814-3816.
[5]   Spackman, M. A.; McKinnon, J. J.; Jayatilaka, D. *CrystEngComm* **2008**, *10*, 377-388.
[6]   Spackman, M. A.; Jayatilaka, D. *CrystEngComm* **2009**, *11*, 19-32.
[7]   Spackman, M. A.; Byrom, P. G. *Chem. Phys. Lett.* **1997**, *267*, 215-220.
[8]   McKinnon, J. J.; Mitchell, A. S.; Spackman, M. A. *Chem. Eur. J.* **1998**, *4*, 2136-2141.
[9]   Wolff, S. K.; Grimwood, D. J.; McKinnon, J. J.; Jayatilaka, D.; Spackman, M. A.; University of Western Australia: Perth, 2010.
[10]   Munshi, P.; Skelton, B. W.; McKinnon, J. J.; Spackman, M. A. *CrystEngComm* **2008**, *10*, 197-206.
[11]   Sheldrick, G. M.; Universität Göttingen: Göttingen, Germany, 1997.
[12]   Marsh, R. E. *Acta Cryst.* **2004**, *B60*, 252-253.

Author's Biography

Aaron D. Finke was born on June 20, 1984 at Langley AFB, VA. He grew up in Henderson, NV and graduated from Green Valley High School in 2002. He went on to study chemistry at the University of Arizona, pursuing independent research in the lab of Prof. Dominic McGrath working on non-aggregating dendritic chromophores. In 2005 he spent a summer at Georgia Tech working in the lab of Prof. Seth Marder on the synthesis of triarylamines for enhanced hole transport in organic LEDs. Aaron received his BS in Chemistry in 2006, then moved to the University of Illinois, Urbana-Champaign to received his Ph.D under the tutelage of Prof. Jeff Moore, working on developing carbon-carbon bond-forming methodologies for the formation of shape-persistent architectures and X-ray crystallographic analysis of shape-persistent architectures. In 2009, Aaron received a Hach graduate fellowship. Upon completion of his graduate studies in early 2011, Aaron will join the lab of Prof. François Diederich at ETH-Zürich, Switzerland, as a postdoctoral researcher.